Vol. 7, no. 2, 2023 eISSN 2587-8999
PEER-REVIEWED SCIENTIFIC AND THEORETICAL JOURNAL

Computational Mathematics and Information Technology

Computational Mathematics

Mathematical Modelling

Information Technologies

www.cmit-journal.ru
DOI 10.23947/2587-8999

Computational Mathematics and Information Technologies

Peer-reviewed scientific and theoretical journal (published since 2017)

eISSN 2587-8999
DOI: 10.23947/2587-8999

Vol. 7, no. 2, 2023

The scope of "Computational Mathematics and Information Technologies" is focused on fundamental and applied research according to the following scientific sections:

1. Computational Mathematics
2. Mathematical Modelling
3. Information Technologies

Indexing:	Russian Scientific Citation Index, Crossref, Cyberleninka
Name of the body that registered the publication	Mass media registration certificate ЭЛ № ФС 77-66529 dated July 21, 2016 issued by the Federal Service for Supervision of Communications, Information Technology and Mass Media.
Founder and publisher	Federal State Budgetary Educational Institution of Higher Education Don State Technical University (DSTU).
Periodicity	Quarterly (4 issues per year)
Address of the founder and publisher	Gagarin Sq. 1, Rostov-on-Don, 344003, Russian Federation.
E-mail	CMIT-EJ@yandex.ru
Telephone	+7(863) 273–85–14
Website	https://cmit-journal.ru
Date of publication	25.06.2023

Computational Mathematics and Information Technologies

Рецензируемый научно-теоретический журнал (издаётся с 2017 года)

eISSN 2587-8999
DOI: 10.23947/2587-8999

Том 7, № 2, 2023

Журнал «Computational Mathematics and Information Technologies» ориентирован на фундаментальные и прикладные исследования по следующим научным разделам:

1. Вычислительная математика
2. Математическое моделирование
3. Информационные технологии

Индексация:	РИНЦ, CrossRef, КиберЛенинка
Наименование органа, зарегистрировавшего издание	Свидетельство о регистрации средства массовой информации ЭЛ № ФС 77 – 66529 от 21 июля 2016 г., выдано Федеральной службой по надзору в сфере связи, информационных технологий и массовых коммуникаций.
Учредитель и издатель	Федеральное государственное бюджетное образовательное учреждение высшего образования «Донской государственный технический университет» (ДГТУ).
Периодичность	4 выпуска в год
Адрес учредителя и издателя	344003, Российская Федерация, г. Ростов-на-Дону, пл. Гагарина, 1.
E-mail	CMIT-EJ@yandex.ru
Телефон	+7(863) 273–85–14
Сайт	https://cmit-journal.ru
Дата выхода в свет	25.06.2023

Contents

Содержание

ВЫЧИСЛИТЕЛЬНАЯ МАТЕМАТИКА

МАТЕМАТИЧЕСКОЕ МОДЕЛИРОВАНИЕ

COMPUTATIONAL MATHEMATICS
ВЫЧИСЛИТЕЛЬНАЯ МАТЕМАТИКА

UDC 519.6

Review article

https://doi.org/10.23947/2587-8999-2023-7-2-7-18

The Discontinuous Galerkin Method and its Implementation in the RAMEG3D Software Package

Vladimir F Tishkin ✉, Marina E Ladonkina

Keldysh Institute of Applied Mathematics of the Russian Academy of Sciences, 4, Miusskaya Sq., Moscow, Russian Federation

✉ v.f.tishkin@mail.ru

Abstract

Currently, the Discontinuous Galerkin Method (DGM) is widely used to solve complex multi-scale problems of mathematical physics that have important applied significance. When implementing it, the question of choosing a discrete approximation of flows for viscous terms of the Navier-Stokes equation is important.

It is necessary to focus on the construction of limiting functions, on the selection of the best discrete approximations of diffusion flows, and on the use of implicit and iterative methods for solving the obtained differential-difference equations for the successful application of DGM on three-dimensional unstructured grids.

First-order numerical schemes and second-order DGM schemes with Godunov, HLLC, Rusanov-Lax-Friedrichs numerical flows and hybrid flows are investigated. For high-order precision methods, it is necessary to use high-order time schemes. The Runge-Kutta scheme of the third order is used in the work. The equations are written as a system of first-order equations, when solving the Navier-Stokes equation by the discontinuous Galerkin method.

Keywords: Discontinuous Galerkin Method (DGM), Navier-Stokes equations, hybrid flows, Runge-Kutta scheme, scheme template.

For citation. Tishkin VF, Ladonkina ME. The discontinuous Galerkin method and its implementation in the RAMEG3D software package. *Computational Mathematics and Information Technologies.* 2023;7(2):7–18. https://doi.org/10.23947/2587-8999-2023-7-2-7-18

Обзорная статья

Разрывный метод Галеркина и его реализация в программном комплексе РАМЕГ3D

В.Ф. Тишкин ✉, М.Е. Ладонкина

Институт прикладной математики им. М. В. Келдыша Российской академии наук, Российская Федерация, г. Москва, Миусская пл., 4

✉ v.f.tishkin@mail.ru

Аннотация

В настоящее время метод Галеркина с разрывными базисными функциями (РМГ) или *Discontinuous Galerkin Method* (DGM) получил широкое распространение для решения сложных разномасштабных задач математической физики, имеющих важное прикладное значение. При его реализации важным является вопрос о выборе дискретной аппроксимации потоков для вязких членов уравнения Навье-Стокса.

Для успешного применения РМГ на трехмерных неструктурированных сетках необходимо сосредоточить внимание на построении лимитирующих функций, на выборе наилучших дискретных аппроксимаций

диффузионных потоков и на применении неявных и итерационных методов решения полученных дифференциально-разностных уравнений.

Исследуются численные схемы первого порядка и схемы РМГ второго порядка с численными потоками Годунова, HLLC, Русанова-Лакса-Фридрихса и гибридными потоками. Для методов высокого порядка точности необходимо использовать схемы высокого порядка по времени.

В работе используется схема Рунге-Кутты третьего порядка. При решении уравнения Навье-Стокса разрывным методом Галеркина уравнения записываются в виде системы уравнений первого порядка.

Ключевые слова: разрывный метод Галеркина, уравнения Навье-Стокса, гибридные потоки, схема Рунге-Кутты, шаблон схемы.

Для цитирования. Тишкин В.Ф., Ладонкина М.Е. Разрывный метод Галеркина и его реализация в программном комплексе РАМЕГ3D. *Computational Mathematics and Information Technologies*. 2023;7(2):7–18. https://doi.org/10.23947/2587-8999-2023-7-2-7-18

One of the main requirements is the use of high-precision numerical methods to obtain high-quality solutions to mathematical physics problems of important applied importance, one of the main requirements is the use of high-precision numerical methods. This is especially relevant for solving complex multi-scale problems in which it is not enough to obtain a solution only by grinding the grid and using first-order accuracy methods.

The *Discontinuous Galerkin Method* (DGM) has been developing especially actively over the past few decades, the first mention of which can be found in [1]. This method refers to numerical methods of an increased order of approximation of the solution, because it provides a given order of accuracy, and on unstructured grids, can be used for grids with an arbitrary cell shape, has a compact template consisting of a calculated cell and one layer of neighboring cells. There are two approaches to improve the accuracy of the resulting solution. One of them is the shredding of the grid in the areas of the existing features of the solution, the second approach is to increase the order of accuracy of the scheme. The use of the discontinuous Galerkin method makes it possible to use both approaches at once: increasing the order of accuracy of the method by increasing the order of the polynomials used, and local grinding of the grid (the so-called *hp*-adaptation) [2, 3].

One of the important issues in the implementation of the method is the choice of the grid on which the solution is being sought. The undoubted advantage of RMG is the possibility of its application on grids of arbitrary structure. Currently, the discontinuous Galerkin method is well developed for both structured [4] and unstructured [5] grids. There are successful DGM software implementations for solving three-dimensional problems on unstructured grids containing elements of only one type (tetrahedral [5–8] or hexahedral [9]), as well as for grids of arbitrary structure [10].

The obvious disadvantage of the method is its extremely high computational cost, but this is covered by a compact template and the creation of efficient parallel software systems. DGM has a significant computational complexity, so the question arises about the most efficient use of all the possibilities of computer technology. In the world research centers dealing with this problem, work is underway to parallelize the implementations of DGM on a super computer [11–13]. In [6], when solving the Navier-Stokes DGM equations, a new grid-operator approach to programming mathematical physics problems was used, which allows to compactly record and effectively apply mathematical formulas, uniformly implement the approach on different types of grids and for various computing architectures, including for CUDA graphics accelerators [14, 15].

Along with the many advantages of using the discontinuous Galerkin method, there are also some difficulties in its implementation. Firstly, in order to ensure the monotony of the solution obtained by this method, it is necessary to introduce slope limiters or limiters, especially if the solution contains strong discontinuities. The most widely used is the Cockburn limiter [16]. The idea of this limiter is easily implemented in the multidimensional case on grids of arbitrary structure. However, this limiter, like all TVD limiters, reduces the accuracy of the resulting solution. Recently, various approaches to solving this problem have been actively developing. One of the approaches to creating a limiter of an increased order of accuracy is proposed in the works of Krivodanova [17]. But this limiter works well only on structured grids. Other approaches to creating limiters of a higher order of accuracy are described in [18–25].

Also important in the implementation of DGM is the question of choosing a discrete approximation of flows for viscous terms of the Navier-Stokes equation. There are several types of such approximations, most often used in real calculations [26, 27], which were investigated in [28]. Nevertheless, the question of the optimal choice of such approximations remains open.

When the order of accuracy of the scheme increases, there is a strict restriction on the time step. Initially, when calculating DGM, time integration was carried out by explicit multistep Runge-Kutta schemes of high order [16, 29, 30]. But the most effective approach is to use implicit time integration methods in order to relax the time step constraint [31–36].

Currently, software implementations of DGM are known by an implicit method for modeling incompressible flows [37] and for solving the Navier-Stokes equations [35].

Another point that the authors had to face when implementing DGM on grids with an arbitrary cell shape is the need to carry out the integration procedure [16] on an arbitrary cell shape. To do this, the transformation of the original irregular-shaped cell into a reference cell for which the position of the quadrature points is known [61]. When constructing such a transformation for the case of a tetrahedron, hexahedron and triangular prism, it is sufficient to use a multilinear transformation that translates the vertices of the cell into the vertices of the original cell. However, for a quadrangular pyramid, this approach does not give the desired result, because when using it, we get curved side faces and edges of the pyramid, which will not allow it to be properly joined with tetrahedral cells. Below in this paper, a transformation is constructed that avoids this drawback.

For the successful implementation of DGM on three-dimensional unstructured grids, it is necessary to focus on several points:

– on the construction of limiting functions;

– on the selection of the best discrete approximations of diffusion flows;

– on the application of implicit and iterative methods for solving the obtained differential-difference equations.

To obtain an accurate numerical solution of mathematical physics problems, it is important to use a high-quality computational grid and a reliable high-precision numerical method, as well as to be sure that the chosen method fully corresponds to the problem being solved. For example, it is known that when using Godunov-type difference schemes in some problems containing shock waves, the development of instability of the “carbuncle” type occurs [38, 39]. The conditions for the appearance of this type of instability are high Reynolds numbers and a low dissipative numerical flow. It was noted in [40] that other types of instabilities may occur under such conditions. One of the established causes of this type of instability is the numerical flows used [41–48]. Flows with low dissipation are most susceptible to the occurrence of this instability, and the use of highly dissipative flows allows avoiding the occurrence of “carbuncle” instability. For this reason, several attempts have been made to develop new methods that suppress the development of instabilities, ensuring low dissipation [49–52]. In [53], a study of the susceptibility to shock-wave instability of specific numerical flows implemented in the RAMEG3D software package was carried out [54]. This type of instability is tested on test problems from the Kerk list [40] in the statements given in [55].

In this paper, we study first-order numerical schemes and second-order DGM schemes with numerical Godunov flows [56], HLLC [57], Rusanov-Lax-Friedrichs flows [58, 59] and hybrid flows [60] used in calculations. The basic formulas of the hybrid flow developed by the authors are also given.

1. Basic formulas of the discontinuous Galerkin method. Consider the Navier-Stokes equations written as a system of first-order equations:

$$\begin{gathered}\partial_t U + \nabla \cdot F(U) - \nabla \cdot G(U, \boldsymbol{\tau}) = 0, \\ \boldsymbol{\tau} = \left(\lambda - \frac{2}{3}\mu\right)\hat{E}(div\ v) + 2\mu \boldsymbol{S}(v), \\ \boldsymbol{S}(v) = \frac{1}{2}\left(\nabla v + (\nabla v)^*\right), \\ q(U) = k\nabla T.\end{gathered} \tag{1}$$

$$\begin{aligned} U &= (\rho, \rho u, \rho v, \rho w, E), \\ F(U) &= (F_x(U), F_y(U), F_z(U)), \\ G(U, \boldsymbol{\tau}) &= (G_x(U, \boldsymbol{\tau}), G_y(U, \boldsymbol{\tau}), G_z(U, \boldsymbol{\tau})). \end{aligned} \tag{2}$$

$$\begin{aligned} F_x(U) &= \left(\rho u, \rho u^2 + p, \rho uv, \rho uw, (E+p)u\right), \\ F_y(U) &= \left(\rho u, \rho uv \rho v^2 + p, \rho uw, (E+p)v\right), \\ F_z(U) &= \left(\rho u, \rho uw \rho vw, \rho w^2 + p, (E+p)w\right), \\ G_x(U, \boldsymbol{\tau}) &= \left(0, \tau_{xx}, \tau_{xy}, \tau_{xz}, u\tau_{xx} + v\tau_{xy} + w\tau_{xz} + q_x\right), \\ G_y(U, \boldsymbol{\tau}) &= \left(0, \tau_{yx}, \tau_{yy}, \tau_{yz}, u\tau_{yx} + v\tau_{yy} + w\tau_{yz} + q_y\right), \\ G_z(U, \boldsymbol{\tau}) &= \left(0, \tau_{zx}, \tau_{zy}, \tau_{zz}, u\tau_{zx} + v\tau_{zy} + w\tau_{zz} + q_z\right), \end{aligned} \tag{3}$$

where ρ is the substance density; u, v, w are the velocity components v, ε is the specific internal energy and $E = \rho\left(\varepsilon + \frac{u^2 + v^2 + w^2}{2}\right)$ is the total energy per unit volume, p is the substance pressure.

The system of equations (1) is closed by the equation of state, in this case, the equation of state of an ideal gas $p = (\gamma - 1)\rho\varepsilon$ with an adiabatic exponent γ.

For each specific task, system (1) is supplemented with suitable initial-boundary conditions.

Let's cover the area Ω, where the solution is sought by the discontinuous Galerkin method with a grid T_h. On each element T_j we will look for an approximate solution of the system of equations (1) in the form of polynomials $P(x)$ of degree N with time-dependent coefficients [1]:

$$\begin{aligned} \boldsymbol{U}_h(x,t) &= \sum_{k=0}^{st} \boldsymbol{U}_k(t)\phi_k(x), \\ q_{ih}(x,t) &= \sum_{k=0}^{st} q_{ik}(t)\phi_k(x), \\ \boldsymbol{\tau}_{ijh}(x,t) &= \sum_{k=0}^{st} \tau_{ij\,k}(t)\phi_k(x), i, j = x, y, z, \end{aligned} \tag{4}$$

where $st = 0, C_{N+3}^3 - 1$ is the dimension of the polynomial space, and $\phi_k(x)$ is the basis function.

For high-order precision methods, it is necessary to use high-order time schemes. In this paper, the Runge-Kutta scheme of the third order is used [1].

The equations are written as a system of first-order equations, and the solution occurs in two stages when solving the Navier-Stokes equation by the discontinuous Galerkin method. At the first stage, the components of the temperature gradient and the viscous stress tensor are calculated. Their approximation, as well as the approximation of the solution, within the grid cell when implementing the modal approach is in the form of polynomials of degree p with time-dependent coefficients. At the boundary of the element, the flow values of the quantities are determined by some rule from the values inside the element and from the values in the cell adjacent to this element.

At the second stage, the components of the vector of conservative variables are determined. In this case, convective flows can be calculated using various variants of the exact or approximate solution of the Riemann problem. Diffusion flows at the element boundary can also be calculated in various ways, a detailed analysis of which was carried out in [63]. Quadrature formulas of the required order are used to calculate integrals. This two-step approach allows us to calculate gradients with the same order of accuracy as conservative variables, while maintaining the compactness of the scheme template.

2. Hybrid flow's building. In [60], a hybrid numerical flow was constructed, the main idea of which was proposed in [52]. This flow is a linear combination of one of the flows (HLLC or Godunov flow) and a stable Rusanov-Lax-Friedrichs flow (RLF).

The direction of the velocity jump determines the normal to the shock wave: when the cell boundary coincides with the shock wave front, the Godunov flow ($\boldsymbol{F}^{\text{Godunov}}$), is used, and when the interface is perpendicular to the shock wave, the Rusanov-Lax-Friedrichs flow ($\boldsymbol{F}^{\text{RLF}}$) is applied. Thus, dissipation increases in the direction coinciding with the shock wave, and instability is eliminated:

$$\hat{\boldsymbol{F}} = \theta \boldsymbol{F}^{HLLC} + (1-\theta)\boldsymbol{F}^{RLF}, \tag{5}$$

$$\hat{\boldsymbol{F}} = \theta \boldsymbol{F}^{\text{Godunov}} + (1-\theta)\boldsymbol{F}^{RLF}, \tag{6}$$

$$\text{where} \quad \theta = \begin{cases} \dfrac{|\Delta u \cdot n|}{|\Delta u|} = \dfrac{|\Delta u n_x + \Delta v n_y + \Delta w n_z|}{\sqrt{\Delta u^2 + \Delta v^2 + \Delta w^2}}, & |\Delta u| > \varepsilon, \\ 1, & |\Delta u| \le \varepsilon, \end{cases} \tag{7}$$

where ε is a small constant to avoid division by zero (for example $\varepsilon = 10^{-6}$); n is the normal to the cell boundary, and $\Delta u = (u_L - u_R, v_L - v_R, w_L - w_R)$ is the jump of the velocity vector across the boundary. The parameter θ is calculated from the normal to the cell boundary and the velocity jump through the cell boundary surface.

Another approach to the construction of a hybrid flow is to add a dissipative term in the areas where it is necessary.

To construct it, we will switch to a local coordinate system with an ort $(\boldsymbol{n}, \boldsymbol{\tau}_1, \boldsymbol{\tau}_2)$, where $\boldsymbol{n}$ is the vector of the external normal to the surface through which the flow is considered; $\boldsymbol{\tau}_1$, $\boldsymbol{\tau}_2$ any single orthogonal vectors lying on this surface. Vectors $\boldsymbol{U}$ and $\boldsymbol{F}$ in this coordinate system (indicated by the index *) will have the form:

$$\begin{gathered} \boldsymbol{U}^* = (\rho, \rho(\boldsymbol{u},\boldsymbol{n}), \rho(\boldsymbol{u},\boldsymbol{\tau}_1), \rho(\boldsymbol{u},\boldsymbol{\tau}_1), E)^T, \\ \boldsymbol{F}^*(\boldsymbol{U}) = (\rho(\boldsymbol{u},\boldsymbol{n}), \rho(\boldsymbol{u},\boldsymbol{n})u_n + p, \rho(\boldsymbol{u},\boldsymbol{n})u_{\tau_1}, \rho(\boldsymbol{u},\boldsymbol{n})u_{\tau_2}, (E+p)(\boldsymbol{u},\boldsymbol{n})). \end{gathered} \tag{8}$$

In order to obtain a new flow with greater dissipation than the Godunov flow (HLLC) and less dissipation than the RLF flow, we choose a certain velocity W in the original coordinate system and switch to an inertial frame of reference moving at this speed.

Let's denote the maximum velocity $W_{\max}$, the minimum velocity — $W_{\min}$ (taking into account the sign) of the waves generated during the decay of an arbitrary discontinuity in the case of using the Godunov flow (or using the HLLC flow). Note that if W is greater than $W_{\max}$, then the values of the gas-dynamic quantities will coincide with $U+$ and after recalculation to the original coordinate system, this flow will be equal, respectively, to use the Godunov flow and the HLLC flow:

$$\hat{\boldsymbol{F}} = \boldsymbol{F}^{*\text{Godunov}}(\boldsymbol{U}^{*+}) - W\boldsymbol{U}^{*+},$$

$$\hat{\boldsymbol{F}} = \boldsymbol{F}^{*\text{HLLC}}(\boldsymbol{U}^{*+}) - W\boldsymbol{U}^{*+}.$$

Accordingly, if $-W$ is less than $W_{\min}$, then the values of the gas-dynamic quantities will coincide with $U-$, and after recalculation to the original coordinate system, this flow will be equal to:

$$\hat{\boldsymbol{F}} = \boldsymbol{F}^{*\text{Godunov}}(\boldsymbol{U}^{*-}) + W\boldsymbol{U}^{*-},$$

$$\hat{\boldsymbol{F}} = \boldsymbol{F}^{*\text{HLLC}}\left(\boldsymbol{U}^{*-}\right) + W\boldsymbol{U}^{*-}.$$

Taking the half-sum of these streams, we get the RLF stream. If W=0, then, respectively, Godunov flows (or HLLC) are obtained.

Thus, if $0<W<W^*_{\max}$, where $W^*_{\max} = \max\left(|W_{\max}|, |W_{\min}|\right)$ get a new flow, the average between the Godunov flow (HLLC) and the RLF flow and having greater dissipation than the Godunov flow (HLLC) and less dissipation than the RLF flow. This type of flow was considered in [62].

The hybrid stream used can be obtained as follows. Consider an inertial coordinate system moving at a speed $W \cdot \boldsymbol{n}$ relative to the original system, and calculate the Godunov flux or HLLC, which we then recalculate in the original coordinate system (Fig. 1). The resulting value is denoted by $\boldsymbol{U}^{*+}$. We will carry out a similar procedure with speed $-W \cdot \boldsymbol{n}$ and denote the corresponding value $\boldsymbol{U}^{*-}$. Taking a half-sum of such flows, we come to the formulas:

$$\hat{\boldsymbol{F}} = \frac{\boldsymbol{F}^{*\text{Godunov}}(\boldsymbol{U}^{*+}) + \boldsymbol{F}^{*\text{Godunov}}(\boldsymbol{U}^{*-})}{2} - W\frac{\boldsymbol{U}^{*+} + \boldsymbol{U}^{*-}}{2}, \tag{9}$$

$$\hat{\boldsymbol{F}} = \frac{\boldsymbol{F}^{*HLLC}(\boldsymbol{U}^{*+}) + \boldsymbol{F}^{*HLLC}(\boldsymbol{U}^{*-})}{2} - W\frac{\boldsymbol{U}^{*+} + \boldsymbol{U}^{*-}}{2}, \tag{10}$$

$$W = \theta W^*, \quad W^* = \max\left(|u+c|, |u-c|\right), \tag{11}$$

$$\theta = \begin{cases} M \le M_{\min}, & W = W^*, \\ M_{\min} < M < M_{\max}, & W = \dfrac{M_{\max} - M}{M_{\max} - M_{\min}} W^*, \\ M \ge M_{\max}, & W = 0, \end{cases} \tag{12}$$

where W^* is the maximum of the modules of the eigenvalues of the matrix $\dfrac{\partial \boldsymbol{F}^*(\boldsymbol{U})}{\partial \boldsymbol{U}^*}$; θ is the parameter [52].

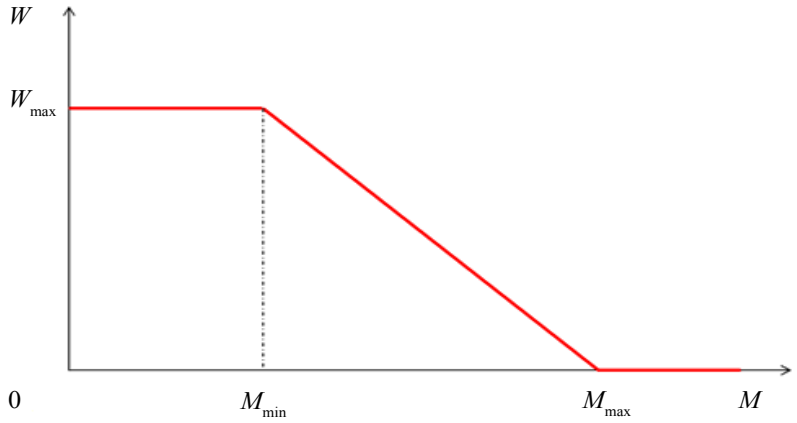

Fig. 1. The constructed hybrid flow, the average between the Godunov flow (HLLC) and the RLF flow

3. Numerical integration on arbitrary cells. Consider the transformation of an arbitrary quadrangular pyramid P with vertices (x_i, y_i, z_i) $i = 1.5$ in the coordinate system $0XYZ$ into a regular quadrangular pyramid P with vertices (0,0,0), (1,0,0), (0,1,0), (1,1,0), (0.5,0.5,1) in the coordinate system 0αβγ (Fig. 2). The base of the pyramid P will be translated into the base of the pyramid P^* using a bilinear transformation:

$$\begin{aligned} x &= a_0 + a_1\alpha + a_2\beta + a_3\alpha\beta, \\ y &= b_0 + b_1\alpha + b_2\beta + b_3\alpha\beta, \\ z &= c_0 + c_1\alpha + c_2\beta + c_3\alpha\beta, \end{aligned} \tag{13}$$

where the coefficients $a_i, b_i, c_i, i = \overline{0,3}$ are defined explicitly:

$$a_0 = x_1, a_1 = x_2 - x_1, a_2 = x_3 - x_1, a_3 = x_4 - x_3 - x_2 + x_1.$$

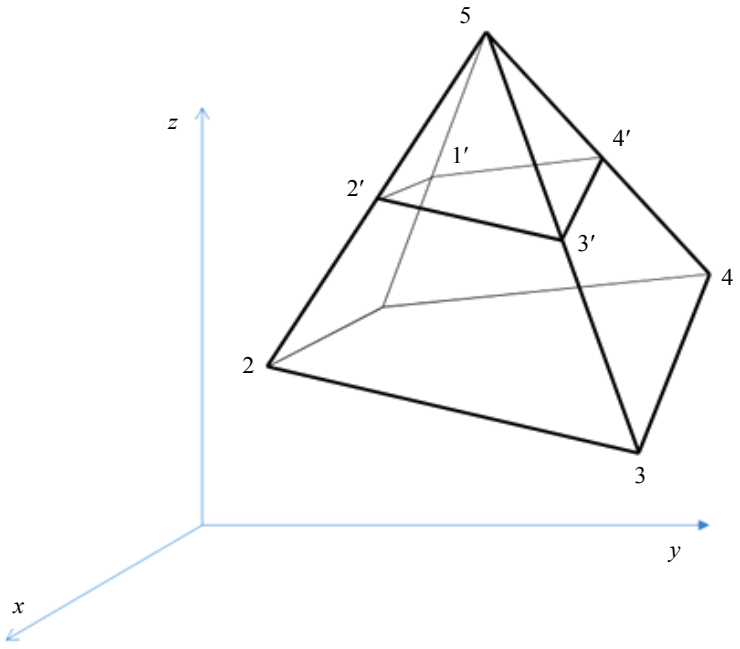

Fig. 2. An arbitrary quadrangular pyramid in space

Let's build an arbitrary pyramid P' with a vertex at point 5 (Fig. 3) and a base with vertices at points 1′–4′, by compressing the original pyramid.

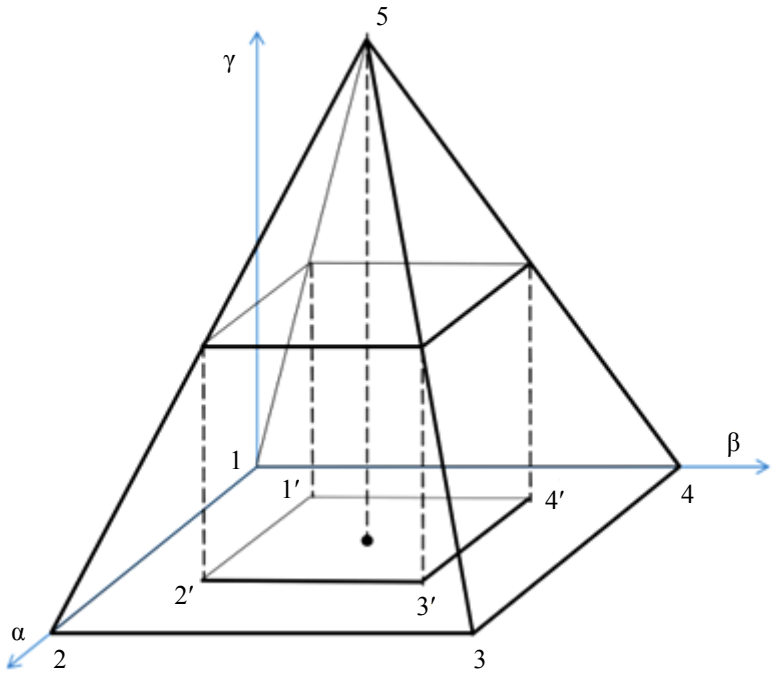

Fig. 3. A regular quadrangular pyramid

The coordinates x'_i can be defined as:

$$\begin{cases} x'_1 = x_1(1-\gamma)+x_5\gamma, \\ x'_2 = x_2(1-\gamma)+x_5\gamma, \\ x'_3 = x_3(1-\gamma)+x_5\gamma, \\ x'_4 = x_4(1-\gamma)+x_5\gamma, \end{cases} \tag{14}$$

where $\gamma\epsilon[0,1]$ is the compression ratio.

Let's make a similar transformation in the reference pyramid with the same compression ratio. The resulting base of the compressed pyramid will be transferred to the base of the reference pyramid. The coordinates of these points in the coordinate system 0αβ are equal to:

$$\begin{aligned} 1' &\to \alpha = \frac{\gamma}{2}, \beta = \frac{\gamma}{2}, \\ 2' &\to \alpha = 1-\frac{\gamma}{2}, \beta = \frac{\gamma}{2}, \\ 3' &\to \alpha = 1-\frac{\gamma}{2}, \beta = 1-\frac{\gamma}{2}, \\ 4' &\to \alpha = \frac{\gamma}{2}, \beta = 1-\frac{\gamma}{2}. \end{aligned} \tag{15}$$

Using the transformation (13)–(15), the coordinates of the points x'_i are:

$$\begin{cases} x'_1 = a_0 + a_1\frac{\gamma}{2} + a_2\frac{\gamma}{2} + a_3\frac{\gamma^2}{4} = x_1(1-\gamma)+x_5\gamma, \\ x'_2 = a_0 + a_1\left(1-\frac{\gamma}{2}\right) + a_2\frac{\gamma}{2} + a_3\left(1-\frac{\gamma}{2}\right)\frac{\gamma}{2} = x_2(1-\gamma)+x_5\gamma, \\ x'_3 = a_0 + a_1\left(1-\frac{\gamma}{2}\right) + a_2\left(1-\frac{\gamma}{2}\right) + a_3\left(1-\frac{\gamma}{2}\right)^2 = x_3(1-\gamma)+x_5\gamma, \\ x'_4 = a_0 + a_1\frac{\gamma}{2} + a_2\left(1-\frac{\gamma}{2}\right) + a_3\left(1-\frac{\gamma}{2}\right)\frac{\gamma}{2} = x_4(1-\gamma)+x_5\gamma. \end{cases} \tag{16}$$

Solving this system of equations (16), the conversion coefficients (13) are:

$$a_3 = \frac{x_4 - x_2 - x_3 + x_1}{1-\gamma},$$

$$a_1 = (x_2 - x_1) - \frac{\gamma}{2(1-\gamma)}(x_4 - x_2 - x_3 + x_1),$$

$$a_2 = (x_3 - x_1) - \frac{\gamma}{2(1-\gamma)}(x_4 - x_2 - x_3 + x_1),$$

$$a_0 = \frac{x_1 + x_2 + x_3 + x_4}{4}(1-\gamma) + \gamma x_5 - \frac{x_2 - 2x_1 + x_3}{2} + \frac{2\gamma - 1}{4(1-\gamma)}(x_4 - x_2 - x_3 + x_1).$$

As a result, get the transformation for the coordinate x:

$$x = \frac{x_1 + x_2 + x_3 + x_4}{4}(1-\gamma) + \gamma x_5 - \frac{x_2 - 2x_1 + x_3}{2} + \frac{2\gamma - 1}{4(1-\gamma)}(x_4 - x_2 - x_3 + x_1) +$$
$$+\left[(x_2 - x_1) - \frac{\gamma}{2(1-\gamma)}(x_4 - x_2 - x_3 + x_1)\right]\alpha +$$
$$+\left[(x_4 - x_1) - \frac{\gamma}{2(1-\gamma)}(x_4 - x_2 - x_3 + x_1)\right]\beta +$$
$$+\left[\frac{x_4 - x_2 - x_3 + x_1}{1-\gamma}\right]\alpha\beta.$$

Similarly, transformation for the y, z coordinates is obtained.

References

1. Reed WH, Hill TR. Triangular mesh methods for the neutron transport equation . Los Alamos Scientific Laboratory Report LA-UR-73-79. USA; 1973. https://www. osti.gov/servlets/purl/4491151

2. Volkov AV. Features of application of the Galerkin method to the solution of spatial Navier-Stokes equations on unstructured hexahedral grids. *Scientific Notes of TsAGI*. 2009;XL(6). (In Russ.).

3. Nastase R, Mavriplis DJ. High-order discontinuous Galerkin methods using an hp-multigrid approach. *Journal of Computational Physics*. 2006;213:330–357.

4. Bosnyakov SM, Mikhailov SV, Podaruyev VYu, et al. Unsteady discontinuous Galerkin method of high order accuracy for modeling turbulent flows. *Mathematical Modeling*. 2018;30(5):37–56. (In Russ.).

5. Krasnov MM, et al. Numerical solution of the Navier-Stokes equations by discontinuous Galerkin method. *Journal of Physics: Conference Series*. 2017;815(1).

6. Krasnov MM, Kuchugov PA, Ladonkina ME, et al. Discontinuous Galerkin method on three-dimensional tetrahedral grids. Using the operator programming method. *Mathematical Modeling*. 2017;29(2):3–22. (In Russ.).

7. Krasnov MM, Ladonkina ME. Discontinuous Galerkin method on three-dimensional tetrahedral grids. Application of template metaprogramming of the C++ language. *Programming*. 2017;3:41–53. (In Russ.).

8. Ladonkina ME, Neklyudova OA, Tishkin VF. Application of the RKDG method for gas dynamics problems. *Mathematical Models and Computer Simulations*. 2014;26(1):17–32. (In Russ.).

9. Volkov AV. Features of application of the Galerkin method to the solution of spatial Navier-Stokes equations on unstructured hexahedral grids. *Scientific Notes of TsAGI*. 2009; XL(6). (In Russ.).

10. Yasue K, Furudate M, Ohnishi N., et al. Implicit discontinuous Galerkin method for RANS simulation utilizing pointwise relaxation algorithm. *Communications in Computational Physics*. 2010;7(3):510–533.

11. Klockner A, Warburton T, Hesthaven JS. Nodal discontinuous Galerkin methods on graphics processors. *Journal of Computational Physics*. 2009;228(21):7863–7882.

12. Lou J, Xia Y, Luo L, et al. OpenACC-based GPU Acceleration of a p-multigrid Discontinuous Galerkin Method for Compressible Flows on 3D Unstructured Grids. *53rd AIAA Aerospace Sciences Meeting, AIAA SciTech Forum,* (AIAA 2015-0822).

13. Chan J, et al. GPU-accelerated discontinuous Galerkin methods on hybrid meshes. *Journal of Computational Physics*. 2015:318.

14. Krasnov MM. Operator library for solving three-dimensional grid problems of mathematical physics using graphics cards with CUDA architecture. *Mathematical Modeling*. 2015;27(3):109–120. (In Russ.).

15. Krasnov MM. Parallel algorithm for calculating hyperplane points of the computing front. *Journal of Computational Mathematics and Mathematical Physics*. 2015;55(1):145–152. (In Russ.).

16. Cockburn. An Introduction to the Discontinuous Galerkin Method for Convection - Dominated Problems, Advanced Numerical Approximation of Nonlinear Hyperbolic Equations. *Lecture Notes in Mathematics*. 1998;1697:151–268.

17. Krivodonova L. Limiters for high-order discontinuous Galerkin methods. *Journal of Computational Physics*. 2007; 226(1):276–296.

18. Shu C-W. High order WENO and DG methods for time-dependent convection-dominated PDEs: A brief survey of several recent developments. *Journal of Computational Physics*. 2016;316:598–613.

19. Luo H, Baum JD, Lohner RA. Hermite WENO-based limiter for discontinuous Galerkin method on unstructured grids. *Journal of Computational Physics*. 2007;225(1):686–713.

20. Zhu J, Zhong X, Shu C-W, et al. Runge-Kutta discontinuous Galerkin method using a new type of WENO limiters on unstructured meshes. *Journal of Computational Physics*. 2013;248:200–220.

21. Dumbser M. Arbitrary high order PNPM schemes on unstructured meshes for the compressible Navier–Stokes equations. *Computers &Fluids*. 2010;39(1):60–76.

22. Peraire J, Persson P-O. *Adaptive High-Order Methods in Computational Fluid Dynamics*. V.2 of Advances in CFD, chap.5 - High-Order Discontinuous Galerkin Methods for CFD. World Scientific Publishing Co; 2011.

23. Volkov AV, Lyapunov CV. Monotonization of the finite element method in problems of gas dynamics. *Scientific Notes of TsAGI*. 2009;XL(4):15–27. (In Russ.).

24. Ladonkina ME, Neklyudova OA, Tishkin VF. Construction of a limiter for the discontinuous Galerkin method based on averaging the solution. *Mathematical Modeling*. 2018;30(5):99–116. (In Russ.).

25. Haga T, Sawada K. *An improved slope limiter for high-order spectral volume methods solving the 3D compressible Euler equations*; 2009.

26. Bassi F, Rebay S. Numerical evaluation of two discontinuous Galerkin methods for the compressible Navier-Stokes equations. *International Journal for Numerical Methods in Fluids*. 2002;40:197–207.

27. Cockburn, Shu C-W. The local discontinuous Galerkin method for time dependent convection diffusion system. *SIAM Journal on Numerical Analysis.* 1998;35(6):2440–2463.

28. Vlasenko VV, Volkov AV, Troshin AI. The choice of the method of approximation of viscous terms in the Galerkin method with discontinuous basis functions. *Scientific Notes of TsAGI*. 2013;XLIV(3).

29. Gottlieb S, Shu C-W, Tadmor E. Strong stability-preserving high-order time discretization methods. *SIAM Review*. 2001;43(1):89–112.

30. Spiteri Raymond J, Ruuth Steven J. A New Class of Optimal High-Order Strong Stability-Preserving Time Discretization Methods. *SIAM Journal on Numerical Analysis*. 2002;40(2):469–491.

31. Rasetarinera P, Hussaini MY. An efficient implicit discontinuous spectral Galerkin method. *Journal of Computational Physics*. 2001;172:718–738.

32. Hartmann R. Adaptive discontinuous Galerkin methods with shock-capturing for the compressible Navier-Stokes equations. *International Journal for Numerical Methods in Fluids*. 2006;51:1131–1156.

33. Hartmann R, Houston P. Symmetric interior penalty DG methods for the compressible Na-vier-Stokes equations I: Method formulation. *International Journal of Numerical Analysis and Modeling*. 2006;3:1–20.

34. Dolejší V. Semi-implicit interior penalty discontinuous Galerkin methods for viscous compressible flows. *Computer Physics Communications*. 2008;4:231–274.

35. Yasue K, Furudate M, Ohnishi N, et al. Implicit discontinuous Galerkin method for RANS simulation utilizing pointwise relaxation algorithm. *Computer Physics Communications.* 2010;7(3):510–533.

36. Jameson A, Yoon S. Lower-upper implicit schemes with multiple grids for the Euler equations. *AIAA Journal.* 1987;25:929–935.

37. Proc. ECCOMAS Thematic Conference: European Conf. on High Order Nonlinear Numerical Methods for Evolutionary PDEs: *Theory and Applications HONOM*. 2017;27.03–31.03.

38. Peery KM, Imlay ST. Blunt body flow simulations. *AIAA Paper.* 1988;88–2924.

39. Rodionov AV. *Artificial viscosity for suppression of shock-wave instability in Godunov-type schemes of increased accuracy.* Russian Federal Nuclear Center VNIIEF. 2018;116:51 p. (In Russ.).

40. Quirk JJ. A contribution to the great Riemann solver debate. ICASE Report 1992;92–64. *International Journal for Numerical Methods in Fluids*. 1994;18:555–574.

41. Rodionov AV. *Development of methods and programs for numerical simulation of nonequilibrium supersonic flows in application to aerospace and astrophysical problems*. Dissertation for the degree of Doctor of Physical and Mathematical Sciences Sarov; 2019. (In Russ.).

42. Pandolfi M, D'Ambrosio D. NumericalI instabilities in Upwind Methods: Analysis and Cures for the "Carbuncle" Phenomenon. *Journal of Computational Physics*. 2001;166:271–301.

43. Dumbser M, Moschetta J-M, Gressier J. A matrix stability analysis of the carbuncle phenomenon. *Journal of Computational Physics*. 2004;197:647–670.

44. Roe P, Nishikawa H, Ismail F, et al. On carbuncles and other excrescences. *AIAA Paper*. 2005;2005–4872.

45. Menart JA, Henderson SJ. Study of the issues of computational aerothermodynamics using a Riemann solver. *AFRL Report.* 2008; 2008–3133.

46. Kitamura K, Shima E. Towards shock-stable and accurate hypersonic heating computations: A new pressure flux for AUSM-family schemes. *Journal of Computational Physics*. 2013;245:62–83.

47. Xie W, Li W, Li H, et al. On numerical instabilities of Godunov-type schemes for strong shocks. *Journal of Computational Physics*. 2017;350:607–637.

48. Gressier J, Moschetta J-M. Robustness versus accuracy in shock-wave computations. *International Journal for Numerical Methods in Fluids*. 2000;33:313–332.

49. Nishikawa H, Kitamura K. Very simple, carbuncle-free, boundary-layer-resolving, rotated-hybrid Riemann solvers. *Journal of Computational Physics*. 2008;227:2560–2581.

50. Guo S, Tao W-Q. *Numerical Heat Transfer*, Part B: Fundamentals. 2018; 73:33–47.

51. Hu LJ, Yuan L. A robust hybrid hllc-force scheme for curing numerical shock instability. *Applied Mechanics and Materials*. 2014;577:749–753.

52. Ferrero A, D'Ambrosio D. An Hybrid Numerical Flux for Supersonic Flows with Application to Rocket Nozzles. *17TH International Conference of Numerical Analysis and Applied Mathematics*. Rhodes, Greece; 2019, 23–28 September.

53. Krasnov MM, Ladonkina ME, Neklyudova OA, et al. On the influence of the choice of numerical flow on the solution of problems with shock waves by the discontinuous Galerkin method. *Preprints of IPM named after M.V.Keldysh*. 2022;91:21 p. (In Russ.). https://doi.org/10.20948/prepr-2022-91

54. Krasnov MM, Ladonkina ME, Tishkin VF. *RAMEG3D software package for numerical simulation of aerothermodynamics problems on high-performance computing systems*. Certificate of state registration of the computer program. No. RU2021615026, 02.04.2021. (In Russ.).

55. Rodionov AV. *Development of methods and programs for numerical simulation of nonequilibrium supersonic flows in application to aerospace and astrophysical problems*. Dissertation for the degree of Doctor of Physical and Mathematical Sciences Sarov; 2019. (In Russ.).

56. Godunov K.The difference method of the calculation of the explosive solutions of the equalization of hydrodynamics. *Mathematical Collection*. 1959;47(89):3:271–306. (In Russ.).

57. Toro EF. *Riemann solvers and numerical methods for fluid dynamics*. Springer, Third Edition. 2010.

58. Rusanov VV. Calculation of interactions with stationary shock waves. *Journal of Computational Mathematics and Mathematical Physics*. 1961;I(2):267–279. (In Russ.).

59. Lax PD. Weak solutions of nonlinear hyperbolic equations and their numerical computation. *Communications on Pure and Applied Mathematics*. 1954;7(1): 159–193.

60. Krasnov MM, Kuchugov PA, Ladonkina ME, et al. Discontinuous Galerkin method on three-dimensional tetrahedral grids. Using the operator programming method. *Mathematical Modeling*. 2017;29(2):3–22,529–543. (In Russ.).

61. Mysovskikh IP. *Interpolation cubature formulas*. Moscow: Nauka; 1981. (In Russ.).

62. Woodward P, Colella Ph. The numerical simulation of two-dimensional fluid flow with strong shocks. *Journal of Computational Physics*. 1984;54(1):115–173.

63. Arnold DN, Brezzi F, Cockburn B, et al. Unified analysis of discontinuous Galerkin methods for elliptic problems. *SIAM Journal on Numerical Analysis*. 2002;29:1749–1779.

About the Authors:

Vladimir F Tishkin, Corresponding Member of the Russian Academy of Sciences, Professor, Keldysh Institute of Applied Mathematics of the Russian Academy of Sciences (4, Miusskaya Sq., Moscow, 125047, RF), Doctor of Physical and Mathematical Sciences, ORCID, tishkin@imamod.ru, v.f.tishkin@mail.ru

Marina E Ladonkina, Senior Researcher, Keldysh Institute of Applied Mathematics of the Russian Academy of Sciences (4, Miusskaya Sq., Moscow, 125047, RF), Candidate of Physical and Mathematical Sciences, ORCID, ladonkina@imamod.ru

Received 05.04.2023.

Revised 24.05.2023.

Accepted 25.05.2023.

Conflict of interest statement

The authors do not have any conflict of interest.

All authors have read and approved the final manuscript.

Об авторах:

Тишкин Владимир Федорович, член-корреспондент РАН, профессор, Институт прикладной математики им. М. В. Келдыша Российской академии наук (125047, РФ, г. Москва, Миусская пл., 4), доктор физико-математических наук, ORCID, tishkin@imamod.ru, v.f.tishkin@mail.ru

Ладонкина Марина Евгеньевна, старший научный сотрудник, Институт прикладной математики им. М. В. Келдыша Российской академии наук (125047, РФ, г. Москва, Миусская пл., 4), кандидат физико-математических наук, ORCID, ladonkina@imamod.ru

Поступила в редакцию 05.04.2023.

Поступила после рецензирования 24.05.2023.

Принята к публикации 25.05.2023.

Конфликт интересов

Авторы заявляют об отсутствии конфликта интересов.

Все авторы прочитали и одобрили окончательный вариант рукописи.

COMPUTATIONAL MATHEMATICS
ВЫЧИСЛИТЕЛЬНАЯ МАТЕМАТИКА

UDC 519.688
https://doi.org/10.23947/2587-8999-2023-7-2-19-30

Original article

Numerical Realization of Shallow Water Bodies' Hydrodynamics Grid Equations using Tridiagonal Preconditioner in Areas of Complex Shape

Vladimir N Litvinov[1,2], Asya M Atayan[1], Natalya N Gracheva[1,2], Nelly B Rudenko[1,2], Natalya Yu Bogdanova[1]

[1]Don State Technical University, 1, Gagarina Sq., Rostov-on-Don, Russian Federation

[2]Azov-Black Sea Engineering Institute of Don State Agrarian University, 21, Lenina St., Zernograd, Russian Federation

LitvinovVN@rambler.ru

Abstract

Introduction. Mathematical modeling of hydrodynamic processes in shallow reservoirs of complex geometry in the presence of coastal engineering systems requires an integrated approach in the development of algorithms for constructing computational grids and methods for solving grid equations. The work is devoted to the description of algorithms that allow to reduce the time for solving SLAE by using an algorithm for processing overlapping geometry segments and organizing parallel pipeline calculations. The aim of the work is to compare the acceleration of parallel algorithms for the methods of Seidel, Jacobi, modified alternately triangular method and the method of solving grid equations with tridiagonal preconditioner depending on the number of computational nodes.

Materials and Methods. The numerical implementation of the modified alternating-triangular iterative method for solving grid equations (MATM) of high dimension is based on parallel algorithms based on a conveyor computing process. The decomposition of the computational domain for the organization of the pipeline calculation process has been performed. A graph model is introduced that allows to fix the connections between neighboring fragments of the computational grid. To describe the complex geometry of a reservoir, including coastal structures, an algorithm for overlapping geometry segments is proposed.

Results. It was found that the efficiency of implementing one step of the MATM on the GPU depends only on the number of threads along the O_z axis, and the step execution time is inversely proportional to the number of nodes of the computational grid along the O_z axis. Therefore, it is recommended to decompose the computational domain into parallelepipeds in such a way that the size along the O_z axis is maximum, and the size along the O_x axis is minimal. Thanks to the algorithm for combining geometry segments, it was possible to speed up the calculation by 14–27 %.

Discussion and Conclusions. An algorithm has been developed and numerically implemented for solving a system of large-dimensional grid equations arising during the discretization of the shallow water bodies' hydrodynamics problem by MATM, adapted for heterogeneous computing systems. The graph model of a parallel-pipeline computing process is proposed. The connection of water body's geometry segments allowed to reduce the number of computational operations and increase the speed of calculations. The efficiency of parallel algorithms for the methods of Seidel, Jacobi, modified alternately triangular method and the method of solving grid equations for problems of hydrodynamics in flat areas, depending on the number of computational nodes, is compared.

Keywords: mathematical modeling, computational domain geometry, parallel programming, graphics accelerator.

Funding information. The study was supported by the Russian Science Foundation no. 21-71-20050. https://rscf.ru/project/21-71-20050/

For citation. Litvinov VN, Atayan AM, Gracheva NN, et al. Numerical realization of shallow water bodies' hydrodynamics grid equations using tridiagonal preconditioner in areas of complex shape. *Computational Mathematics and Information Technologies*. 2023;7(2):19–30. https://doi.org/10.23947/2587-8999-2023-7-2-19-30

Научная статья

Численная реализация сеточных уравнений гидродинамики мелководных водоёмов с использованием трехдиагонального предобуславливателя в областях сложной формы

В.Н. Литвинов[1,2] ✉, **А.М. Атаян**[1], **Н.Н. Грачева**[1,2], **Н.Б. Руденко**[1,2], **Н.Ю. Богданова**[1]

[1]Донской государственный технический университет, Российская Федерация, г. Ростов-на-Дону, пл. Гагарина, 1

[2]Азово-Черноморский инженерный институт ФГБОУ ВО Донской ГАУ, Российская Федерация, г. Зерноград, ул. Ленина, 21

✉ LitvinovVN@rambler.ru

Аннотация

Введение. Математическое моделирование гидродинамических процессов в мелководных водоёмах сложной геометрии при наличии прибрежных инженерных систем требует комплексного подхода при разработке алгоритмов построения расчетных сеток и методов решения сеточных уравнений. Работа посвящена описанию алгоритмов, позволяющих уменьшить время решения СЛАУ за счёт использования алгоритма обработки наложения сегментов геометрии и организации параллельно-конвейерных вычислений. Целью работы является сравнение ускорения параллельных алгоритмов для методов Зейделя, Якоби, модифицированного попеременно-треугольного метода и метода решения сеточных уравнений с трехдиагональным предобуславливателем в зависимости от количества вычислительных узлов.

Материалы и методы. Численная реализация модифицированного попеременно-треугольного итерационного метода решения сеточных уравнений (МПТМ) высокой размерности основана на параллельных алгоритмах, построенных на основе конвейерного вычислительного процесса. Произведена декомпозиция расчётной области для организации процесса конвейерного вычисления. Введена графовая модель, позволяющая зафиксировать связи между соседними фрагментами расчетной сетки. Для описания сложной геометрии водоёма, включающей прибрежные сооружения, предложен алгоритм наложения сегментов геометрии.

Результаты исследования. В ходе исследований было установлено, что время расчета одного шага МПТМ на GPU зависит от количества потоков по оси O_z и обратно пропорционально количеству узлов расчетной сетки по данной оси. Поэтому рекомендуется декомпозировать расчетную область на параллелепипеды таким образом, чтобы их размер по оси O_x был наименьшим, а по O_z — наибольшим. Предложенный алгоритм объединения сегментов геометрии позволил уменьшить время вычислений на величину от 14 до 27 %.

Обсуждение и заключения. Разработан и численно реализован алгоритм решения системы сеточных уравнений большой размерности, возникающих при дискретизации задачи гидродинамики мелководного водоема методом МПТМ, адаптированный для гетерогенных вычислительных систем. Предложена графовая модель параллельно-конвейерного вычислительного процесса. Соединение сегментов геометрии водного объекта позволило сократить количество вычислительных операций и увеличить скорость расчетов. Проведено сравнение эффективности параллельных алгоритмов для методов Зейделя, Якоби, модифицированного попеременно-треугольного метода и метода решения сеточных уравнений для задач гидродинамики в плоских областях в зависимости от количества вычислительных узлов.

Ключевые слова: математическое моделирование, геометрия расчетной области, параллельное программирование, графический ускоритель.

Финансирование. Исследование выполнено за счет гранта Российского научного фонда № 21-71-20050. https://rscf.ru/project/21-71-20050/

Для цитирования. Литвинов В.Н., Атаян А.М., Грачева Н.Н. и др. Численная реализация сеточных уравнений гидродинамики мелководных водоёмов с использованием трехдиагонального предобуславливателя в областях сложной формы. *Computational Mathematics and Information Technologies*. 2023;7(2):19–30. https://doi.org/10.23947/2587-8999-2023-7-2-19-30

Introduction. Mathematical modeling is used to predict the state of shallow reservoirs in emergency situations caused by human activity or natural and climatic disasters. It is necessary to take into account such features of each specific water body as the geometry of the reservoir and its coastal zone, climatic conditions and hydrodynamic regimes. Such problems

actualize the improvement of methods for solving systems of grid equations of high dimension in the case of a non-self-adjoint operator. It is necessary to use multiprocessor computing systems and video adapters to increase the speed of obtaining a solution, due to the large amount of data and the complexity of calculations.

Modeling of many hydrophysical and hydrobiological problems reduces to the need to solve the diffusion-convection-reaction equation with a non-self-adjoint operator. The review of actual numerical methods of solution is carried out in the work of P. Vabishevich [1], where a number of theorems are formulated that allow determining the numerical parameters and the limits of applicability of the studied methods for solving grid equations. Iterative methods for solving such problems are actively developing. In the work of Geiser, Hueso, Martinez [2], various types of splitting methods are analyzed, modifications of SLIS and SQIS methods are proposed, on the basis of which effective adaptive algorithms are built that allow increasing the time step without reducing the accuracy of calculations.

There has been a significant increase in the number of studies aimed at developing algorithms that are efficient in computing speed and designed to solve systems of high-dimensional grid equations over the past few years. Russian and foreign scientists are developing parallel algorithms for heterogeneous computing environments, studying the performance of cluster computing systems for various methods of discretization of various differential equations. For example, Subbaian G. and Reddy Sathi [3, 4] analyzed the performance of several iterative methods for solving the Navier-Stokes equation with accelerated computing on a graphics processor (GPU) using CUDA technology. Scientists Lakshmiranganatha S., Muknahallipatna S., Paliwal M., Chilla R., Prasanth N., Goundar S. and Raja S.P. compared the performance of various parallel algorithms for finding solutions to time-dependent ordinary differential equations on CPU and GPU using three parallelization technologies: OpenMP, OpenACC and CUDA. It was found that CUDA technology is the most effective accelerator for solving these equations as a result of the study [5, 6]. Russian and Kazakh scientists have developed parallel algorithms for finding solutions to systems of linear algebraic equations. The algorithms were implemented on multicore processors using OpenMP technology [7, 8]. The efficiency of parallel algorithms for solving the one-dimensional thermal conductivity problem for three finite-difference approximation methods was tested on central and graphics processors in the programming languages C (CPU) and CUDA C (GPU). GPU computing acceleration increased up to 60 times [9, 10]. In [11], the construction of parallel algorithms based on the functional decomposition of the counter-run method for solving tridiagonal grid equations is considered. D. B. Volkov-Bogorodsky, G. B. Sushko and S. A. Kharchenko in their work [12] describe hybrid parallel algorithms for approximating solutions of the nonstationary thermal conductivity equation with phase transitions based on the analytical method blocks, namely MPI+threads technology.

It is necessary to develop a parallel version of the algorithm, which will reduce the time of solving SLAE by using an algorithm for processing the overlapping of geometry segments and parallelizing the calculation process, in this study,

Materials and Methods

1. Problem statement. Shallow water bodies' hydrodynamics mathematical model includes [13]:

– Navier-Stokes equations:

$$u_t' + uu_x' + vu_y' + wu_z' = -\frac{1}{\rho}P_x' + \left(\mu u_x'\right)_x' + \left(\mu u_y'\right)_y' + \left(\mu u_z'\right)_z' + 2\Omega\left(v\sin\vartheta - w\cos\vartheta\right), \quad (1)$$

$$v_t' + uv_x' + vv_y' + wv_z' = -\frac{1}{\rho}P_y' + \left(\mu v_x'\right)_x' + \left(\mu v_y'\right)_y' + \left(v v_z'\right)_z' + 2\Omega u\sin\vartheta, \quad (2)$$

$$w_t' + uw_x' + vw_y' + ww_z' = -\frac{1}{\rho}P_z' + \left(\mu w_x'\right)_x' + \left(\mu w_y'\right)_y' + \left(v w_z'\right)_z' + 2\Omega u\cos\vartheta + g; \quad (3)$$

– continuity equation in the case of variable density:

$$\rho_t' + \left(\rho u\right)_x' + \left(\rho v\right)_y' + \left(\rho w\right)_z' = 0, \quad (4)$$

where $V = \{u, v, w\}$ are the velocity vector components; P is the total hydrodynamic pressure; ρ is the aqueous medium density; μ, v are the horizontal and vertical turbulent exchange coefficient components; $\Omega = \Omega \cdot (\cos\vartheta \cdot j + \sin\vartheta \cdot k)$ is

the angular velocity of the Earth›s rotation; ϑ is the latitude of the place; g is the acceleration of gravity; f_T, f_s are the sources of heat and salt (located on the region border).

The initial hydrodynamics model (1–4) is divided into several subtasks [14, 15]. The first subtask is represented by the diffusion-convection-reaction equation, which is used to calculate the components of the velocity vector field on the intermediate layer in time:

$$\frac{\widetilde{u}-u}{\tau}+u\overline{u}_x'+v\overline{u}_y'+w\overline{u}_z'=\left(\mu\overline{u}_x'\right)_x'+\left(\mu\overline{u}_y'\right)_y'+\left(v\overline{u}_z'\right)_z'+2\Omega(v\sin\theta-w\cos\theta),$$

$$\frac{\widetilde{v}-v}{\tau}+u\overline{v}_x'+v\overline{v}_y'+w\overline{v}_z'=\left(\mu\overline{v}_x'\right)_x'+\left(\mu\overline{v}_y'\right)_y'+\left(v\overline{v}_z'\right)_z'-2\Omega u\sin\theta, \tag{5}$$

$$\frac{\widetilde{w}-w}{\tau}+u\overline{w}_x'+v\overline{w}_y'+w\overline{w}_z'=\left(\mu\overline{w}_x'\right)_x'+\left(\mu\overline{w}_y'\right)_y'+\left(v\overline{w}_z'\right)_z'+2\Omega u\cos\theta+g\left(\frac{\rho_0}{\rho}-1\right).$$

The Krank-Nicholson scheme was used to approximate the diffusion-convection-reaction equation (5) in time. Here, $\overline{u}=\sigma\widetilde{u}+(1-\sigma)u$, $\sigma\in[0,1]$ is the diagram weight.

2. Methods for solving grid equations. Modified alternately triangular iterative method. Let's introduce three-dimensional uniform computational grid [14]:

$$\overline{w}_h=\{t^n=n\tau, x_i=ih_x,\ y_j=jh_y,\ z_k=kh_z;\ n=\overline{0,n_t-1},\ i=\overline{0,n_1-1},$$

$$j=\overline{0,n_2-1},\ k=\overline{0,n_3-1};\ (n_t-1)\tau=T,(n_1-1)h_x=l_x,(n_2-1)h_y=l_y,(n_3-1)h_z=l_z\},$$

where τ is the time step; h_x, h_y, h_z is the size of the steps along the coordinate directions; n_t is the number of time layers; T is the upper bound by time coordinate; n_1, n_2, n_3 are the number of nodes by spatial coordinates; l_x, l_y, l_z are the spatial dimensions of the calculated area.

Let's get a system of grid equations when constructing a discrete model. Each equation of the system can be presented in canonical form, and we will use a seven-point template:

$$c(m_0)u(m_0)-\sum_{i=1}^{6}c(m_0,m_i)u(m_i)=F(m_0),$$

where $m_0(x_i,y_j,z_k)$ is the template center; $M'(P)=\{m_1(x_{i+1},y_j,z_k),\ m_2(x_{i-1},y_j,z_k),\ m_3(x_i,y_{j+1},z_k),\ m_4(x_i,y_{j-1},z_k),\ m_5(x_i,y_j,z_{k+1}),\ m_6(x_i,y_j,z_{k-1})\}$ is the neighborhood of the center; $c_0\equiv c(m_0)$ is the coefficient of the template center; $c_i\equiv c(m_0,m_i)$ are the coefficients of the neighborhood of the template center; F is the vector of the right parts; u is the calculated vector.

The MATM algorithm consists of four stages:

1) calculation of the residual vector r^m;

2) calculation of the correction vector w^m;

3) calculation of scalar products based on iterative parameters τ_{m+1}, ω_{m+1};

4) transition to a new iterative layer.

The condition for the end of the iterative process is that the norm of the residual vector r^m reaches the specified accuracy. At the same time, the most time-consuming part of the algorithm is the calculation w^m, which boils down to solving SLAE with lower-triangular and upper-triangular matrices.

3. Method for solving grid equations with tridiagonal preconditioner. If the steps along one of the spatial coordinates are significantly smaller than the steps along the others (for example, when solving problems of heat and mass transfer in shallow reservoirs), the dimensions of the calculated area in the vertical direction can be hundreds to thousands of times smaller than the horizontal dimensions. To solve problem (1) on the basis of difference schemes with relatively small labor costs for the transition between time layers, compared with the explicit scheme (1.5–2 times larger), with large time steps (about 30 times more), we will use splitting schemes into two-dimensional and one-dimensional problems [16–17]:

$$\frac{c^{n+1/2}-c^n}{\tau}+u\left(c^n\right)'_x+v\left(c^n\right)'_y=\left(\mu\left(c^n\right)'_x\right)'_x+\left(\mu\left(c^n\right)'_y\right)'_y, \tag{6}$$

$$\frac{c^{n+1}-c^{n+1/2}}{\tau}+w\left(c^{n+(\sigma+1)/2}\right)'_z=\left(v\left(c^{n+(\sigma+1)/2}\right)'_z\right)'_z+f^{n+(\sigma+1)/2}, \tag{7}$$

where $c^{n+(\sigma+1)/2}=\sigma c^{n+1}+(1-\sigma)c^{n+1/2}$; σ is the weight of the scheme [7].

The spatial grid is introduced for the numerical implementation of a discrete mathematical model of the problem [18]:

$$\overline{w}_h=\{t^n=n\tau, x_i=ih_x, y_j=jh_y; n=\overline{0,n_t-1}, i=\overline{0,n_1-1},$$

$$j=\overline{0,n_2-1};\ (n_t-1)\tau=T,(n_1-1)h_x=l_x,(n_2-1)h_y=l_y\}.$$

To approximate the homogeneous equation (2), splitting schemes in spatial coordinate directions will be used:

$$\begin{aligned}\frac{c^{n+1/4}-c^n}{\tau}+u\left(c^n\right)'_x&=\left(\mu\left(c^n\right)'_x\right)'_x,\\ \frac{c^{n+1/2}-c^{n+1/4}}{\tau}+v\left(c^{n+1/4}\right)'_y&=\left(\mu\left(c^{n+1/4}\right)'_y\right)'_y.\end{aligned} \tag{8}$$

To solve real problems of hydrophysics of shallow water bodies, three-layer difference schemes based on a linear combination of the Upwind Leapfrog and Standart Leapfrog difference schemes with weight coefficients 2/3 and 1/3, respectively, are used. To increase the accuracy of calculations, a scheme is used that takes into account the fullness of the calculation cells [19–21]:

– difference scheme for the equation describing the transfer along the direction O_x:

$$\frac{2q_{2,i,j}+q_{0,i,j}}{3}\frac{c_{i,j}^{n+1/4}-c_{i,j}^n}{\tau}+5u_{i-1/2,j}q_{2,i,j}\frac{c_{i,j}^n-c_{i-1,j}^n}{3h_x}+u_{i+1/2,j}\min\left(q_{1,i,j},q_{2,i,j}\right)\frac{c_{i+1,j}^n-c_{i,j}^n}{3h_x}+$$

$$+\frac{2\Delta_x c_{i-1,j}^n q_{2,i,j}+\Delta_x c_{i,j}^n q_{0,i,j}}{3}=2\mu_{i+1/2,j}q_{1,i,j}\frac{c_{i+1,j}^n-c_{i,j}^n}{h_x^2}-2\mu_{i-1/2,j}q_{2,i,j}\frac{c_{i,j}^n-c_{i-1,j}^n}{h_x^2}-$$

$$-\left|q_{1,i,j}-q_{2,i,j}\right|\mu_{i,j}\frac{\alpha_x c_{i,j}^n+\beta_x}{h_x},\ u_{i,j}\geq 0,$$

where $\Delta_x c_{i,j}^n=\dfrac{c_{i,j}^{n-3/4}-c_{i,j}^{n-1}}{\tau}$;

– difference scheme for equation (4) describing the transfer along the direction O_y:

$$\frac{2q_{4,i,j}+q_{0,i,j}}{3}\frac{c_{i,j}^{n+1/2}-c_{i,j}^{n+1/4}}{\tau}+5v_{i,j-1/2}q_{4,i,j}\frac{c_{i,j}^{n+1/4}-c_{i,j-1}^{n+1/4}}{3h_y}+v_{i,j+1/2}\min\left(q_{3,i,j},q_{4,i,j}\right)\frac{c_{i,j+1}^{n+1/4}-c_{i,j}^{n+1/4}}{3h_y}+$$

$$+\frac{2\Delta_y c_{i,j-1}^{n+1/4}q_{4,i,j}+\Delta_y c_{i,j}^{n+1/4}q_{0,i,j}}{3}=2\mu_{i,j+1/2}q_{3,i,\mathrm{j}}\frac{c_{i,j+1}^{n+1/4}-c_{i,j}^{n+1/4}}{h_y^2}-2\mu_{i,j-1/2}q_{4,i,j}\frac{c_{i,j}^{n+1/4}-c_{i,j-1}^{n+1/4}}{h_y^2}-$$

$$-\left|q_{3,i,j}-q_{4,i,j}\right|\mu_{i,j}\frac{\alpha_y c_{i,j}^{n+1/4}+\beta_y}{h_y},\ v_{i,j}\geq 0,$$

where $\Delta_y c_{i,j}^{n+1/4}=\dfrac{c_{i,j}^{n-1/2}-c_{i,j}^{n-3/4}}{\tau}$.

Where q_0, q_1, q_2, q_3, q_4 are the degrees of control areas occupancy.

To obtain difference schemes approximating the system of equations (4), with $u_{i,j}<0$ and $v_{i,j}<0$ from the approximations presented, it is necessary to direct the corresponding coordinate axes O_x and O_y in opposite directions. Equation (3) is solved by the run-through method.

The splitting scheme into two-dimensional and one-dimensional problems has an advantage for solving non-stationary problems. The two-dimensional problem is solved on the basis of explicit schemes, and the one-dimensional one is approximated by schemes with weights and solved by the run-through method in this case. Schemes with weights are used, when solving stationary problems. Using this approach allows to reduce the initial problem to solving grid equations by iterative methods [22].

4. Geometry Segment overlay algorithm. It is necessary to take into account the complex geometry of the reservoir formed by a combination of the bottom surface and coastal engineering structures when drawing up SLAE. Programmatically, an approach is proposed and implemented that allows modeling the geometry of the object under study as a set of geometric primitives. A feature of the approach is the support for superimposing primitives on each other. In the class library developed with the software implementation, all geometric primitives are inherited from the abstract Geometry2DPrimitive class (Fig. 1), which contains data such as the _dS0 offset coordinates, the _primitiveType primitive type, and a logical property characterizing the "cutout" (_isCavity).

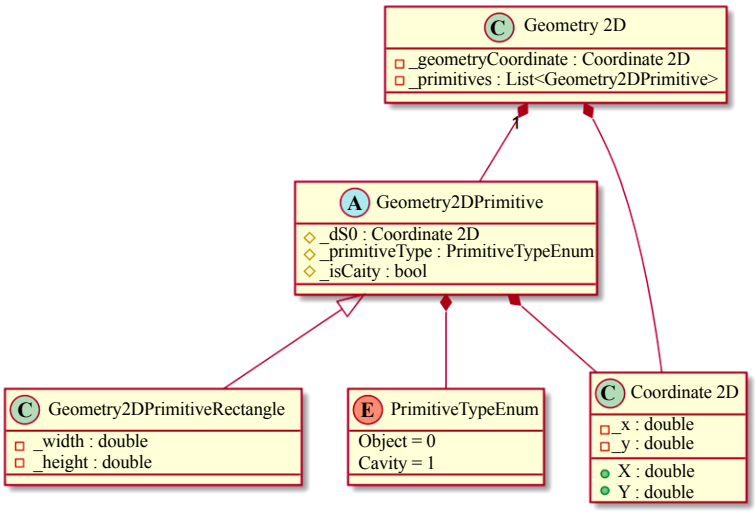

Fig. 1. Research object geometry. Class diagram

Object-oriented modeling of a geometry segment is performed using a typed class GeometryPrimitiveSegment<T>, in which type T is a class used to store data about the coordinates of the beginning and end of the segment.

Let's denote the coordinates of the beginning and end of the first and second segments c_{11}, c_{12} ,c_{21}, c_{22}.

Let's introduce logical variables: $A = c_{11} < c_{21}$, $B = c_{11} == c_{21}$, $C = c_{11} > c_{21}$, $D = c_{12} < c_{22}$, $E = c_{12} == c_{22}$, $F = c_{12} > c_{22}$, $G = c_{11} == c_{22}$, $H = c_{12} == c_{21}$, $I = c_{12} < c_{21}$, $J = c_{11} > c_{22}$. K, L are the types of the first and second segments; M, N are the fullness of the space under the first and second segments; V is the flag indicating that the second segment is a "cutout".

All possible combinations of overlapping geometry segments are summarized in Table 1.

The basis of the original linear algorithm is to take into account various combinations of geometric primitives. To increase productivity, a number of modifications based on conditional constructions have been introduced:

1. Initialization: c_{11}, c_{12} ,c_{21}, c_{22}.
2. Calculation: A, B, C, D, E, F, G, H, I, J, K, L, M, N, V.
3. Checking the correctness condition: $L \wedge \overline{N} \vee K \wedge \overline{M} \neq \text{true}$.
4. Definition of the overlay type.
5. Further actions are performed for the found overlay type. For example, option No. 1 is described (Table 1). For other types, the actions are the same.
6. If the first segment is not a boundary $(K = \text{true})$, then go to step 12.
7. If the second segment is not a boundary $(L = \text{true})$, then go to step 10.
8. Calculating expressions $\overline{M} \wedge \overline{N} \wedge \overline{V}$, $\overline{M} \wedge \overline{N} \wedge V$, $\overline{M} \wedge N \wedge \overline{V}$, $\overline{M} \wedge N \wedge V$, $M \wedge \overline{N} \wedge \overline{V}$, $M \wedge \overline{N} \wedge V$ $M \wedge N \wedge \overline{V}$, $M \wedge N \wedge V$ and creating the resulting segments.

9. Go to step 17.
10. Calculating $\overline{M} \wedge N \wedge V$, $M \wedge N \wedge \overline{V}$, $M \wedge N \wedge V$, $\overline{M} \wedge N \wedge \overline{V}$ and creating the resulting segments.
11. Go to step 17.
12. If the second segment is boundary $(L =$ false$)$, then transition to step 15, otherwise transition to step 17.
13. Checking the conditions $M \wedge N \wedge V$, $M \wedge \overline{N} \wedge V$, $M \wedge \overline{N} \wedge \overline{V}$, $M \wedge N \wedge \overline{V}$.
14. Creating and returning the resulting segments.
15. Go to step 17.
16. Calculation $M \wedge N \wedge V$, $M \wedge N \wedge \overline{V}$ and creation of the resulting segments.
17. The end.

Table 1

Options for overlapping geometry segments

Overlay option	Graphical interpretation	Logical expression
1		H
2		G
3		$B \wedge E$
4		$A \wedge F$
5		$C \wedge D$
6		$B \wedge F$
7		$B \wedge D$
8		$A \wedge E$
9		$C \wedge E$
10		$C \wedge F$
11		$A \wedge D \wedge \bar{I}$
12		I
13		J

5. Parallel implementation. The pipeline parallel algorithm has been developed that allows using all available computing resources for the numerical implementation of the MATM applicable to a high-dimensional SLAE. At the same time, each computer (CPU core or GPU computing unit) processes only the fragments of the computational domain assigned to it.

The connections between fragments and the organization of the parallel-pipeline computing process are described by a graph model, where nodes represent fragments of the computational domain. The computational process is organized according to the values of the counter of the calculation stages $s = k \cdot i + j$.

The developed graph model is used in the algorithm for solving SLAE with a lower-triangular matrix (Fig. 3). The input parameters of the algorithm are the coefficients of grid equations c_0, c_2, c_4, c_6 and the constant ω. The result is the velocity vector of the water flow *r*. When starting the software implementation of the algorithm in the CUDA C language, it is necessary to set the values of the dimensions of the CUDA computing blocks *blockDim.x, blockDim.z*. The parallel-pipelined computing process is organized as a cycle (line 6).

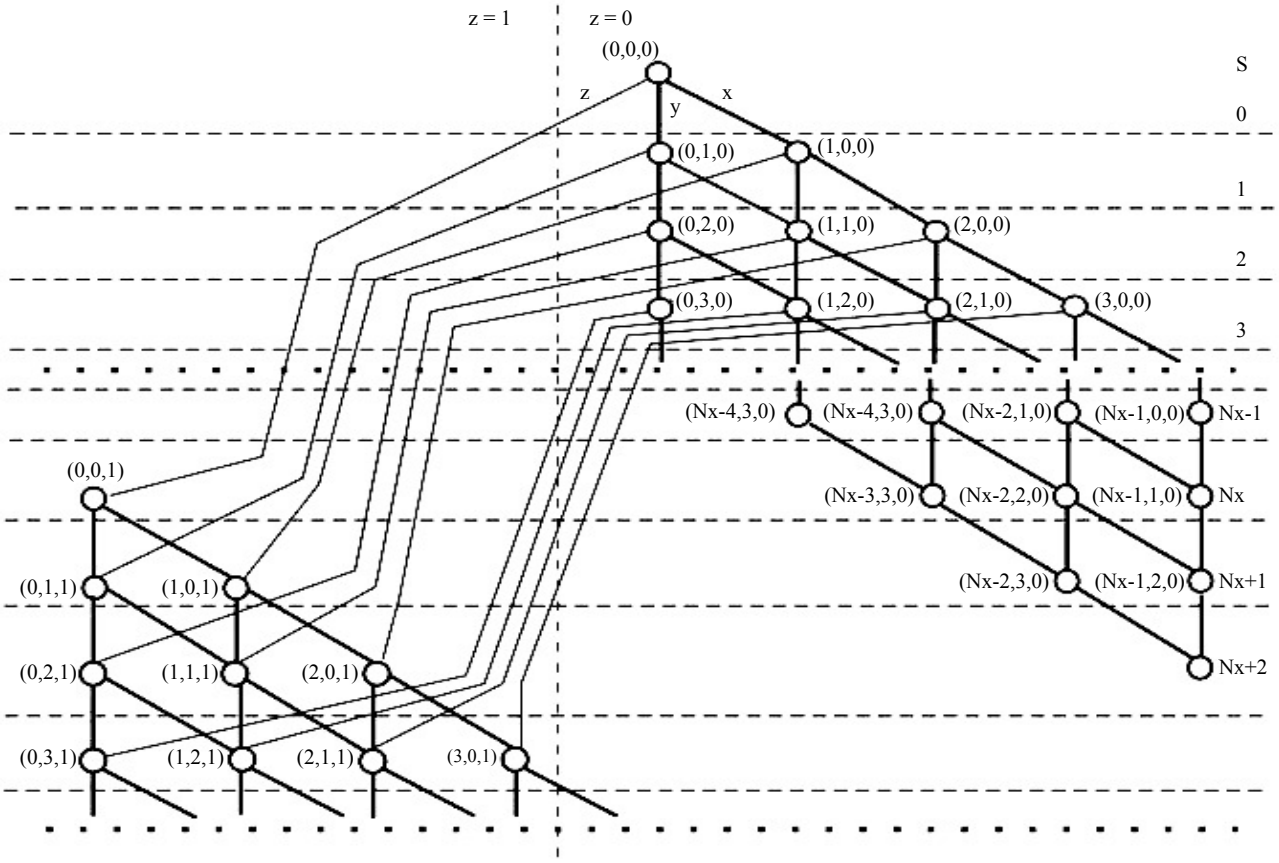

Fig. 2. Graph model of parallel-pipeline computing process

Algorithm 1 ptmKernel3(IN: $c_0, c_2, c_4, c_6, \omega$ IN/OUT: r;)

1: $threadX \leftarrow blockDim.x \cdot blockIdx.x + threadIdx.x$;
2: $threadZ \leftarrow blockDim.z \cdot blockIdx.z + threadIdx.z$;
3: $i \leftarrow threadX + 1$;
4: $j \leftarrow 1$;
5: $k \leftarrow threadZ + 1$;
6: **for** $s \in [3; n_1 + n_2 + n_3 - 3]$ **do**
7: **if** $(i + j + k = s) \wedge (s < i + n_2 + k)$ **then**
8: $m_0 \leftarrow i + (blockDim.x + 1) \cdot j + n_1 \cdot n_2 \cdot k$;
9: **if** $c0[m0] > 0$ **then**
10: $m_2 \leftarrow m_0 - 1$;
11: $m_4 \leftarrow m_0 - n_1$;
12: $m_6 \leftarrow m_0 - n_1 \cdot n_2$;
13: $rm4 \leftarrow 0$;
14: **if** $(s > 3 + threadX + threadZ)$ **then**
15: $rm4 \leftarrow cache[threadX][threadZ]$;
16: **else**
17: $rm4 \leftarrow r[m_4]$;
18: $rm2 \leftarrow 0$;
19: **if** $(threadX \neq 0) \wedge (s > 3 + threadX + threadZ)$ **then**
20: $rm2 \leftarrow cache[threadX - 1][threadZ]$;
21: **else**
22: $rm2 \leftarrow r[m_2]$;
23: $rm6 \leftarrow 0$;
24: **if** $(threadZ \neq 0) \wedge (s > 3 + threadX + threadZ)$ **then**
25: $rm6 \leftarrow cache[threadX][threadZ - 1]$;
26: **else**
27: $rm6 \leftarrow r[m_6]$;
28: $rm0 \leftarrow (\omega \cdot (c2[m_0] \cdot rm2 + c4[m_0] \cdot rm4 + c6[m_0] \cdot rm6) + r[m_0])/((0.5 \cdot \omega + 1) \cdot c_0[m_0])$;
29: $cache[threadX][threadZ] \leftarrow rm0$;
30: $r[m_0] \leftarrow rm0$;
31: $j \leftarrow j + 1$;

Fig. 3. Algorithm for solving a system of equations with a lower triangular matrix

Two-dimensional array *cache*, placed in shared GPU memory has been introduced to reduce the number of reads from global video memory. It stores the intermediate results of calculations on the current layer along the axis O_y, which speeds up the calculation process by 30 %.

The results of the study. Computational experiment comparing the performance of the basic and modified algorithms was conducted on a computer system with an Intel Core i5 3.3 GHz processor and 32 GB DDR4 RAM (Table 2). The modified algorithm recorded a decrease in the calculation time by up to 27 %.

Table 2

Results of comparing the performance of the basic and modified algorithms for combining geometry segments

Number of unions, $\times 10^6$	1	2	3	4	5	6	7	8	9	10
Basic algorithm, s	0.53	0.75	0.13	0.16	0.19	0.23	0.26	0.29	0.35	0.38
Modified algorithm, s	0.41	0.55	0.97	0.12	0.15	0.20	0.22	0.25	0.29	0.31

The numerical experiment was carried out to determine the number of GPU threads along the axes O_x and O_z the calculated grid (X, Z) with a fixed value of grid nodes along the axis O_y, equal to 10000, which allows to reduce the calculation time of one step of the MATM (T_{GPU}) on the GPU. The levels of variation of the factors X and Z and the results of the numerical experiment are shown in Table 3.

Table 4

Results of the experiment

№	X	Z	T_{GPU}, s
1.	16	64	0.064
2.	32	32	0.065
3.	64	16	0.081
4.	128	8	0.109
5.	256	4	0.100
6.	512	2	0.103

In the experiment, it was found that the calculation time of one MATM step on the GPU is inversely proportional to the number of nodes of the calculated grid along the axis O_z. The smallest value of the objective function is obtained at X and Z, equal to 16 and 64, respectively.

Table 5

Comparison of parallel algorithms' acceleration

P	Jacobi		Seidel		MATM		MSGE with a tridiagonal preconditioner	
	Speed-up ratio	Efficiency	Speed-up ratio	Efficiency	Speed-up ratio	Efficiency	Speed-up ratio	Efficiency
1	1.00	100.00	1.00	100.00	1.00	100.00	1.00	100.00
2	1.95	97.50	1.95	97.50	1.94	97.00	1.84	92.00
3	2.96	98.67	2.92	97.33	2.82	94.00	2.97	99.00
4	3.98	99.50	3.75	93.75	3.82	95.50	3.32	83.00
8	7.36	92.00	7.02	87.75	7.31	91.38	8.03	100.38
16	13.29	83.06	12.92	80.75	12.78	79.88	15.80	98.75
24	16.93	70.54	16.49	68.71	17.03	70.96	19.53	81.38

Table 4 presents a comparison of the speed-up ratio of parallel algorithms for the Seidel, Jacobi methods, the modified alternately triangular method and the method for solving grid equations with a tridiagonal preconditioner on the number of computational nodes. Calculations were made on a grid of one million calculation cells. The launches were carried out sequentially, starting from the launch on one computing node and ending with the connection of all available nodes.

Discussion and Conclusions. Algorithms for solving SLAE obtained by discretizing the problem of hydrodynamics of a shallow reservoir, MATM using NVIDIA CUDA technology are proposed. The proposed method of decomposition of the computational grid and the graph model make it possible to efficiently organize parallel pipeline calculations on computing systems of various configurations.

Numerical experiments have been carried out to determine the best two-dimensional configuration of threads in the computing unit, minimizing the time of one step of the MATM on the GPU, – $X = 16$ and $Z = 64$.

The maximum speed-up ratio was shown by the method of solving grid equations for hydrodynamic problems in flat areas, which is based on an explicit-implicit scheme. MATM, in comparison with the methods of Jacobi and Seidel, requires significantly fewer iterations for convergence. With a good optimization of the parallel MATM algorithm, the speed-up ratio differs by no more than 10 % by the number of computing nodes up to 24 compared to the acceleration of the parallel algorithm of the Jacobi method.

The developed software tools make it possible to more effectively use the computing resources of the GPU used to solve computationally time-consuming spatial-three-dimensional problems of hydrophysics.

Combining segments of the geometry of the object under study leads to a reduction in the number of computational operations, which allows to increase the performance of calculations.

References

1. Vabishchevich P. Iterative Methods for Solving Convection-diffusion Problem. *Computational Methods in Applied Mathematics*. 2002;2(4):410–444. https://www.doi.org/10.2478/cmam-2002-0023

2. Geiser J, Hueso J, Martinez E. Adaptive Iterative Splitting Methods for Convection-Diffusion-Reaction Equations. *Mathematics.* 2020;8:302. https://www.doi.org/10.3390/math8030302

3. Subbaian G, Reddy S. *Performance Analysis of Different Iterative Solvers Parallelized On GPU Architecture*. 2023;2:215–220. https://www.doi.org/10.1007/978-981-19-6970-6_39

4. Lakshmiranganatha S, Muknahallipatna S. Performance Analysis of Accelerator Architectures and Programming Models for Parareal Algorithm Solutions of Ordinary Differential Equations. *Journal of Computer and Communications.* 2021;9(2):29–56. https://www.doi.org/10.4236/jcc.2021.92003

5. Temirbekov A, Baigereyev D, Temirbekov N, et al. Amantayeva A. Parallel CUDA implementation of a numerical algorithm for solving the Navier-Stokes equations using the pressure uniqueness condition. AIP Conference Proceedings; 2021;2325:020063. https://www.doi.org/10.4236/jcc.2021.9200310.1063

6. Paliwal M, Chilla R, Prasanth N, et al. Parallel implementation of solving linear equations using OpenMP. *International Journal of Information Technology*. 2022;14:1677–1687. https://www.doi.org/10.1007/s41870-022-00899-9

7. Akimova EN, Sultanov MA, Misilov VE, et al. Parallel sweep algorithm for solving direct and inverse problems for time-fractional diffusion equation. *Numerical Methods and Programming (Vychislitel'nye Metody i Programmirovanie)*. 2022;23(4):275–287. (In Russ.). https://www.doi.org/10.26089/NumMet.v23r417

8. Sultanov M, Akimova E, Misilov V, et al. Parallel Direct and Iterative Methods for Solving the Time-Fractional Diffusion Equation on Multicore Processors. *Mathematics*. 2022;10(3):323. https://www.doi.org/10.3390/math10030323

9. Sechenov P, Rybenko I. Solving the problem of one-dimensional thermal conductivity on graphics processors using CUDA technology. *Applied Mathematics and Control Sciences*. 2021;4:23–41. https://www.doi.org/10.15593/2499-9873/2021.4.02

10. Khimich A, Polyanko V, Chistyakova T. Parallel Algorithms for Solving Linear Systems on Hybrid Computers. *Cybernetics and Computer Technologies*. 2020:53–66. https://www.doi.org/10.34229/2707-451X.20.2.6

11. Golovashkin DL. Parallel algorithms for solving tridiagonal grid equations based on the method of counter runs. *Mathematical modeling*. 2005;17(11):118–128. (In Russ.).

12. Volkov-Bogorodsky DB, Sushko GB, Kharchenko SA. Combined MPI+threads parallel implementation of the block method for modeling thermal processes in structurally inhomogeneous media. *Computational methods and programming*. 2010;11(1):127–136. (In Russ.).

13. Munk DJ, Kipouros T, Vio GA. Multi-physics bi-directional evolutionary topology optimization on GPU-architecture. *Engineering with Computers*. 2019;35(4):1059–1079. https://www.doi.org/10.1007/s00366-018-0651-1

14. Sukhinov AI, Chistyakov AE, Shishenya AV, et al. Predictive Modeling of Coastal Hydrophysical Processes in Multiple-Processor Systems Based on Explicit Schemes. *Mathematical Models and Computer Simulations*. 2018;10(5):648–658. https://www.doi.org/10.1134/S2070048218050125

15. Konovalov AN. The method of rapid descent with an adaptive alternately triangular preconditioner. Differential equations. 2004;40(7):953–963. (In Russ.).

16. Samarskiy AA, Vabishevich PN. *Numerical methods for solving convection-diffusion problems, Stereotype Publishing House*. Moscow: Book House «LIBROCOM»; 2015. 248 p. (In Russ.).

17. Oyarzun G, Borrell R, Gorobets A, et al. MPI-CUDA sparse matrix–vector multiplication for the conjugate gradient method with an approximate inverse preconditioner. *Computers and Fluids*. 2014;92:244–252. https://www.doi.org/10.1016/j.compfluid.2013.10.035

18. Khokhlov NI, Petrov IB. Application of the grid-characteristic method for solving the problems of the propagation of dynamic wave disturbances in high-performance computing systems. *Proceedings of ISP RAS*. 2019;31:237–252.

19. Sukhinov AI, Belova YuV, Chistyakov AE. Solution of the matter transport problem at high Peclet numbers. *Numerical methods and programming*. 2017;18(4):371–380.

20. Sukhinov AI, Chistyakov AE, Protsenko EA, et al. Accounting method of filling cells for the hydrodynamics problems solution with complex geometry of the computational domain. *Mathematical Models and Computer Simulations*. 2019;31(8):79–100. https://www.doi.org/10.1134/S0234087919080057

21. Sukhinov AI, Chistyakov AE, Protsenko EA. Upwind and Standard Leapfrog Difference Schemes. *Numerical methods and programming*. 2019;20(2):170–181. https://www.doi.org/0.26089/NumMet.v20r216; Sukhinov AI, Chistyakov AE, Kuznetsova IY, et al. Modelling of suspended particles motion in channel. *Journal of Physics: Conference Series*. 2020;1479(1). https://www.doi.org/10.1088/1742-6596/1479/1/012082

22. Sukhinov AI, Chistyakov AE. Adaptive analog-SSOR iterative method for solving grid equations with nonselfadjoint operators. *Mathematical Models and Computer Simulations*. 2012;4(4):398–409.

About the Authors:

Vladimir N Litvinov, Associate Professor of the Mathematics and Computer Science Department, Don State Technical University (1, Gagarin Sq., Rostov-on-Don, 344003, RF), PhD. (Tech.), ScopusID, ORCID, LitvinovVN@rambler.ru

Asya M Atayan, Assistant of the Computer Engineering and Automated Systems Software Department, Don State Technical University (1, Gagarin Sq., Rostov-on-Don, 344003, RF), ScopusID, ORCID, atayan24@mail.ru

Natalia N Gracheva, PhD. (Tech.), Associate Professor of the Mathematics and Bioinformatics Department, Azov-Black Sea Engineering Institute of the Donskoy GAU (21, Lenin St., Zernograd, 347740, RF), ScopusID, ORCID, grann72@mail.ru

Nelly B Rudenko, Associate Professor of the Mathematics and Bioinformatics Department, Azov-Black Sea Engineering Institute of the Donskoy GAU (21, Lenin St., Zernograd, 347740, RF), PhD. (Tech.), ScopusID, ORCID, nelli-rud@yandex.ru

Natalia Yu Bogdanova, Lecturer of the Mathematics and Computer Science Department, Don State Technical University (1, Gagarin Sq., Rostov-on-Don, 344003, RF), nat_bogdanova07@mail.ru

Claimed contributorship:

VN Litvinov: development of mathematical models and algorithms. AM Atayan: conducting numerical experiments. NN Gracheva: statistical processing of experimental data. NB Rudenko: software implementation, preparation of illustrations. NYu Bogdanova: conducting numerical experiments.

Received 04.04.2023.
Revised 16.05.2023.
Accepted 17.05.2023.

Conflict of interest statement

The authors do not have any conflict of interest.

All authors have read and approved the final manuscript.

Об авторах:

Литвинов Владимир Николаевич, доцент кафедры математики и информатики, Донской государственный технический университет (344003, РФ, г. Ростов-на-Дону, пл. Гагарина, 1), кандидат технических наук, ScopusID, ORCID, LitvinovVN@rambler.ru

Атаян Ася Михайловна, ассистент кафедры программного обеспечения вычислительной техники и автоматизированных систем, Донской государственный технический университет (344003, РФ, г. Ростов-на-Дону, пл. Гагарина, 1), ScopusID, ORCID, atayan24@mail.ru

Грачева Наталья Николаевна, доцент кафедры математики и биоинформатики, Азово-Черноморский инженерный институт ФГБОУ ВО Донской ГАУ (347740, РФ, г. Зерноград, ул. Ленина, 21), кандидат технических наук, ScopusID, ORCID, grann72@mail.ru

Руденко Нелли Борисовна, доцент кафедры математики и биоинформатики, Азово-Черноморский инженерный институт ФГБОУ ВО Донской ГАУ (347740, РФ, г. Зерноград, ул. Ленина, 21), кандидат технических наук, ScopusID, ORCID, nelli-rud@yandex.ru

Богданова Наталья Юрьевна, старший преподаватель кафедры математики и информатики, Донской государственный технический университет (344003, РФ, г. Ростов-на-Дону, пл. Гагарина, 1), nat_bogdanova07@mail.ru

Заявленный вклад соавторов:

Литвинов В.Н. — разработка математических моделей и алгоритмов. Атаян А.М. — проведение численных экспериментов. Грачева Н.Н. — статистическая обработка экспериментальных данных. Руденко Н.Б. — программная реализация, подготовка иллюстраций. Богданова Н.Ю. — проведение численных экспериментов.

Поступила в редакцию 04.04.2023.

Поступила после рецензирования 16.05.2023.

Принята к публикации 17.05.2023.

Конфликт интересов

Авторы заявляют об отсутствии конфликта интересов.

Все авторы прочитали и одобрили окончательный вариант рукописи.

COMPUTATIONAL MATHEMATICS
ВЫЧИСЛИТЕЛЬНАЯ МАТЕМАТИКА

UDC

Original article

https://doi.org/10.23947/2587-8999-2023-7-2-31-39

A Second-Order Difference Scheme for Solving a Class of Fractional Differential Equations

Aslanbek Kh Hibiev, Anatoly A Alikhanov✉, Mohammad Shahbaziasl, Ruslan A Chernobrovkin

North-Caucasus Center for Mathematical Research, North-Caucasus Federal University, 1, Pushkin St., Stavropol, Russian Federation

✉ aaalikhanov@gmail.com

Abstract

Introduction. Increasing accuracy in the approximation of fractional integrals, as is known, is one of the urgent tasks of computational mathematics. The purpose of this study is to create and apply a second-order difference analog to approximate the fractional Riemann-Liouville integral. Its application is investigated in solving some classes of fractional differential equations. The difference analog is designed to approximate the fractional integral with high accuracy.

Materials and Methods. The paper considers a second-order difference analogue for approximating the fractional Riemann-Liouville integral, as well as a class of fractional differential equations, which contains a fractional Caputo derivative in time of the order belonging to the interval (1, 2).

Results. To solve the above equations, the original fractional differential equations have been transformed into a new model that includes the Riemann-Liouville fractional integral. This transformation makes it possible to solve problems efficiently using appropriate numerical methods. Then the proposed difference analogue of the second order approximation is applied to solve the transformed model problem.

Discussion and Conclusions. The stability of the proposed difference scheme is proved. An a priori estimate is obtained for the problem under consideration, which establishes the uniqueness and continuous dependence of the solution on the input data. To evaluate the accuracy of the scheme and verify the experimental order of convergence, calculations for the test problem were carried out.

Keywords: Fractional differential equation, Caputo derivative, Riemann-Liouville integral, Difference scheme.

Founded information. The study was supported by the Russian Science Foundation grant no. 22-21-00363. https://rscf.ru/project/22-21-00363/

For citation. Hibiev AKh, Alikhanov AA, Shahbaziasl M, et al. A second-order difference scheme for solving a class of fractional differential equations. *Computational Mathematics and Information Technologies*. 2023;7(2):31–39. https://doi.org/10.23947/2587-8999-2023-7-2-31-39

Научная статья

Разностная схема второго порядка для решения класса дифференциальных уравнений дробного порядка

А.Х. Хибиев, А.А. Алиханов✉, М. Шахбазиасль, Р.А. Чернобровкин

Северо-Кавказский центр математических исследований, Северо-Кавказский федеральный университет, Российская Федерация, г. Ставрополь, ул. Пушкина, 1

✉ aaalikhanov@gmail.com

Аннотация

Введение. Повышение точности при аппроксимация дробных интегралов, как известно, является одной из актуальных задач вычислительной математики. Цель настоящего исследования — создание и применение разност-

ного аналога второго порядка для аппроксимации дробного интеграла Римана-Лиувилля. Его применение исследуется при решении некоторых классов дифференциальных уравнений дробного порядка. Разностный аналог предназначен для аппроксимации дробного интеграла с высокой точностью.

Материалы и методы. В работе рассматривается разностный аналог второго порядка для аппроксимации дробного интеграла Римана-Лиувилля, а также класс дифференциальных уравнений дробного порядка, который содержит дробную производную Капуто по времени порядка, принадлежащего интервалу (1, 2).

Результаты исследования. Для решения вышеупомянутых уравнений преобразованы исходные дифференциальные уравнения дробного порядка в новую модель, которая включает дробный интеграл Римана-Лиувилля. Это преобразование позволяет эффективно решать задачи с использованием соответствующих численных методов. Затем предложенный разностный аналог второго порядка аппроксимации применяется для решения преобразованной модельной задачи.

Обсуждение и заключения. Доказана устойчивость предложенной разностной схемы. Получена априорная оценка для рассматриваемой задачи, которая устанавливает единственность и непрерывную зависимость решения от входных данных. Для оценки точности схемы и проверки экспериментального порядка сходимости проведены расчеты для тестовой задачи.

Ключевые слова: дифференциальное уравнение дробного порядка, производная Капуто, интеграл Римана-Лиувилля, разностная схема.

Финансирование. Исследование выполнено за счет гранта Российского научного фонда № 22-21-00363. https://rscf.ru/project/22-21-00363/

Для цитирования. Хибиев А.Х., Алиханов А.А., Шахбазиасль М. и др. Разностная схема второго порядка для решения класса дифференциальных уравнений дробного порядка. *Computational Mathematics and Information Technologies*. 2023;7(2):31–39. https://doi.org/10.23947/2587-8999-2023-7-2-31-39

Introduction. Fractional calculus (FC) is a branch of mathematics that investigates and applies derivatives and integrals of real and complex order. While the concept originated centuries ago, it gained significant interest in the late 1960s among engineers who realized its potential for accurately modeling real-world systems compared to conventional integer order calculus [1]. The delay in its adoption can be attributed to various factors such as the lack of a clear interpretation for fractional derivatives, the perceived adequacy of integer calculus, and the inherent complexity of FC [2]. Nowadays, FC has become a well-established field, finding extensive applications across various fields, including science, engineering, and mathematics. The extensive literature highlights the broad usage of FC in numerous subject areas such as control systems, acoustics, medical and biological sciences, optics, waves, finance, economics, signal processing, and more [3, 4].

Mathematical models based on differential equations with integer order derivatives have proven useful in studying the dynamics of real-world systems. However, these models have limitations in capturing long-range temporal memory or long-range spatial interactions that are inherent in many real-world phenomena. This restriction arises due to the omission of these features in integer order derivatives [5]. In contrast, FDEs offer a significant advantage as they exhibit nonlocal behavior. This implies that fractional calculus serves as a powerful tool for capturing the memory and evolutionary properties exhibited by a wide range of physical phenomena and complex systems [6, 7]. Consequently, mathematical models based on FDE are more realistic and practical compared to classical integer-order models [8].

The need to accurately model and understand various phenomena and processes, coupled with the effectiveness of FDE models in capturing long-range memory and non-local interactions, has propelled the quest for efficient numerical or analytical solution techniques. Researchers strive to develop innovative methods that can handle the complexities and challenges associated with FDEs, enabling a deeper comprehension of the systems under investigation. However, obtaining analytical solutions for FDEs is generally challenging and exact solutions often involve infinite series representations such as the Mittag-Leffler function, the Fox H-function, or the hyperbolic geometry function, which can pose computational difficulties during evaluation [9]. Consequently, there is a growing interest in the development of computationally efficient numerical algorithms for solving FDEs. These methods include a variety of high-performance computing techniques such as finite difference methods:

– predictor-corrector methods;
– finite element methods, spectral methods;
– boundary particle methods;
– implicit meshless methods;
– Galerkin methods, finite volume methods;
– local radial basis function methods (see [10] and the citations provided within).

In the past few years, there has been a significant focus on the development of numerical methods for solving one-dimensional time FDEs. Numerous studies have been published in order to investigate and advance these numerical approaches [11, 12, 13]. Yand et al. [14] applied the Lubich's fractional multistep method for numerical solution of fractional diffusion-wave equation by transforming the original model into a equivalent integro-differential equation. They demonstrated that their method achieves a temporal order of accuracy of α for $1 \le \alpha \le 1.71832$. In [15], the authors presented a method of order 3-α for $0 < \alpha < 1$ to approximate the Caputo derivative. They then proposed a discrete difference scheme by introducing two new variables to transform the original equation into a lower-order system of equations. Two alternating direction implicit schemes for solving two-dimensional time fractional nonlinear super-diffusion equations is introduced in [16]. These schemes are based on the equivalent partial integro-differential equations of the original problem. The Riemann-Liouville fractional integral is discretized using the classical first-order approximation. The authors prove that both schemes exhibit first-order accuracy in time, ensuring convergence of the numerical solutions. Khibiev et al. [13] developed a second-order difference analog to approximate the generalized Caputo derivative. They successfully applied this difference analog for numerically solving the generalized time-fractional diffusion equation, specifically focusing on cases with smooth solutions.

Based on the insights gained from the discussion and the comprehensive review of relevant literature in this Section, our objective is to develop a second-order difference analog for approximating the Riemann-Liouville fractional integral and then apply this difference analog to solving a class of FDEs. The paper is organized as follows. In Section 2, we introduce the class of FDEs that contain a fractional Caputo derivative of order $\alpha + 1$, where $0 < \alpha < 1$. We transform the FDE model into a form that includes the Riemann-Liouville fractional integral, and present an a priori estimate for the solution of the differential model in subsection 2.1. In Section 3, we propose a difference analog for approximating the Riemann-Liouville fractional integral. We also estimate the truncation error of the method and apply it to solve the new FDE model. Additionally, we investigate the stability of the numerical method in the subsection 3.1. In Section 4, we perform numerical simulations to validate the accuracy and efficiency of the proposed method for solving the considered FDE. We also investigate the method's experimental order of convergence. Finally, in Section 5, we provide a brief conclusion summarizing the key findings and contributions of our study.

Materials and Methods. In this section, we present a specific class of initial-value FDEs and propose a methodology to effectively solve these models. In this study, a new effective and precise numerical scheme is being sought to approximate the solutions of the following initial-value FDEs:

$$\partial_{0t}^{\alpha+1} y(t) + \varkappa y(t) = g(t), \tag{1}$$

$$y(0) = y_0, \; y_t(0) = y_{1,}, \tag{2}$$

In which $\varkappa$ is a positive constant, $0 < \alpha < 1$ and $0 < t \le T$.

There exist multiple definitions for derivatives and integral operators in the context of fractional calculus. Some widely used definitions include the Caputo derivative and the Riemann-Liouville derivative. These definitions differ in the way they capture the fractional order behavior of a function. In the Caputo derivative, the fractional derivative is defined by considering the fractional order differentiation of the function while preserving the initial conditions. This makes it particularly suitable for modeling real-life processes where the initial conditions are crucial in determining the behavior of the system [17, 1]. For this reason, in our study, we adopt the fractional derivative in equation (1) in the Caputo sense. This choice is motivated by the compatibility of the Caputo derivative with real-life applications and its ability to accurately capture the initial conditions of the system. The Caputo derivative is defined as follows:

$$\partial_{0t}^{\alpha+1} y(t) = \frac{1}{\Gamma(1-\alpha)} \int_0^t (t-\eta)^{-\alpha} y''(\eta) d\eta, \; 0 < \alpha < 1,$$

where α represents the fractional order, and Γ(·) denotes the gamma function. By utilizing the Caputo derivative, we are able to effectively capture the fractional order behavior of the system and account for the influence of past history on the current state. This definition allows us to model various real-life phenomena where the initial conditions play a crucial role in determining the system's dynamics [18, 2].

Applying the Riemann-Liouville fractional integration operator of order α, denoted by $D_{0t}^{-\alpha} y(t)$ to the both sides of the model (1), we reach:

$$\frac{dy}{dt} + \varkappa D_{0t}^{-\alpha} y = f(t),\ 0 < t \le T, \tag{3}$$

where $f(t) = D_{0t}^{-\alpha} g(t) + y_1$ and the Riemann-Liouville fractional integration operator is defined as:

$$D_{0t}^{-\alpha} y(t) = \frac{1}{\Gamma(\alpha)} \int_0^t (t-\xi)^{\alpha-1} y(\xi) d\xi. \tag{4}$$

The model (3) is subject to the initial condition $y(0)=y_0$. In Eq. (3), as t approaches 0, we have $y_t(0)=f(0)=y_1$. Therefore, the second initial condition in Eq. (2) can be derived.

A priori estimate for the solution of the differential problem. The following theorem presents an a priori estimate for the solution of the differential problem (3), which provides valuable insights into the behavior and properties of the solution, allowing for a better understanding and analysis of the model. Before presenting the main theorem, it is essential to introduce the following corollary, which is derived from the results presented in [19].

Corollary 1. For any function $y(t)$ absolutely continuous on $[0,T]$ the following inequality takes place:

$$\int_0^t y(s) D_{0s}^{-\alpha} y(s) ds \ge 0,\ 0 < \alpha < 1.$$

Theorem 1. The solution $y(t)$ of the problem (3) satisfies the following a priori estimate:

$$y^2(t) \le C_1 \left(y_0^2 + \int_0^t f^2(s) ds \right),\ C_1 = \max\{2, 4T\}.$$

Proof. Multiplying Eq. (3) by $y(t)$, then changing the variable t to s and integrating over the time variable s from 0 to t, we get:

$$\int_0^t y(s) y'(s) ds + \varkappa \int_0^t y(s) D_{0s}^{-\alpha} y(s) ds = \int_0^t y(s) f(s) ds. \tag{5}$$

From corollary 1 and the fact that $\varkappa > 0$, the second term of left-hand side of (5) is non-negative and can be omitted. In this way we have:

$$\frac{1}{2}(y^2(t) - y_0^2) \le \int_0^t \left(\varepsilon y^2(s) + \frac{1}{4\varepsilon} f^2(s) \right) ds,$$

$$y^2(t) \le 2\varepsilon \int_0^t y^2(s) ds + y_0^2 + \frac{1}{2\varepsilon} \int_0^t f^2(s) ds. \tag{6}$$

To complete the proof, we need to estimate the integral $\int_0^t y^2(s) ds$. For this purpose, we integrate (6) with respect to the variable t form 0 to t. Set $\varepsilon = \frac{1}{(4T)}$, taking into account the following inequality:

$$\int_0^t d\xi \int_0^\xi y^2(s) ds = \int_0^t (t-s) y^2(s) ds \le T \int_0^t y^2(s) ds,$$

we can reach the following conclusion:

$$\int_0^t y^2(s) ds \le 2T y_0^2 + 4T^2 \int_0^t f^2(s) ds. \tag{7}$$

Now, by substituting equation (7) into equation (6) and setting $\varepsilon = \frac{1}{(4T)}$, one can complete the proof.

Derivation of the difference scheme for approximation FDE. The objective of this subsection is to introduce a difference analog that effectively approximates the Riemann-Liouville fractional integral. Subsequently, we employ this difference analog to devise a robust and accurate second-order difference scheme specifically developed for approximating the model (3).

To construct a difference method to approximate the Riemann-Liouville fractional integral (4), for an integer number N and a given time T, we discretize the interval $[0,T]$ into equally spaced $t_j=j\tau$, $j=0,1,\ldots,N$, where $\tau = \frac{T}{N}$ is the temporal step length. For notational brevity, we denote the numerical solution of $y(t_j)$ at the point t_j by y^j. To approximate the Riemann-Liouville fractional integral at $t=t_{j+1}$, where $j=1,2,\ldots,N$, we employ a generalized trapezoidal formula. This formula is utilized in the following manner:

$$D^{-\alpha}_{0t_{j+1}} y(t) = \frac{1}{\Gamma(\alpha)} \int_0^{t_{j+1}} (t_{j+1}-\xi)^{\alpha-1} y(\xi) d\xi = \frac{1}{\Gamma(\alpha)} \sum_{s=0}^{j} \int_{t_s}^{t_{s+1}} (t_{j+1}-\xi)^{\alpha-1} y(\xi) d \approx$$

$$\approx \frac{1}{\Gamma(\alpha)} \sum_{s=0}^{j} \int_{t_s}^{t_{s+1}} (t_{j+1}-\xi)^{\alpha-1} \left(y(t_{s+1}) \frac{\xi - t_s}{\tau} + y(t_s) \frac{t_{s+1}-\xi}{\tau} \right) = \tag{8}$$

$$= \frac{\tau^{\alpha}}{\Gamma(\alpha+2)} \left(\sum_{s=0}^{j} c^{(\alpha)}_{j-s} y^{s+1} + c^{-(\alpha)}_{j+1} y^0 \right) = \Delta^{-v}_{0t_{j+1}} y,$$

in which $c_0^{(\alpha)}=1$ and

$$c_s^{(\alpha)} = (s+1)^{\alpha+1} - 2s^{\alpha+1} + (s-1)^{\alpha+1},$$
$$c_s^{-(\alpha)} = (\alpha+1)(s+1)^{\alpha} - ((s+1)^{\alpha+1} - s^{\alpha+1}).$$

The truncation error of the operator $\Delta^{-v}_{0t_{j+1}}$ in (8) is characterized by the following lemma.

Lemma 1. Suppose $y(t)\in c^2[0,t_{j+1}]$. For any $\nu\in(0,1)$, $\Delta^{-v}_{0t_{j+1}}$ is defined in (8). Then we have:

$$\left| D^{-v}_{0t_{j+1}} y(t) - \Delta^{-v}_{0t_{j+1}} y \right| = O(\tau^2).$$

Proof. By using the Lagrange interpolation remainder formula, it follows that:

$$\left| D^{-v}_{0t_{j+1}} y(t) - \Delta^{-v}_{0t_{j+1}} y \right| \le \sum_{s=0}^{j} \int_{t_s}^{t_{s+1}} (t_{j+1}-\xi)^{v-1} \left| \frac{C^2}{2} (t_{s+1}-\xi)(\xi - t_s) \right| d\xi \le$$

$$\le \frac{C_2}{8} \tau^2 \sum_{s=0}^{j} \int_{t_s}^{t_{s+1}} (t_{j+1}-\xi)^{v-1} d\xi = \frac{C_2}{8} \tau^2 \int_0^{t_{j+1}} (t_{j+1}-\xi)^{v-1} d\xi \le \frac{C_2 T^v}{8} \tau^2 = O(\tau^2),$$

here $C_2 = \max_{0\le t\le T} \left| y''(t) \right|$.

The validity of this approximation can be readily confirmed through the application of Taylor's Theorem.

In the uniform domain $\Omega=\{t_j; j=0,1,\ldots,N\}$, we consider the fractional differential model (3) at the point t_{j+1}, with $j=1,2,\ldots,N-1$. Applying the proposed difference scheme (8) as well as the approximation (9) to the model (3), we propose the following difference scheme:

$$\frac{3y^{j+1} - 4y^j + y^{j-1}}{2\tau} + \varkappa \Delta^{-\alpha}_{0t_{j+1}} y = f(t_{j+1}), \tag{10}$$

$$y^0 = y_0. \tag{11}$$

At the initial time step t_1, we estimate the value of y^1 by employing Taylor's theorem as follows:

$$y^1 = y_0 + \tau y_1 + O(\tau^2). \tag{12}$$

Taking into account Lemma 1 and equation (9) and (12), one can conclude that if the solution of the differential model (3) satisfies the smoothness condition $y(t)\in C_t^2(\Omega)$, then the difference scheme (10)–(11) demonstrates an order of accuracy of $O(\tau^2)$.

Theoretical analysis of the proposed difference scheme. Consider the error $z^j=Y^j-y^j$, with $Y^j=y(t_j)$. Substituting $y^j=z^j+Y$ into the model (3), we obtain the problem for the error as follows:

$$\frac{3z^{j+1}-4z^j+z^{j-1}}{2\tau}+\varkappa\Delta^{-\alpha}_{0t_{j+1}}z=R_i^{j+1}, \tag{13}$$

$$z^0=u_0,\ z^1=\mu,$$

where

$$R_i^{j+1}=-\frac{3Y^{j+1}-4Y^j+Y^{j-1}}{2\tau}-\varkappa\Delta^{-\alpha}_{0t_{j+1}}Y+f(t_{j+1})=O(\tau^2),$$

$$\mu=-y^1+y_0+\tau y_1=O(\tau^2).$$

Before presenting the main theorem for the stability of the proposed difference scheme, it is essential to introduce the following two Lemmas.

Lemma 2 [6]. For any real constants r_0, r_1 such that $r_0\geq\max\{r_1,-3r_1\}$, and $\{v_j\}_{j=0}^{j=N}$ the following inequality holds:

$$v_{j+1}(r_0v_{j+1}-(r_0-r_1)v_j-r_1v_{j-1})\geq E_{j+1}(r_0,r_1)-E_j(r_0,r_1),\ j=1,...,N-1,$$

where

$$E_j(r_0,r_1)=\left(\frac{1}{2}\sqrt{\frac{r_0-r_1}{2}}+\frac{1}{2}\sqrt{\frac{r_0+3r_1}{2}}\right)^2v_j^2+$$

$$+\left(\sqrt{\frac{r_0-r_1}{2}}v_j-\left(\frac{1}{2}\sqrt{\frac{r_0-r_1}{2}}+\frac{1}{2}\sqrt{\frac{r_0+3r_1}{2}}\right)v_{j-1}\right)^2.$$

Lemma 3 [20]. Assume that the sequence $\{a_n\}_{n=0}^{\infty}$ of real numbers is satisfy the following properties:

$$a_n\geq 0,\ a_n-a_n+1\geq 0,\ a_n-2a_{n+1}+a_n+2\geq 0.$$

Let $c_0=\frac{a_0}{2}$ и $c_j=a_j$ for $j\geq 1$. Then:

$$\sum_{s=1}^{n}\sum_{k=1}^{s}c_{s-k}\xi_s\xi_k\geq 0,\ \forall(\xi_1,\xi_2...,\xi_n)\in R^n.$$

Theorem 2. The difference scheme (3) is unconditionally stable and the following a priori estimate is valid for its solution:

$$(z^{j+1})^2\leq C_3\left(\sum_{s=1}^{j}(R^{s+1})^2\tau+\mu^2\right),$$

where C_3 is a positive constant independent of τ and h.

Proof. The proof follows a similar approach to that of Theorem 1. By multiplying equation (13) by $z^{j+1}\tau$ and replacing j with s, we then sum over s from 1 to j and utilize the results from Lemma 2 and Lemma 3. Due to the similarity in methodology, the detailed proof is omitted here for brevity.

Results. To evaluate the performance of the numerical method and gain insights into its convergence behavior, a comprehensive set of numerical experiments is conducted in this section. The primary objective is to analyze the numerical errors by comparing the exact solution with the computed numerical solution. Additionally, the convergence order of the numerical algorithm with respect to the step size τ is investigated. The experimental orders of convergence (EOC) are calculated using the following relations:

$$\mathrm{EOC}=\log_{\tau_1/\tau_2}\frac{E(\tau_1)}{E(\tau_2)},$$

where the maximum absolute error $E(\tau)$ is calculated by:

$$E(\tau)=\max_{1\leq j\leq N}\left|y(t_j)-y^j\right|,$$

with the step size τ.

Example 1. Consider the model (3) with an exact analytical solution given by the following expression $y(t)=t^2+t^{3+\alpha}$. The corresponding source term and initial conditions for the given problem can be obtained as follows:

$$f(t) = 2t + (3+\alpha)t^{2+\alpha} + \varkappa \frac{2}{\Gamma(3+\alpha)} t^{\alpha+2} + \varkappa \frac{\Gamma(4+\alpha)}{\Gamma(4+2\alpha)} t^{3+2\alpha}, \; y(0) = y_t(0) = 0.$$

We solve this problem with the presented difference scheme (10).

Table 1 presents the results obtained by varying the values of the step length τ, displaying the maximum error and EOC for different values of α with $\varkappa = 4$, at the time $T = 1$. The Table demonstrates that the method exhibits excellent accuracy even for very small grid sizes, and the EOC consistently reaches the expected value of 2 for all cases.

We proceed with an investigation of the long time performance of the proposed scheme method with the aim of further assessing the precision and reliability of the scheme. Table 2 showcases the maximum error and EOC for different values of a with $\varkappa = 2$, at the time $T = 10$. The Table provides further evidence of the method's high accuracy, even for extended time intervals and very small mesh sizes. The EOC consistently remains at 2, indicating the method's reliability and robustness in accurately solving the problem. These findings confirm the effectiveness and reliability of our numerical scheme in accurately solving the considered problem across different time ranges.

Discussion and Conclusions. In this study, we have presented a second-order numerical analog for approximating the Riemann-Liouville fractional integral and demonstrated its effectiveness in solving a class of ordinary FDEs. By transforming the original FDEs into a model that incorporates the Riemann-Liouville fractional integral, we were able to extend the applicability of our proposed method to solve the model. Furthermore, we established a priori estimates for the solution, which demonstrate the uniqueness and continuous dependence of the solution on the input data. The stability analysis of the proposed difference scheme is also investigated. Numerical simulations are performed to assess the accuracy, efficiency, and long-term reliability of the proposed method. The simulations demonstrate the method's effectiveness in solving FDEs, even for extended time intervals and with small mesh sizes. The experimental order of convergence (EOC) is also investigated, confirming the expected EOC of 2 for different cases.

Table 1

The maximum error and the experimental orders of convergence (EOC) for example 1 with decreasing time-grid size $\tau = T/N$, for $\alpha = 0.1, 0.5, 0.9$, with $\varkappa = 4$, at the time $T = 1$

$\tau = T/N$	$\alpha = 0.1$		$\alpha = 0.5$		$\alpha = 0.9$	
N	$E(\tau)$	CO	$E(\tau)$	CO	$E(\tau)$	CO
80	2.1178e-04		2.2420e-04		3.9043e-04	
160	5.4976e-05	1.9457	5.7336e-05	1.9673	9.8674e-05	1.9843
320	1.4126e-05	1.9604	1.4501e-05	1.9833	2.4799e-05	1.9924
640	3.5885e-06	1.9769	3.6458e-06	1.9918	6.2161e-06	1.9962
1280	9.0518e-07	1.9871	9.1379e-07	1.9963	1.5560e-06	1.9981
2560	2.2750e-07	1.9923	2.2870e-07	1.9984	3.8926e-07	1.9991

Table 2

Long time performance of the proposed scheme for solving example 1 with decreasing time-grid size $\tau = T/N$, for $\alpha = 0.1, 0.5, 0.9$, with $\varkappa = 2$, at the time $T = 10$

	$\alpha = 0.1$		$\alpha = 0.5$		$\alpha = 0.9$	
N	$E(\tau)$	CO	$E(\tau)$	CO	$E(\tau)$	CO
80	3.1602e-02		3.1247e-01		1.1045e+00	
160	8.8350e-03	1.8387	7.9023e-02	1.9834	2.7524e-01	2.0046
320	2.4257e-03	1.8648	1.9915e-02	1.9884	6.8737e-02	2.0016
640	6.5691e-04	1.8846	5.0069e-03	1.9919	1.7177e-02	2.0006
1280	1.7599e-04	1.9002	1.2567e-03	1.9943	4.2936e-03	2.0002
2560	4.6740e-05	1.9128	3.1505e-04	1.9960	1.0733e-03	2.0001

References

1. Asl MS, Javidi M, Yan Y. High order algorithms for numerical solution of fractional differential equations. *Advances in Difference Equations*. SpringerOpen. 2021;2021(1):1–23.

2. Asl MS, Javidi M. An improved PC scheme for nonlinear fractional differential equations: Error and stability analysis. *Journal of Computational and Applied Mathematics*. Elsevier; 2017;324:101–117.

3. Roohi M, Aghababa P, Haghighi AR. Switching adaptive controllers to control fractional-order complex systems with unknown structure and input nonlinearities. *Complexity*. Wiley Online Library; 2015;21(2):211–223.

4. Taheri M, et al. A Finite-time Sliding Mode Control Technique for Synchronization Chaotic Fractional-order Laser Systems With Application on Encryption of Color Images. *Optik*. Elsevier; 2023:170948.

5. Zaslavsky G, Edelman M, Tarasov V. Dynamics of the chain of forced oscillators with long-range interaction: From synchronization to chaos. Chaos: *An Interdisciplinary Journal of Nonlinear Science. American Institute of Physics*. 2007;17(4):043124.

6. Alikhanov AA, Huang C. A high-order L2 type difference scheme for the time-fractional diffusion equation. *Applied Mathematics and Computation*. Elsevier; 2021;411:126545.

7. Asl MS, Javidi M. Novel algorithms to estimate nonlinear FDEs: applied to fractional order nutrient-phytoplankton-zooplankton system. *Journal of Computational and Applied Mathematics*. Elsevier; 2018;339:193–207.

8. Kumar V, Kumari N. Stability and bifurcation analysis of fractional-order delayed prey–predator system and the effect of diffusion. *International Journal of Bifurcation and Chaos*. World Scientific; 2022;32(01): 2250002.

9. Deng W. Short memory principle and a predictor–corrector approach for fractional differential equations. *Journal of Computational and Applied Mathematics*. Elsevier; 2007;206(1):174–188.

10. Xie J, Deng D, Zheng H. Fourth-order difference solvers for nonlinear delayed fractional sub-diffusion equations with variable coefficients. *International Journal of Modelling and Simulation*. Taylor & Francis; 2017;37(4):241–251.

11. Li C, He C. Fractional-order diffusion coupled with integer-order diffusion for multiplicative noise removal. *Computers and Mathematics with Applications*. Elsevier; 2023;136:34–43.

12. Xu Y, et al. A novel meshless method based on RBF for solving variable-order time fractional advection-diffusion-reaction equation in linear or nonlinear systems. *Computers and Mathematics with Applications*. Elsevier; 2023;142:107–120.

13. Khibiev A, Alikhanov AA, Huang C. A second-order difference scheme for generalized time-fractional diffusion equation with smooth solutions. *Computational Methods in Applied Mathematics*. 2023.

14. Yang J, et al. Numerical solution of fractional diffusion-wave equation based on fractional multistep method. *Applied Mathematical Modelling*. Elsevier; 2014;38(14):3652–3661.

15. Sun Z, Wu X. A fully discrete difference scheme for a diffusion-wave system. *Applied Numerical Mathematics*. Elsevier; 2006;56(2):193–209.

16. Huang J, et al. Alternating direction implicit schemes for the two-dimensional time fractional nonlinear super-diffusion equations. *Journal of Computational Mathematics*. 2019;37(3).

17. Asl MS, Javidi M, Ahmad B. New predictor-corrector approach for nonlinear fractional differential equations: error analysis and stability. *Journal of Applied Analysis and Computation*. 2019;9(4):1527–1557.

18. Asl MS, Javidi M. Numerical evaluation of order six for fractional differential equations: stability and convergency. *Bulletin of the Belgian Mathematical Society-Simon Stevin*. The Belgian Mathematical Society; 2019;26(2):203–221.

19. Vabishchevich PN. Numerical solution of the Cauchy problem for Volterra integrodifferential equations with difference kernels. *Applied Numerical Mathematics*. Elsevier; 2022;174:177–190.

20. McLean WV. Thomée Numerical solution of an evolution equation with a positive-type memory term. *The ANZIAM Journal*. Cambridge University Press; 1993;35(1):23–70.

About the Authors:

Aslanbek Kh Khibiev, Trainee researcher of the Computational Methods Department, North Caucasus Center for Mathematical Research, North Caucasus Federal University (1, Pushkin St., Stavropol, 355017, RF), ORCID, akkhibiev@gmail.com

Anatoly A Alikhanov, Vice-Rector for Research and Innovation, Associate Professor, North Caucasus Center for Mathematical Research, North Caucasus Federal University (1, Pushkin St., Stavropol, 355017, RF), Candidate of Physical and Mathematical Sciences, ScopusID, ORCID, aaalikhanov@gmail.com

Mohammad Shahbaziasl, Researcher, North Caucasus Center for Mathematical Research, North Caucasus Federal University (1, Pushkin St., Stavropol, 355017, RF)

Ruslan A Chernobrovkin, Laboratory Assistant of the Computational Methods Department, North Caucasus Center for Mathematical Research, North Caucasus Federal University (1, Pushkin St., Stavropol, 355017, RF) Conflict of interest statement

Received 06.04.2023.
Revised 19.05.2023.
Accepted 22.05.2023.

Conflict of interest statement
The authors do not have any conflict of interest.

All authors have read and approved the final manuscript.

Об авторах:
Хибиев Асланбек Хизирович, стажер-исследователь отдела вычислительных методов, Северо-Кавказский центр математических исследований, Северо-Кавказский федеральный университет (355017, РФ, г. Ставрополь, ул. Пушкина, 1), ORCID, akkhibiev@gmail.com

Алиханов Анатолий Алиевич, проректор по НИР И ИД, доцент, Северо-Кавказский центр математических исследований, Северо-Кавказский федеральный университет (355017, РФ, г. Ставрополь, ул. Пушкина, 1), кандидат физико-математических наук, ScopusID, ORCID, aaalikhanov@gmail.com

Шахбазиасль Мохаммад, научный сотрудник, Северо-Кавказский центр математических исследований, Северо-Кавказский федеральный университет (355017, РФ, г. Ставрополь, ул. Пушкина, 1)

Чернобровкин Руслан Алексеевич, лаборант отдела вычислительных методов, Северо-Кавказский центр математических исследований, Северо-Кавказский федеральный университет (355017, РФ, г. Ставрополь, ул. Пушкина, 1)

Поступила в редакцию 06.04.2023.
Поступила после рецензирования 19.05.2023.
Принята к публикации 22.05.2023.

Конфликт интересов
Авторы заявляют об отсутствии конфликта интересов.

Все авторы прочитали и одобрили окончательный вариант рукописи.

MATHEMATICAL MODELING
МАТЕМАТИЧЕСКОЕ МОДЕЛИРОВАНИЕ

UDC 51-77
https://doi.org/10.23947/2587-8999-2023-7-2-40-51

Review article

Optimal Control in Neurological Models of Information Warfare

Alexander P Petrov

Keldysh Institute of Applied Mathematics RAS, 4, Miusskaya Sq., Moscow, Russian Federation

petrov.alexander.p@yandex.ru

Abstract

Two neurological models of information warfare are considered. For each of them, the optimal control problem is considered, assuming that the Campaign Planner is associated with the governing body of one of the belligerent parties and distributes the volume of propaganda broadcasting in time.

The cost functional reflects the Planner's desire to maximize the number of their supporters at a given time while minimizing costs during the campaign.

The problem is studied analytically, using the Pontryagin's maximum principle.

Optimal control is obtained for various combinations of parameters.

The "increasing" type of campaign is aimed at ensuring that for most individuals information is received immediately before the finish line, and that the impression of this information does not have time to weaken. In contrast, the strategy of a "decreasing" campaign implies a high role of interpersonal communication: it is based on convincing a significant number of individuals of their position at the very beginning, who will then retell it to their interlocutors.

Keywords: mathematical model, information warfare, optimal control, Pontryagin's maximum principle.

For citation. Petrov AP. Optimal control in neurological models of information warfare. *Computational Mathematics and Information Technologies.* 2023;7(2):40–51. https://doi.org/10.23947/2587-8999-2023-7-2-40-51

Обзорная статья

Оптимальное управление в нейрологических моделях информационного противоборства

А.П. Петров

Институт прикладной математики им. М. В. Келдыша РАН, Российская Федерация, г. Москва, Миусская пл., 4

petrov.alexander.p@yandex.ru

Аннотация

Рассматриваются две нейрологические модели информационного противоборства. Для каждой из них предложено решение задачи оптимального управления. При этом предполагается, что Планировщик кампании ассоциируется с управляющим органом одной из противоборствующих партий и распределяет во времени доступный ему объем пропагандистского вещания. Таким образом, интенсивность пропагандистского вещания одной из сторон противоборства имеет смысл управления.

Целевой функционал отражает стремление Планировщика максимизировать численность своих сторонников в заданный момент времени при минимизации затрат в течение кампании.

Исследование задачи управления проводится аналитически, с помощью принципа максимума Понтрягина.

Получено оптимальное управление для различных комбинаций параметров.

Стратегия пропагандистской кампании, в зависимости от параметров системы, может быть как «нарастающей» (т. е. проходящей с неубывающей интенсивностью пропагандистского вещания), так и «убывающей» (проходящей с невозрастающей интенсивностью). При «нарастающей» кампании информация предоставляется только на финише, с тем, чтобы впечатление от этой информации не успело потерять силу. В основе стратегии «убывающей» кампании — межличностное общение. Сначала нужно убедить в своей позиции как можно больше индивидов, которые затем будут пересказывать ее собеседникам. Параметры системы определяют баланс между этими типами стратегий.

Ключевые слова: математическая модель, информационное противоборство, оптимальное управление, принцип максимума Понтрягина.

Для цитирования. Петров А.П. Оптимальное управление в нейрологических моделях информационного противоборства. *Computational Mathematics and Information Technologies*. 2023;7(2):40–51. https://doi.org/10.23947/2587-8999-2023-7-2-40-51

The following problem is considered in the article. Consider the information war between the two sides. By associating ourselves with one of them, we will try to maximize the number of our supporters at a certain point in time, while minimizing the costs of broadcasting in the media. This moment in time can be considered as an election date. The question is to determine the most profitable strategy: for example, whether to start a campaign with a low intensity of propaganda in the media and strengthen it over time. Or, on the contrary, you need to start a campaign with intensive propaganda, and then reduce it. Or some more complex, non-monotonic strategy is optimal. For simplicity, let›s assume that the propaganda of the other side has a constant intensity.

This paper uses a neurological model of information warfare in society to study this problem [1]. Therefore, from an applied point of view, the analysis is aimed not so much at obtaining quantitative results as at identifying qualitative patterns. For these revealed patterns, the final section presents a transparent sociological interpretation that allows for the practical application of the results. The conclusions obtained in this case do not contradict intuition, but, according to the authors, are not obvious and could hardly be obtained on the basis of general considerations, i.e. without the use of mathematical modeling methods.

Meaningfully, this work relates to such a direction as mathematical modeling of information processes in society [2–4]. In this field, information processes are studied by methods of text analysis [5, 6], network analysis and opinion dynamics [7–11], etc. At the same time, the task of management in the formulation of this work has not been previously considered.

The model of information warfare. The neurological model of information warfare in society [1] (and its application [3]) is based on the traditional neurological scheme [12, 13] and has the form:

$$\frac{d\psi}{dt} = c\left(2\int_{-\psi}^{\infty} n(\varphi)\,d\varphi - N_0\right) + u - b - a\psi. \tag{1}$$

Here the parameters a, b, c, u are positive, and their meaningful meaning is defined in Rashevsky's theory [12, 13]. They depend both on the stimulus that come from the social environment and on the internal parameters of the neurological system. For the purposes of this work, it is important that a and b are related to the intensity of the mass media supporting the Right and Left parties, respectively.

In the most general terms, the sociological meaning of the position selection model and equation (1) can be explained as follows. It is assumed that in a society consisting of individuals, there is an information struggle between two sides (parties): Left and Right. Each individual makes a decision to support a particular party based on his attitude and incentives coming from the social environment.

Next, we will consider in turn what these incentives and attitudes are, and then we will describe the decision-making mechanism.

Stimuli in the authors' model are understood as informational influence on an individual by the media and other individuals. Under this influence, an individual can change his party affiliation over time. At the same time, he himself creates incentives for other individuals by agitating them for his current party. As a result, there is a social dynamics described by equation (1). If the intensity of media propaganda is constant, then the dynamic process ends with the

formation of a stationary state. Quite often, several stationary states are possible, in this case, which of them is achieved depends on the initial condition. Next, the optimal control problem is formulated, in which the Planner is identified with one of the sides of the warfare (with the Right Party), and the intensity of its propaganda through the media is taken as a control parameter, and the objective function takes into account this intensity (as an indicator of expenses) and the number of supporters of this party at a given time (the end of the warfare).

Now let's look at the model in more detail.

Each of the individuals N_0 is characterized by an attitude, i. e. their predisposition φ to support a particular party, related to their fundamental belonging to a certain ideology, previous experience, social status, etc. This value is assumed to be constant for a period of time, during which the information struggle lasts.

Thus, it is assumed that there is a constant in time, exogenously defined distribution of individuals along the axis of attitudes $n(\varphi)$, while the negative attitude corresponds to the support of the first batch, the positive one corresponds to the support of the second batch, and the absolute value reflects the strength of support.

Here the function $n(\varphi)$ is equal to zero outside the segment at $\varphi_{\min} \le \varphi \le \varphi_{\max}$ and further we will assume that on this segment the function $n(\varphi)$ is positive, except, perhaps, a finite number of isolated points at which it turns to zero.

Obviously:

$$N_0 = \int_{-\infty}^{\infty} n(\varphi) d\varphi.$$

The rule by which an individual relates himself to a particular party can be expressed as follows: if the sum of the stimulus and the attitude is negative, then the individual relates himself to the Left party, if positive — to the Right.

The variant of the model considered in this paper assumes that the influence of mass media is evenly distributed throughout society, in particular, this means that selective use of the media is not taken into account (for example, "conservatives read only conservative newspapers, liberals read only liberal newspapers"). The incentive to support a certain party associated with the campaigning carried out by the supporters of this party is assumed to be proportional to its current number.

The numbers of supporters of the Left (L) and Right (R) parties are equal, respectively:

$$L(t) = \int_{\varphi_{\min}}^{-\psi(t)} n(\varphi) d\varphi, \tag{2.1}$$

$$R(t) = \int_{-\psi(t)}^{\varphi_{\max}} n(\varphi) d\varphi. \tag{2.2}$$

The initial condition $\psi(0)$, necessary for an unambiguous definition $\psi(t)$, is found from the distribution of individuals between parties at the moment t=0 and has the form:

$$L(0) = \int_{-\psi(0)}^{\varphi_{\max}} n(\varphi) d\varphi \tag{3}$$

or, equivalently:

$$R(0) = \int_{\varphi_{\min}}^{-\psi(0)} n(\varphi) d\varphi.$$

Here $L(0)$ (and also $R(0)$) is an observable quantity and each of these equalities can be considered as an equation for $\psi(0)$, having a unique solution if the function $N(\varphi)$ is positive for almost all φ.

Obviously, $\psi(0) = \varphi_{\max}$, if $X(0) = 0$ and $\psi(0) = \varphi_{\min}$, if $Y(0) = 0$. The realistic assumption is that $0 < X(0) < N_0$, so that $\varphi_{\min} < \psi(0) < \varphi_{\max}$.

Note that, the function $\psi(t)$ can take values in a wider range, up to $-\infty < \psi < \infty$. For example, inequality $\psi(t) > \varphi_{\max}$ corresponds to a situation where absolutely all members of society support the first party, i. e. its advantage in the intensity of propaganda is so great that it outweighs the installation of even the most radical supporter of the second party. This situation seems unrealistic. Therefore, in this analysis, we will choose the areas of parameter changes so that $\varphi_{\min} < \psi(t) < \varphi_{\max}$ for all $0 \le t \le T$.

So, the function $\psi(t)$ is found as a solution to the initial problem (1), (3).

Rashevsky [12, 13] analyzed a stationary equation corresponding to (1) in the case $u=b=0$ (in terms of this model, this corresponds to a process taking place in the absence of mass media propaganda) and an even function $n(\varphi)$. He showed that for sufficiently small values of the ratio c/a there is a single stationary solution, it is asymptotically stable and corresponds to an equal distribution of individuals between parties, i. e. $R(t) - L(t) \to 0$, at $t \to \infty$. This corresponds to the case when the reaction of (each) individual is significantly more determined by his attitude than the opinion of other individuals. And, conversely, with sufficiently large values c/a an individual's reaction is more determined by the opinion of other individuals than by his own attitude. As a result, the balance between the parties is unstable: if one of them has a numerical superiority at $t=0$, then it allows you to create an advantage in the strength of the incentive (i. e., in the number of individuals campaigning for it), which increases over time. As a result, stable stationary solutions correspond to situations in which one of the parties acquires a substantial majority. It is precisely such cases that are of the greatest interest for analysis and it is to them that the most attention is paid in this work.

Statement of the management problem. We will consider the process of informational warfare in the time interval $(0;T)$, where an exogenously given moment of time T can be conditionally interpreted as "election day". At the same time, the intensity u of the propaganda broadcast of the Right-wing Party is accepted as management and has a limitation:

$$0 \le u \le u_m. \tag{4}$$

The target functionality reflects the Planner's desire to maximize the number of his supporters at time T while minimizing costs during the campaign:

$$J = -\frac{k}{2}\int_0^T u^2 dt + R(T) \to \max,$$

so

$$J = -\frac{k}{2}\int_0^T u^2 dt + \int_{-\psi(T)}^{\varphi_{\max}} n(\varphi) d\varphi \to \max. \tag{5}$$

In this case, we limit ourselves to the case of a uniform symmetric distribution: $\varphi_{\max} = -\varphi_{\min} = \varphi_m$ and $N(\varphi) = \text{const} > 0$, at $-\varphi_m < \varphi < \varphi_m$.

Methods of solving the management problem

A. Basic equations. The Hamiltonian of the optimal control problem (1)–(5) has the form:

$$H(\psi, p, u) = \left[c\left(2\int_{-\psi(t)}^{\varphi_m} n(\varphi) d\varphi - N_0\right) + u - b - a\psi\right] p - \frac{ku^2}{2}.$$

Therefore,

$$\frac{d\psi}{dt} = c\left(2\int_{-\psi}^{\varphi_m} n(\varphi) d\varphi - N_0\right) + u - b - a\psi, \tag{6}$$

$$\frac{dp}{dt} = \left[-2cn(-\psi) + a\right] p, \tag{7.1}$$

$$p(T) = n(-\psi(T)). \tag{7.2}$$

The immediate goal is to maximize the control Hamiltonian. We have:

$$\frac{\partial H}{\partial u} = p - ku.$$

This derivative turns to zero at:

$$u = \frac{p}{k}.$$

Taking into account the constraint (4), we obtain that the optimal control has the form:

$$u^* = \begin{cases} 0, & p < 0, \\ p/k, & 0 \le p \le ku_m, \\ u_m, & p > ku_m. \end{cases} \tag{8}$$

Taking into account the fact that the authors limited themselves to the case of a uniform symmetric distribution: $N(\varphi) = \text{const} > 0$, at $-\varphi_m < \varphi < \varphi_m$, hence:

$$\int_{-\psi}^{\varphi_m} n(\varphi)d\varphi = \begin{cases} 0, & \psi < -\varphi_m, \\ \dfrac{N_0}{2}\left(1 + \dfrac{\psi}{\varphi_m}\right), & -\varphi_m \le \psi \le \varphi_m, \\ N_0, & \psi > \varphi_m. \end{cases}$$

Stationary solutions of the differential equation (6) are found from the equation:

$$f(\psi) = a\psi. \tag{9}$$

where

$$f(\psi) = \begin{cases} -cN_0 + u - b, & \psi < -\varphi_m, \\ cN_0 \dfrac{\psi}{\varphi_m} + u - b, & -\varphi_m \le \psi \le \varphi_m, \\ cN_0 + u - b, & \psi > \varphi_m. \end{cases}$$

It is not difficult to see that if $a > cN_0 / \varphi_m$, then equation (9) has one solution for any constant u. If $a < cN_0 / \varphi_m$, then it has three roots at $a\varphi_m - cN_0 < u - b < -a\varphi_m + cN_0$ and only one root at or $u - b < a\varphi_{\text{m}} - cN_0$ or $-a\varphi_m + cN_0 < u - b$ (this paper does not consider a special case $a = cN_0 / \varphi_m$).

For the brevity of the record , we introduce the notation:

$$\lambda = a - \frac{cN_0}{\varphi_m}. \tag{10}$$

Tasks (6), (7) take the form:

$$\frac{d\psi}{dt} = \begin{cases} -cN_0 + u - b - a\psi, & \psi < -\varphi_m, \\ -\lambda\psi + u - b, & -\varphi_{\text{m}} \le \psi \le \varphi_m, \\ cN_0 + u - b - a\psi, & \psi > \varphi_m. \end{cases} \tag{11}$$

$$\frac{dp}{dt} = \begin{cases} ap, & \psi < -\varphi_m, \\ \lambda p, & -\varphi_m \le \psi \le \varphi_m, \\ ap, & \psi > \varphi_m. \end{cases} \tag{12}$$

Taking into account the case under consideration $-\varphi_m \le \psi(t) \le \varphi_m$ for all t, we have:

$$\frac{d\psi}{dt} = -\lambda\psi + u - b, \ \psi(0) = \psi^0, \tag{13}$$

$$\frac{dp}{dt} = \lambda p, \ \ p(T) = N_0 / 2\varphi_m. \tag{14}$$

The solution of problem (14) for the conjugate equation has the form:

$$p(t) = \frac{N_0}{2\varphi_m}\exp[\lambda(t - T)]. \tag{15}$$

Thus, the function $p(t)$ either increases strictly (if $\lambda > 0$), or decreases strictly (if $\lambda < 0$), or is constant (if $\lambda = 0$). Let's consider the first two options sequentially.

B. Strictly increasing function $p(t)$

We will assume that:

$$a - cN_0 / \varphi_m > 0. \tag{16}$$

Then there can be three cases (Fig. 1).

Case 1 (Fig. 1 *a*): $ku_m \ge p(T)$, i. e.:

$$N_0 / 2\varphi_m \le ku_m.$$

Case 2 (Fig. 1 *b*): $p(0) < ku_m < p(T)$, i. e.:

$$\frac{N_0}{2\varphi_m}\exp[-\lambda T] < ku_m < \frac{N_0}{2\varphi_m}.$$

Case 3 (Fig.1 *c*): $ku_m \le p(0)$, i. e.:

$$ku_m \le \frac{N_0}{2\varphi_m}\exp[-\lambda T].$$

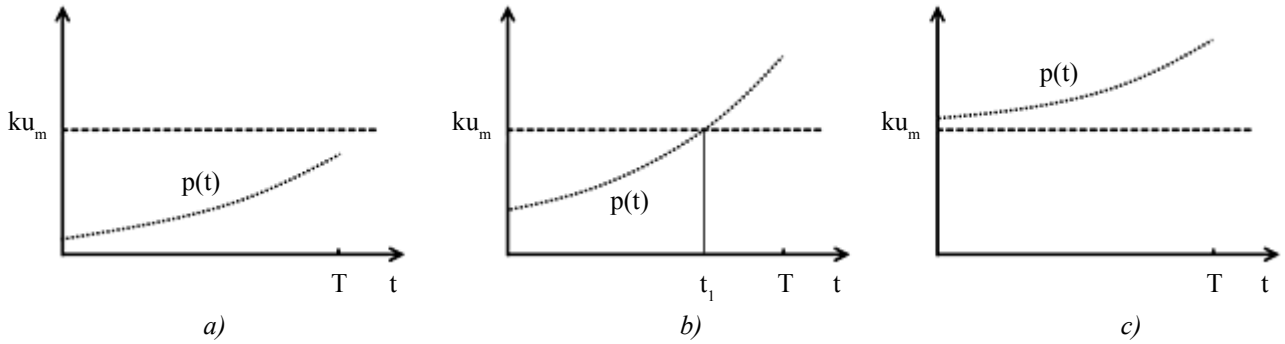

a) *b)* *c)*

Fig. 1. Three options for the location of the function $y=p(t)$ relative to a straight line $y=ku_m$: cases 1–3

Let's consider each of these cases.

Case 1. $\lambda > 0,\ ku_m \ge p(T)$.

Then $p(t) \le ku_m$ at $t \in [0;T]$. Then it follows from equation (8) that:

$$u^*(t) = \frac{N_0}{2k\varphi_m}\exp[\lambda(t-T)]. \tag{17}$$

Substituting this into (13), we get:

$$\frac{d\psi}{dt} = -\lambda\psi + \frac{N_0}{2k\varphi_m}\exp[\lambda(t-T)] - b, \tag{18}$$

The solution to this Cauchy problem has the form:

$$\psi(t) = \frac{N_0\exp[\lambda(t-T)]}{4\lambda k\varphi_m} - \frac{b}{\lambda} + \left[\psi^0 - \frac{N_0\exp[-\lambda T]}{4\lambda k\varphi_m} + \frac{b}{\lambda}\right]\exp[-\lambda t], \tag{19}$$

at $0 \le t \le T$.

Case 2. $\lambda > 0,\ p(0) < ku_m < p(T)$.

Then there is a point $t_1 \in (0;T)$, such that $p(t_1) = ku_m$ (Fig. 1 *b*). In other words, t_1 is determined by equating the function $p(t)$, given by expression (15) to the value ku_m. We have an equation for this value $N_0/(2\varphi_m)\exp[\lambda(t_1 - T)] = ku_m$, i. e.:

$$t_1 = T - \frac{1}{\lambda}\ln\frac{N_0}{2\varphi_m ku_m}. \tag{20}$$

Calculated in this way t_1 is positive due to the condition $p(0) < ku_m < p(T)$, defining Case 2 (non-positivity would mean that $p(0) > ku_m$, i. e., Case 3 takes place). For optimal control, we obtain:

$$u^* = \begin{cases} p(t)/k, & 0 \le t \le t_1, \\ u_m, & t_1 < t \le 1. \end{cases}$$

Substituting $u=u^*$ into equation (13), we obtain for the function $\psi(t)$ the Cauchy problem with the right part given separately on the segments $0 \le t \le t_1$ and $t_1 \le t \le 1$:

$$\frac{d\psi}{dt} = -\lambda\psi + \frac{N_0}{2k\varphi_m}\exp[\lambda(t-T)] - b,\ 0 \le t \le t_1,\ \psi(0) = \psi^0, \tag{21}$$

$$\frac{d\psi}{dt} = -\lambda\psi + u_m - b,\ t_1 \le t \le 1,\ \psi(t_1 + 0) = \psi(t_1 - 0). \tag{22}$$

Sequentially solving problems (21), (22), we obtain:

$$\psi(t) = \frac{N_0 \exp[\lambda(t-T)]}{4\lambda k\varphi_m} - \frac{b}{\lambda} + \left[\psi^0 - \frac{N_0 \exp[-\lambda T]}{4\lambda k\varphi_m} + \frac{b}{\lambda}\right]\exp[-\lambda t], \quad 0 \le t \le t_1; \tag{23}$$

$$\psi(t) = \frac{u_m - b}{\lambda} + \left[\psi(t_1) - \frac{u_m - b}{\lambda}\right]\exp[-\lambda(t-t_1)], \quad t_1 \le t \le 1.$$

Case 3. $\lambda > 0, \ ku_m \le p(0)$.

In this case $p(t) \ge ku_m$ for $t \in [0;T]$, in particular $p(T) = N_0 / 2\varphi_m > ku_m$. It follows from (8) that the optimal control then has the form:

$$u^*(t) = u_m, \ \ t \in [0;T]. \tag{25}$$

Substituting $u=u^*$ into equation (13), we obtain for the function $\psi(t)$ задачу the Cauchy problem:

$$\frac{d\psi}{dt} = -\lambda\psi + u_m - b, \ \ \psi(0) = \psi^0,$$

the solution of which has the form:

$$\psi(t) = \frac{u_m - b}{\alpha} + \left[\psi^0 - \frac{u_m - b}{\alpha}\right]\exp[-\alpha t]. \tag{26}$$

C. Strictly decreasing function $p(t)$

We will assume that:

$$\lambda = a - cN_0 / \varphi_m < 0. \tag{27}$$

For convenience, we will rewrite the formula (15):

$$p(t) = \frac{N_0}{2\varphi_m}\exp[\lambda(t-T)].$$

There may be three cases (Fig. 2).

Case 4 (Fig. 2 *a*): $ku_m \ge p(0)$, i. e.:

$$ku_m \ge \frac{N_0}{2\varphi_m}\exp[-\lambda T].$$

Case 5 (Fig. 2 *b*): $p(T) < ku_m < p(0)$, i. e.:

$$\frac{N_0}{2\varphi_m} < ku_m < \frac{N_0}{2\varphi_m}\exp[-\lambda T].$$

Case 6 (Fig. 2 c): $ku_m \le p(T)$, i. e.:

$$ku_m \le \frac{N_0}{2\varphi_m}.$$

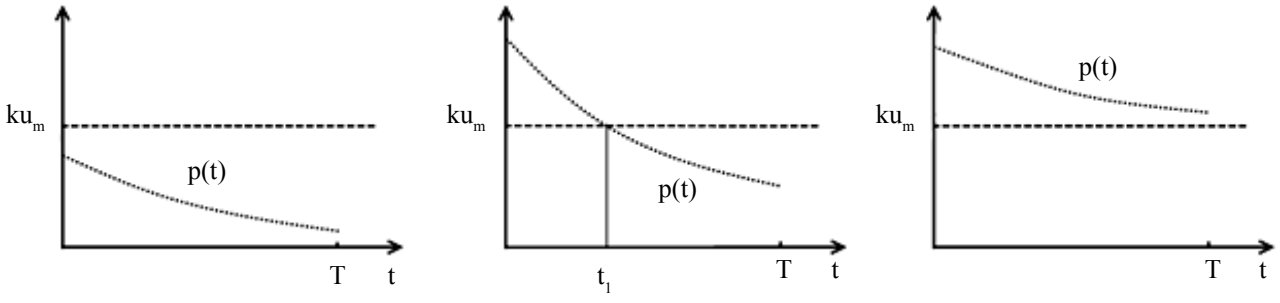

a) *b)* *c)*

Fig. 2. Three options for the location of the function $y=p(t)$ relative to a straight line $y=ku_m$: cases 4–6

Let's consider these cases sequentially.

Case 4. $\lambda < 0, \ \ p(0) \le ku_m$.

Thus, $\frac{N_0}{2\varphi_m}\exp[-\lambda T] \le ku_m$. In this case $p(t) \le ku_m$ for $t \in [0;T]$. Then it follows from (8) that:

$$u^*(t) = \frac{N_0}{2k\varphi_m}\exp[\lambda(t-T)]. \tag{28}$$

Substituting $u=u^*$ into equation (13), we obtain the Cauchy problem for the function $\psi(t)$:

$$\frac{d\psi}{dt} = -\lambda\psi + \frac{N_0}{2k\varphi_m}\exp\left[\lambda(t-T)\right] - b, \quad \psi(0) = \psi^0. \tag{29}$$

Its solution at has the form:

$$\psi(t) = \frac{N_0\exp\left[\lambda(t-T)\right]}{4\lambda k\varphi_m} - \frac{b}{\lambda} + \left[\psi^0 - \frac{N_0\exp\left[-\lambda T\right]}{2\lambda k\varphi_m} + \frac{b}{\lambda}\right]\exp\left[-\lambda t\right]. \tag{30}$$

Case 5. $\lambda < 0, \ p(T) < ku_m < p(0)$.

Thus, $N_0/(2\varphi_m) < ku_m < N_0/(2\varphi_m)\exp\left[-\lambda T\right]$. Then there is a point $t_1 \in (0;T)$, such that $p(t_1) = ku_m, t_1$ is determined by equating the function $p(t)$, given by formula (15) to the value ku_m. We will get:

$$t_1 = T - \frac{1}{\lambda}\ln\frac{N_0}{2\varphi_m k u_m}. \tag{31}$$

Then the optimal control has the form:

$$u^* = \begin{cases} u_m, & 0 \le t \le t_1, \\ p(t)/k, & t_1 < t \le 1. \end{cases} \tag{32}$$

Substitute this in (13). We will get:

$$\frac{d\psi}{dt} = -\lambda\psi + u_m - b, \ 0 \le t \le t_1, \ \psi(0) = \psi^0. \tag{33}$$

$$\frac{d\psi}{dt} = -\lambda\psi + \frac{N_0}{2k\varphi_m}\exp\left[\lambda(t-T)\right] - b, \ t_1 \le t \le 1, \ \psi(t_1+0) = \psi(t_1-0). \tag{34}$$

Having solved these problems at the appropriate time intervals, we get:

$$\psi(t) = \frac{u_m - b}{\lambda} + \left[\psi^0 - \frac{u_m - b}{\lambda}\right]\exp\left[-\lambda t\right], \tag{35}$$

$$\psi = \left\{\frac{\frac{N_0}{2k\varphi_m}\exp\left[\alpha(t-T)\right]}{2\alpha} - \frac{b}{a}\right\} + C\exp\left[-\alpha(t-T)\right], \tag{36}$$

where

$$\begin{aligned} C = {} & \frac{u_m - b}{\alpha}\exp\left[\alpha(t_1 - T)\right] + \left[\psi^0 - \frac{u_m - b}{\alpha}\right]\exp\left[-\alpha T\right] - \\ & - \exp\left[\alpha(t_1 - T)\right]\left\{\frac{N_0\exp\left[\alpha(t_1 - T)\right]}{4\alpha k\varphi_m} - \frac{b}{\alpha}\right\}. \end{aligned} \tag{37}$$

Case 6. $\lambda < 0, \ ku_m \le p(T)$.

In this case $p(t)/k \ge u_m$ for $t \in [0;T]$. It follows from (8) that the optimal control has the form:

$$u^*(t) = u_m \text{ for all } t \in [0;T]. \tag{38}$$

Substituting this into (13), we get the Cauchy problem:

$$\frac{d\psi}{dt} = -\lambda\psi + u_m - b, \ \psi(0) = \psi^0, \tag{39}$$

the solution of which is the function:

$$\psi(t) = \frac{u_m - b}{\alpha} + \left[\psi^0 - \frac{u_m - b}{\alpha}\right]\exp\left[-\alpha t\right]. \tag{40}$$

The main conclusions of this section are:

– at sufficiently high values of the relaxation parameter *a* and/or sufficiently small values of the intensity of information transmission in interpersonal communication (parameter *c*), the optimal strategy is non-decreasing (Fig. 1);

– in the opposite case, the optimal strategy is non-increasing (Fig. 2).

Extended model: a society consisting of two groups. This section is devoted to the analysis of a model that considers society in more detail compared to the model from the previous section. The main goal is to determine whether the conclusion of the previous section on the influence of parameters *a*, c on the nature of the optimal campaign is preserved for this more complex model.

The model has the form:

$$\frac{d\psi_1}{dt} = f_1(\psi_1, \psi_2, u) - a\psi_1, \tag{41}$$

$$\frac{d\psi_2}{dt} = f_2(\psi_1, \psi_2, u) - a\psi_2, \tag{42}$$

$$J(n,u) = -\frac{k}{2}\int_0^T u^2 dt + \int_{-\psi_1(T)}^{\varphi_m} n_1(\varphi)d\varphi + \int_{-\psi_2(T)}^{\varphi_m} n_2(\varphi)d\varphi \to \max, \tag{43}$$

where

$$f_1(\psi_1, \psi_2, u) = c\left[\gamma\left(2\int_{-\psi_1}^{\varphi_m} n_1(\varphi)d\varphi - N_1\right) + (1-\gamma)\left(2\int_{-\psi_2}^{\varphi_m} n_2(\varphi)d\varphi - N_2\right)\right] + (u-b),$$

$$f_2(\psi_1, \psi_2, u) = c\left[(1-\gamma)\left(2\int_{-\psi_1}^{\varphi_m} n_1(\varphi)d\varphi - N_1\right) + \gamma\left(2\int_{-\psi_2}^{\varphi_m} n_2(\varphi)d\varphi - N_2\right)\right] + (u-b)$$

and there is still a limitation:

$$0 \le u \le u_m. \tag{44}$$

Here it is assumed that the system consists of two groups of individuals. Each of them is characterized by its own distribution $n_1(\varphi)$, $n_2(\varphi)$. At the same time, each individual communicates more with members of his group than a stranger, which is described by the parameter γ (at the same time γ=1 corresponds to the fact that there is no intergroup communication, but γ=0.5 corresponds to homogeneous communication when groups are actually absent. Next, we will assume that $0.5 < \gamma < 1$). Let's denote the number of the first group by N_1, the number of the second group by N_2. Let's assume that the distribution of individuals by installation within each of the groups is similar to the distribution from the model discussed in the previous section. In other words, the distributions are uniform over some exogenously given interval $(-\varphi_m, \varphi_m)$, so that:

$$\int_{-\psi}^{\varphi_m} n_i(\varphi)d\varphi = \begin{cases} 0, & \psi < -\varphi_m, \\ \dfrac{N_i}{2}\left(1 + \dfrac{\psi}{\varphi_m}\right), & -\varphi_m \le \psi \le \varphi_m, \\ N_i, & \psi > \varphi_m, \end{cases}$$

(here and in formulas (45) *i*=1,2). We have for the numbers of supporters of the Right and Left parties in the first and groups:

$$R_i(t) = \int_{-\psi_i(t)}^{\varphi_m} n_i(\varphi)d\varphi, \tag{45.1}$$

$$L_i(t) = \int_{-\varphi_m}^{-\psi_i(t)} n_i(\varphi)d\varphi. \tag{45.2}$$

In addition, it is assumed here that the groups are equally exposed to the media propaganda of each of the parties.

Taking into account the selected type of functions $f_i(\psi_1, \psi_2, u), n_i(\varphi)$ formulas (41)–(43) take the form:

$$\frac{d\psi_1}{dt} = c\left[\gamma N_1 \frac{\psi_1}{\varphi_m} + (1-\gamma)N_2 \frac{\psi_2}{\varphi_m}\right] + (u-b) - a\psi_1, \quad -\varphi_m \le \psi_1 \le \varphi_m, \tag{46}$$

$$\frac{d\psi_2}{dt} = c\left[(1-\gamma)N_1 \frac{\psi_1}{\varphi_m} + \gamma N_2 \frac{\psi_2}{\varphi_m}\right] + (u-b) - a\psi_2, \quad -\varphi_m \le \psi_2 \le \varphi_m, \tag{47}$$

$$J(n,u) = -\frac{k}{2}\int_0^T u^2 dt + \frac{N_1}{2}\frac{\varphi_m + \psi_1(T)}{\varphi_m} + \frac{N_2}{2}\frac{\varphi_m + \psi_2(T)}{\varphi_m} \to \max. \quad (48)$$

The Hamiltonian has the form:

$$H(\psi_1, \psi_2, p_1, p_2, u) = \left\{c\left[\gamma N_1 \frac{\psi_1}{\varphi_m} + (1-\gamma)N_2 \frac{\psi_2}{\varphi_m}\right] + (u-b) - a\psi_1\right\}p_1 +$$
$$+ \left\{c\left[(1-\gamma)N_1 \frac{\psi_1}{\varphi_m} + \gamma N_2 \frac{\psi_2}{\varphi_m}\right] + (u-b) - a\psi_2\right\}p_2 - \frac{ku^2}{2}.$$

The immediate goal is to maximize the control Hamiltonian. Here:

$$\frac{\partial H}{\partial u} = p_1 + p_2 - ku.$$

This function has a maximum when:

$$u = \frac{p_1 + p_2}{k}.$$

Taking into account the constraint (44), we obtain optimal control, which has the form:

$$u^* = \begin{cases} 0, & p_1 + p_2 < 0, \\ (p_1 + p_2)/k, & 0 \le p_1 + p_2 \le ku_m, \\ u_m, & p_1 + p_2 > ku_m. \end{cases} \quad (49)$$

The conjugate system has the form:

$$\frac{dp_1}{dt} = -\left(\frac{\gamma c N_1}{\varphi_m} - a\right)p_1 - \frac{(1-\gamma)cN_1}{\varphi_m}p_2, \quad p_1(T) = \frac{N_1}{2\varphi_m},$$

$$\frac{dp_2}{dt} = -\frac{(1-\gamma)cN_2}{\varphi_m}p_1 - \left(\frac{\gamma c N_2}{\varphi_m} - a\right)p_2, \quad p_2(T) = \frac{N_2}{2\varphi_m}.$$

It is not difficult to see that due to the positivity of the values $p_1(T)$, $p_2(T)$ the functions $p_1(t)$, $p_2(t)$ are positive for $0 \le t \le T$. It is also obvious that each of the derivatives dp_1/dt, dp_2/dt is positive for sufficiently large values of parameter a and/or small values of parameter c and negative in the opposite case. Consequently, the optimal control given by formula (49) is non-decreasing at sufficiently high values of the relaxation parameter a and non-increasing at sufficiently small values. Thus, the model of this section retains the basic property of the simpler model discussed in the previous section.

Let's give a meaningful interpretation of the results obtained. It follows from the formulas obtained for both models considered that the parameters affect the optimal strategy as follows:

– relaxation parameter a: large values contribute to an increasing campaign, small values to a decreasing one;

– the duration of the confrontation T and the intensity b of the broadcast of the opposing party does not affect the choice of strategy (provided that this intensity is constant);

– the intensity of information transmission through interpersonal communication (parameter c), the size of the society, as well as the consolidation of the group parameter φ_{max}: large values contribute to a decreasing campaign, small values contribute to an increasing one.

Information is distributed through the media and through interpersonal communication (rumors): from individual to individual. At the same time, the influence of information on a particular individual after he receives it gradually decreases, so he can be "turned over" by more recent enemy information.

Accordingly, the "growing" campaign is focused on ensuring that for most individuals, information is received immediately before the finish line, and the impression of it does not have time to weaken. The flip side of such a strategy is that individuals will not have time to widely disseminate the information received "by word of mouth", because each act of interpersonal communication requires a certain amount of time. In contrast, the strategy of a "decreasing" campaign implies an effective role of interpersonal interaction and is based on convincing a significant number of individuals of their position at the very beginning, who will then retell it to others. This strategy also has a downside: over time, the

interest of individuals in this position will fade, so that by the end of the campaign, the enemy can "turn over" them due to more intensive broadcasting. Thus, the conclusions obtained in the work are not obvious, but they do not contradict intuitio.

References

1. Petrov AP, Maslov AI, Tsaplin NA. Modeling of the choice of positions by individuals in the information confrontation in society. *Mathematical modeling*. 2015;27(12):137–148. (In Russ.). http://www.mathnet.ru/php/archive.phtml?wshow=paper&jrnid=mm&paperid=3684

2. Mikhailov AP, Pronchev GB, Proncheva OG. Mathematical Modeling of Information Warfare in Techno-Social Environments. Troussov A., Maruev S. "Techno-Social Systems for Modern Economical and Governmental Infrastructures". *IGI Global*. 2019:174–210. https://www.doi.org/10.4018/978-1-5225-5586-5, https://www.igi-global.com/chapter/mathematical-modeling-of-information-warfare-in-techno-social-environments/208385

3. Proncheva OG. On the influence of the degree of polarization of society on the outcome of the information confrontation. *Preprints of the IPM named after M. V. Keldysh*. 2016;75. 29 p. (In Russ.). https://www.doi.org/10.20948/prepr-2016-75, http://library.keldysh.ru/preprint.asp?id=2016-75

4. Pronchev GB. On the problems of information security of the use of information and communication technologies and artificial intelligence in digital healthcare. *Social and humanitarian knowledge*. 2022;2:100–107. (In Russ.). https://www.doi.org/10.34823/SGZ.2022.2.51777

5. Boldyreva A, Alexandrov M, Koshulko O, et al. *Queries to Internet as a tool for analysis of the regional police work and forecast of the crimes in regions.* In: Proc. of 14-th Mexican Intern. Conf. on Artif. Intell. (MICAI-2016). Springer Cham, LNAI. 2017;10061(25):290–302. https://doi.org/10.1007/978-3-319-62434-1_25

6. Boldyreva A, Sobolevskiy O, Alexandrov M, et al. *Creating collections of descriptors of events and processes based on Internet queries*. In: Proc. of 14-th Mexican Intern. Conf. on Artif. Intell. (MICAI-2016). Springer Cham, LNAI. 2017;10061(26):303–314. https://doi.org/10.1007/978-3-319-62434-1_26

7. Gubanov DA, Novikov DA. Models of joint dynamics of opinions and actions in online social networks. Part 1. Initial data and primary analysis. *Management problems*. 2023;2:37–53. (In Russ.).

8. Gubanov DA. Methods of analyzing information influence in active network structures. *Automation and telemechanics*. 2022;5:87–101. (In Russ.).

9. Chartishvili AG, Kozitsin IV, Goiko VL, et al. *On an approach to measure the level of polarization of individuals' opinions.* Twelfth International Conference "Management of large-scale system development" (MLSD). 2019;1–5. https://doi.org/10.1109/MLSD.2019.8911015

10. Kozitsin IV. A general framework to link theory and empirics in opinion formation models. *Scientific reports*. 2022;12:5543.

11. Chkhartishvili AG. The problem of finding the median preference of individuals in a stochastic model. *Automation and telemechanics*. 2021;5:139–150. (In Russ.).

12. Rashevsky N. *Outline of a Physico-mathematical Theory of Excitation and Inhibition*. Protoplasma; 1933.

13. Rashevsky N. Two models: imitative behavior and status distribution. Edited by GV Osipov. *Mathematical methods in modern bourgeois sociology. Collection of articles*. Moscow: Progress; 1966. pp. 175–197. (In Russ.).

About the Author:

Alexander Phoun Zho Petrov, Leading Researcher, Keldysh Institute of Applied Mathematics of the Russian Academy of Sciences (4, Miusskaya Sq., Moscow, 125047, RF), Dr. (Physical and Mathematical Sciences), ORCID, eLibrary.ru, ИСТИНА, ResearcherID, ScopusID, petrov.alexander.p@yandex.ru

Received 24.04.2023.

Revised 30.05.2023.

Accepted 31.05.2023.

Conflict of interest statement

The author does not have any conflict of interest.

The author has read and approved the final manuscript.

Об авторе:

Петров Александр Пхоун Чжо, ведущий научный сотрудник Института прикладной математики им. М. В. Келдыша РАН (РФ, 125047, г. Москва, Миусская пл., 4), доктор физико-математических наук, ORCID, eLibrary.ru, ИСТИНА, ResearcherID, ScopusID, petrov.alexander.p@yandex.ru

Поступила в редакцию 24.04.2023.
Поступила после рецензирования 30.05.2023.
Принята к публикации 31.05.2023.

Конфликт интересов

Автор заявляет об отсутствии конфликта интересов.

Автор прочитал и одобрил окончательный вариант рукописи.

MATHEMATICAL MODELLING
МАТЕМАТИЧЕСКОЕ МОДЕЛИРОВАНИЕ

UDC 519.6

https://doi.org/10.23947/2587-8999-2023-7-2-52-59

Original article

Modeling and Analysis of Quasi-2D Turbulence Dynamics in Shallow Waters

Sofia V Protsenko, Elena A Protsenko ✉

Taganrog Institute named after A. P. Chekhov (branch) of RSUE, 48, Initiative St., Taganrog, Russian Federation

✉ eapros@rambler.ru

Abstract

Introduction. The work is devoted to the study of the generation and development of turbulent structures in shallow-water flows. For optimal water resource management, it is necessary to know what the consequences will be if the flow system changes as a result of human intervention. Basically, all fluid flows that relate to the practice of civil engineering are turbulent in nature. These are, for example, river and channel flows, tidal currents in the oceans and coastal seas. Shallow currents in the environment often include a wide range of vortex scales, ranging from micro-scale vortices to large-scale coherent structures with horizontal length scales that far exceed the depth of water ($L >> H$). The existence of such large structures is a typical characteristic of turbulence in shallow flow. This indicates the need for a systematic analysis of the problem, as well as modeling of such complex formalized systems. The purpose of this work is to model and analyze the dynamics of quasi-2D turbulence structures.

Materials and Methods. Large-scale quasi-2D coherent structures (2 DCS) are investigated depending on the source and localization in the liquid column. Turbulent flows in the channel satisfying incompressible Navier-Stokes equations are considered. The numerical experiment was carried out on the basis of the “large eddy simulation” (LES) approach.

The Results of the Study. Scenario of the dynamics of quasi-2D turbulence structures of the coastal zone is constructed, the formation of vortex structures is predicted.

Discussion and Conclusions. The development of two-dimensional turbulence in shallow flows illustrates the processes that control quasi-two-dimensional turbulence, including the merging of individual vortices. The main mechanism controlling the decay of 2DCS is the loss of energy due to friction on the bottom, while the larger the size of the vortex relative to the depth, the faster the direct dissipation of its kinetic energy occurs.

Keywords: turbulent structures, shallow water channels, large-scale quasi-2D coherent structures (2PCS), quasi-2D turbulence, vortex scale.

Founded information. The study was supported by the Russian Science Foundation grant No. 22-11-00295. https://rscf.ru/project/22-11-00295/

For citation. Protsenko SV, Protsenko EA. Modeling and analysis of quasi-2D turbulence dynamics in shallow waters. *Computational Mathematics and Information Technologies*. 2023;7(2):52–59. https://doi.org/10.23947/2587-8999-2023-7-2-52-59

Научная статья

Моделирование и анализ динамики квази-2D-турбулентности в мелководных водоемах

С.В. Проценко, Е.А. Проценко

Таганрогский институт им. А. П. Чехова (филиал) РГЭУ (РИНХ), Российская Федерация, Ростовская область, г. Таганрог, ул. Инициативная, 48

eapros@rambler.ru

Аннотация

Введение. Работа посвящена изучению генерации и развития турбулентных структур в мелководных потоках. Для оптимального управления водным ресурсом необходимо знать, какие будут последствия при изменении системы течения в результате вмешательства человека. В основном все потоки жидкости, которые относятся к практике гражданского строительства, имеют турбулентный характер. Это, например, речные и русловые потоки, приливные течения в океанах и прибрежных морях. Неглубокие течения в окружающей среде часто включают в себя широкий диапазон масштабов вихрей, начиная от микромасштабных вихрей и заканчивая крупномасштабными когерентными структурами с горизонтальными масштабами длины, которые намного превышают глубину воды ($L >> H$). Существование таких крупных структур — типичная характеристика турбулентности при мелком течении. Это указывает на необходимость проведения системного анализа проблемы, а также моделирования подобных сложно формализуемых систем. Целью данной работы является моделирование и анализ динамики структур квази-2D-турбулентности.

Материалы и методы. Исследуются крупномасштабные квази-2D когерентные структуры (2DCS) в зависимости от источника и локализации в столбе жидкости. Рассматриваются турбулентные течения в канале, удовлетворяющие несжимаемым уравнениям Навье-Стокса. Численный эксперимент выполнен на основе подхода «моделирование крупных вихрей» (LES).

Результаты исследования. Построен сценарий динамики структур квази-2D-турбулентности береговой зоны. Предсказано формирование вихревых структур.

Обсуждение и заключения. Развитие двумерной турбулентности в неглубоких потоках служит иллюстрацией процессов, которые управляют квази-двумерной турбулентностью, включая слияние отдельных вихрей. Основным механизмом, управляющим распадом 2DCS, являются потери энергии из-за трения о дно. При этом, чем больше размер вихря относительно глубины, тем быстрее происходит прямое рассеивание его кинетической энергии.

Ключевые слова: турбулентные структуры, мелководные потоки, крупномасштабные квази-2D когерентные структуры (2DCS), квази-2D-турбулентность, масштаб вихрей.

Финансирование. Исследование выполнено за счет гранта Российского научного фонда № 22-11-00295. https://rscf.ru/project/22-11-00295/

Для цитирования. Проценко С.В., Проценко Е.А. Моделирование и анализ динамики квази-2D-турбулентности в мелководных водоемах. *Computational Mathematics and Information Technologies*. 2023;7(2):52–59. https://doi.org/10.23947/2587-8999-2023-7-2-52-59

Introduction. In the context of fluid mechanics in the environment, it can be stated that almost all fluid flows have a turbulent character. Typically, a turbulent flow contains vortices, also called “coherent structures” or “turbulence structures”. These are dynamic recirculation structures resulting from the instability of the internal flow. Despite the fact that the size and boundaries of individual vortices cannot usually be identified unambiguously, it is often possible to determine the length and velocity scales to characterize the behavior of various types of vortices in the flow, especially dominant energy-containing large vortices. Shallow flows include a wide range of vortex scales, including large-scale coherent structures. Such vortices are often observed in areas with large horizontal velocity differences or near obstacles where the flow separates from the wall.

The turbulence of a shallow current, like any other, in the environment cannot be directly predicted in detail due to its chaotic nature. Careful experimental work (field or laboratory data) and detailed numerical modeling are required to predict the behavior of turbulence in real situations with some accuracy. This is of practical importance for improving the understanding and modeling of large-scale turbulence in shallow water. For optimal management of a water resource,

it is necessary to know with a high degree of probability what consequences will occur when the flow system changes (including turbulence) as a result of human intervention.

Turbulent flows are present everywhere in nature, shallow turbulent flows among them form an important subgroup. In fact, turbulence is a chaotic phenomenon. However, turbulence in shallow currents can be described as "organized chaos". The organization in such flows is visible due to turbulent structures with length scales, usually exceeding the depth of water, which can have a relatively long lifetime.

A shallow flow is defined as three-dimensional, one dimension of which is significantly smaller than the other two dimensions. In the context of environmental hydromechanics, this smaller dimension is usually the depth of the water. G. H. Jirka [1] describes several mechanisms that cause large-scale turbulence structures, which are typical for shallow flows. Such large vortices are predominantly two-dimensional in nature. Their dynamics differ significantly from smaller-scale vortices ($L < H$), which have a completely three-dimensional character, i. e. relatively short lifetime ($T \approx L/U$), weaker cross-correlation and a continuous tendency to break up into smaller vortices. Although all turbulence in nature is essentially three-dimensional, shallow flow turbulence is often referred to as "quasi-2D" [2]. G. H. Jirka [1] introduced the abbreviation 2DCS to denote large-scale quasi-2D coherent structures. It is obvious that 2D objects in the stream are always accompanied by three-dimensional structures of a smaller scale. Figure 1 shows a color-synthesized image of the Taganrog Bay of the Azov Sea, obtained in March 2020 from the Landsat 8 remote sensing satellite, the figure shows the structures of turbulent currents in the Taganrog Bay, which have a quasi-two-dimensional character.

Turbulence is usually caused by a shift in the direction perpendicular to the local flow velocity, as a result of which the flow becomes unstable. The origin of such a lateral shift can always be traced either to wall friction (wall turbulence) or to a transverse velocity gradient within the region (free turbulence). An important mechanism responsible for the occurrence of internal velocity gradients is flow separation. Separation occurs when the boundary layer of the flow loses contact with the corresponding solid wall and breaks away from it. This may be due to geometric reasons (for example, the flow is not able to follow the complex shape of the boundary or smoothly bend around the corner) or for dynamic reasons (the pressure gradient in the flow disrupts the equilibrium of the local boundary layer). Separating flows include an area of strong transverse shear downstream from the separation site, which leads to a high intensity of turbulence and is often an area of flow recirculation [3–5].

Fig. 1. Color-synthesized image of the Taganrog Bay of the Azov Sea from the Landsat 8 remote sensing satellite, resolution 30 m

Shallow flows, jets and mixing layers are three common types of free, shallow, shear flows. In other cases, the presence of side walls leads to the fact that the separating flow creates a recirculation area.

Materials and methods

1. Shallow water and its effect on turbulence. Turbulent flows in the channel satisfy incompressible Navier-Stokes equations in a conservative form [6]:

$$\frac{\partial u_i}{\partial x_i} = 0, \tag{1}$$

$$\frac{\partial u_i}{\partial t}+\frac{\partial u_i u_j}{\partial x_j}+\frac{\partial P/\rho}{\partial x_i}-\frac{\partial}{\partial x_j}v\left(\frac{\partial u_i}{\partial x_j}+\frac{\partial u_j}{\partial x_i}\right)=f_i, \tag{2}$$

where u is the velocity vector of the liquid (m/s); P is the hydrodynamic pressure (kg/ms^2); ρ is the constant density (fresh water, 1000 kg/m^3); v is the constant kinematic molecular viscosity (10^{-6} m^2/s) and f is the vector of body force per unit mass (m/s^2), which usually constitutes gravity, $i,j\in\{1,2,3\}$. The velocity field u is called divergence-free or solenoidal. The gravity of the body can be eliminated by including it in the pressure gradient. If we set $f_i=-\partial(g\,x_3)/\partial x_i$ (with acceleration of gravity g = 9.81 m/s^2) and determine the so-called non-hydrostatic normalized pressure through $\rho=P/\rho+g\,x_3$, equation (2) can be rewritten as:

$$\frac{\partial u_i}{\partial t}+\frac{\partial u_i u_j}{\partial x_j}+\frac{\partial \rho}{\partial x_i}-\frac{\partial}{\partial x_j}\acute{\imath}\left(\frac{\partial u_i}{\partial x_j}+\frac{\partial u_j}{\partial x_i}\right)=0. \tag{3}$$

Equations (1) and (3) must be supplemented with appropriate initial and boundary conditions. On impermeable solid walls, the boundary condition of non-slip is physically fulfilled, whereas on the surface (considered either as a movable free surface or as a rigid cover), the condition of free slip applies (wind and atmospheric influences are neglected in this study) [7–9].

Fluid motion is induced by hydrodynamic pressure gradients, while the velocity field is constantly deformed under the action of nonlinear momentum advection and viscosity. When equation (3) is written in dimensionless form, using the velocity scale U and the length scale L, the ratio of advective and viscous forces can be expressed by one dimensionless parameter — the Reynolds number (Re):

$$Re=\frac{UL}{v}. \tag{4}$$

Two features in the Navier-Stokes equations are a significant cause of turbulence. At large values of Re, the flow problem can become hydrodynamically unstable and eventually exhibit chaotic behavior. The action of viscous forces (in combination with the boundary conditions of non-slip) introduces rotation (or vorticity) into the velocity field, even if the initial flow field did not contain rotation. Due to the presence of vorticity, the chaotic flow field will always contain vortices or "vortices" [10].

Because of the important role of vorticity, turbulence is, in fact, a three-dimensional phenomenon. From a physical point of view, the growing chaos in turbulent flows is illustrated by the fact that vortices are unstable and tend to break up into smaller vortices. This basically means that turbulent kinetic energy is transferred towards smaller scales until the smallest vortices reach length scales at which their energy is converted into heat under the action of viscosity (the so-called Kolmogorov scales). This ongoing release of turbulent kinetic energy is often referred to as a "3D energy cascade" [11]. The energy flow towards smaller length scales often leaves its mark in the energy density spectrum of turbulent motion. As for the three-dimensional energy cascade, the spectrum of spatial energy density E (m^3/s^2) at small scales of isotropic turbulence (inertial range) should have the following form:

$$E(k)\approx \tau^{2/3}k^{-5/3}, \tag{5}$$

where τ (m^2/s^3) is the rate of energy dissipation per unit mass; and k ($m-1$) is the "wave number" associated with a certain scale of turbulence length. Vorticity plays a vital role in the mechanism of the energy cascade. This can be seen by taking the curvature of equation (3), which gives the vorticity equation:

$$\frac{D\omega_i}{Dt}\equiv\frac{\partial\omega_i}{\partial t}+u_j\frac{\partial\omega_i}{\partial x_j}=\omega_j\frac{\partial u_i}{\partial x_j}+v\frac{\partial^2\omega_i}{\partial x_i^2}, \tag{6}$$

where ω ($s-1$) — is the vorticity vector. This equation shows that the material derivative of the vorticity of a moving fluid particle is determined by the right side of the equation. The first term describes the interaction between the vorticity field and the velocity deformation field; the second one describes the diffusion of vorticity through molecular viscosity [12–14].

The first term is responsible for the vortex stretching and can be rewritten as:

$$\omega_j\frac{\partial u_i}{\partial x_j}=\frac{1}{2}\omega_j\left(\frac{\partial u_i}{\partial x_j}+\frac{\partial u_j}{\partial x_i}\right)=\frac{1}{2}\omega_j s_{ij}. \tag{7}$$

If the velocity field is stretched in the direction of the vector of local vorticity (i. e., normal to the corresponding plane of the vortex, (Fig. 2 *a*)), the local vorticity in this direction will increase; the kinetic energy of rotation will be transmitted to higher frequencies and, consequently, to smaller scales, both in space and in time. This vortex stretching mechanism is responsible for the spectral energy flow in the 3D energy cascade.

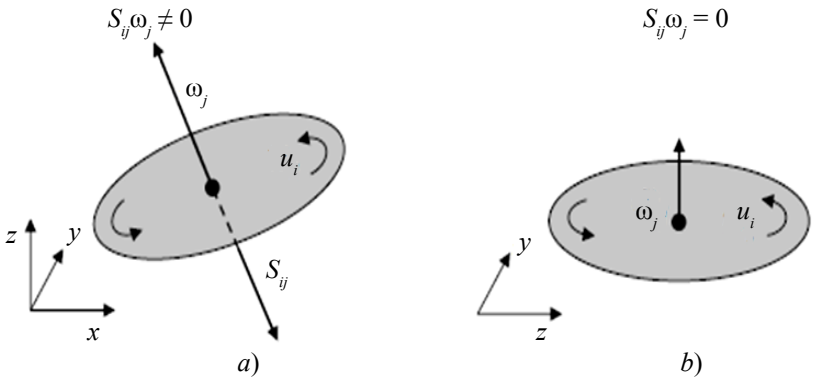

a) *b*)

Fig. 2. 2D and 3D vortex dynamics: *a* — in three-dimensional space, vortices can be stretched in the direction of the local vorticity vector perpendicular to the plane of the vortex; *b* — a vortex in a two-dimensional plane cannot be stretched in the direction perpendicular to this plane

2. Theoretical study of the quasi-2D turbulence structures dynamics. Despite the inherent three-dimensionality of turbulence, many areas of turbulent flow in nature are limited to the vertical direction. Such a flow is called shallow; its large-scale turbulence is often regarded as quasi-two-dimensional. Although 2D turbulence is *contradictio in terminis*, this classification still makes sense, since in practice the dynamics of quasi-2D turbulence structures can differ significantly from "normal" 3D turbulence. This can be shown by referring to the vorticity equation (6). In two dimensions, the velocity vector consists of only one component and is perpendicular to the two-dimensional velocity field everywhere (Fig. 2 *b*). However, stretching of the two-dimensional velocity field is impossible in this perpendicular direction. Consequently, the vortex stretching term vanishes, which leads to:

$$\frac{D\omega_i}{Dt} \equiv \nu \frac{\partial^2 \omega_i}{\partial x_j^2}. \tag{8}$$

The remaining terms show that, theoretically, vorticity is a conserved quantity in 2D. Moreover, it follows from (8) that the total entropy (a measure of the amount of kinetic energy of rotation) is also approximately conserved, with the exception of a small quadratic dissipation term due to viscosity:

$$\frac{D\Omega}{Dt} = \frac{\partial \Omega}{\partial t} + u_j \frac{\partial \Omega}{\partial x_j} = \nu \frac{\partial^2 \Omega}{\partial x_j^2} - \nu \left(\frac{\partial \omega_i}{\partial x_j} \right)^2, \tag{9}$$

where $\Omega = \frac{1}{2}\omega_i^2 \left(s^{-2} \right)$ is the general enstrophy. The principle of enstrophy conservation is similar to the principle of energy conservation: kinetic energy is also conserved, except for the quadratic dissipation term. This result follows from multiplying equation (3) by u_i:

$$\frac{DE_k}{Dt} + \frac{\partial u_i \rho}{\partial x_i} = \frac{\partial}{\partial x_j} \nu u_i \left(\frac{\partial u_i}{\partial x_j} + \frac{\partial u_j}{\partial x_i} \right) - \frac{\nu}{2} \left(\frac{\partial u_i}{\partial x_j} + \frac{\partial u_j}{\partial x_i} \right)^2, \tag{10}$$

where $E_k = \frac{1}{2} u_i^2 \left(m^2 / s^2 \right)$ is the total kinetic energy. Consequently, in the viscosity limit, the energy balance of a two-dimensional flow in time and space is limited by two conservation laws (9) and (10) (instead of only (10) for the 3D case). The stored values E_k and Ω can be written in spectral form:

$$E_k = \frac{1}{2} u_i^2 = \int_0^\infty E_k(k)\, dk, \tag{11}$$

$$\Omega = \frac{1}{2} \omega_i^2 = \int_0^\infty k^2 E_k(k)\, dk. \tag{12}$$

Consequently, Ω can be expressed as the second moment of the spectral distribution of kinetic energy. This means that in a two-dimensional flow, not only the total amount of kinetic energy is preserved, but also its dispersion over all length scales. This fact implies two simultaneous energy cascades. Suppose that the situation with a two-dimensional flow is violated by some forced mechanism with a characteristic length scale, then it is possible to determine the wave number of the impact $k_i \approx L^{-1}$, at which kinetic energy is added to the system. The combination of conservation laws (9) and (10) will cause a redistribution of energy: if kinetic energy is transferred from the k_i scale to higher wave numbers (small scales) $k > k_i$ there must be a compensating energy flow in the direction of lower wavenumbers (large scales) $k < k_i$ in order to maintain dispersion. This energy transfer towards a longer length and time scales is often called backscattering or reverse energy cascade. Consider spectral forms to account for these two simultaneous processes:

$$E(k) = \begin{cases} t^{2/3} k^{-5/3}, \text{if } k < k_i, \\ \eta^{2/3} k^{-3}, \text{if } k > k_i, \end{cases} \tag{13}$$

where τ (m^2/s^3) is the rate of energy dissipation; and η ($s - 3$) is the rate of energy dissipation per unit mass. The existence of an inverse energy cascade in the region implies that after some initial stage, kinetic energy tends to concentrate in large-scale vortices that are stable and do not decay. This principle is often called "self-organization".

As a result of experiments and simulations, specific types of vortices are identified, monopolar, dipole and tripolar vortex formations can be distinguished. These configurations are characterized by the fact that neighboring two-dimensional vortices are able to coexist when they have opposite signs of vorticity. On the other hand, two monopolar two-dimensional vortices with the same sign of vorticity are able to combine and form a new, larger vortex. This phenomenon is known as vortex fusion, which is very noticeable and impressive due to the existence of a reverse energy cascade and a natural analogue of the vortex stretching mechanism, which is responsible for their destruction (Fig. 3).

Research results

Numerical simulation of the quasi-2D turbulence structures dynamics. Shallow turbulent flows exhibit many two-dimensional characteristics, which is called quasi-two-dimensional flow behavior. Although the vortex stretching mechanism is not completely excluded in a shallow flow, it is at least very difficult in vertical measurement. If large-scale quasi-two-dimensional coherent structures are present in a shallow flow, it is often observed that they are quite stable and only weakly dissipative.

A typical quasi-2D problem, characterized by both small 3D turbulence and 2DCS. The latter are clearly distinguishable large-scale structures that remain intact for a relatively long time during passage through the flow region.

Figure 3 shows an example of vortex fusion in 2D modeling of large vortices (LES), it demonstrates graphs of vorticity contours at four stages of the fusion process.

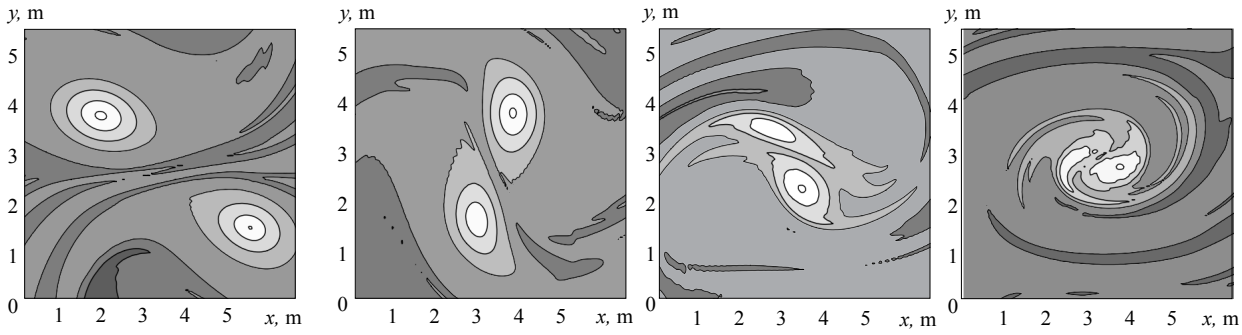

Fig. 3. Results of 2D modeling of the LES vortex fusion due to the existence of an inverse energy cascade: vorticity contours graphs

The term "coherent structures" is used to consider related large-scale turbulent fluid masses that spread uniformly throughout the water depth and contain phase-correlated vorticity, with the exception of a thin bottom boundary layer. In the case of internal instability with transverse shear, separation does not occur: due to the difference in lateral velocities, hydrodynamic instabilities will arise, which will gradually develop into 2DCS. Differences in lateral velocity can be caused, for example, by river mergers or differences in depth and irregularities (complex channels).

Discussion and conclusions. In all cases, the generation and development of 2DCS sequences requires a certain transit time and a certain spatial distance from their source. There are three different regions of 2DCS development, based on the ratio of the distance of the vortex propagation x and the depth of the water H. In the "near field" region ($x / H < 1$) three-dimensional small-scale turbulence prevails, but the average transverse shift present is usually two-dimensional, mainly due to the shape of the geometry. In the "far field" ($x / H > 10$) 2DCS are well developed in the horizontal direction and eventually dissipate due to friction on the bottom. Both medium flow and large-scale turbulence have a pronounced 2D character. The "middle field" ($1 < x / H < 10$) is characterized by the interaction between the growing 2DCS, the average flow and 3D turbulence of the bottom, which leads to the effects of the average secondary flow and 3D effects inside the 2DCS, for example, areas of ascending and descending fluid flows.

The development of two-dimensional turbulence in shallow channels often serves as a good illustration of the processes that control quasi-two-dimensional turbulence, including the merging of individual vortices. 2DCS usually grow when moving in a downstream direction. Eventually the 2DCS will decay in the far field area. The main mechanism controlling this decay is the loss of energy due to friction on the bottom. The larger the size of the vortex relative to the depth, the faster the direct dispersion of its kinetic energy occurs. This fact limits the maximum size of the vortex λ that can be detected in real shallow flows. In cases of very shallow flow, even the formation of 2DCS can already be suppressed by friction against the bottom.

Among the many shallow flow configurations that can contain 2DCS, there are several main types: traces, mesh turbulence, jets and mixing layers. These basic configurations, based on general studies of 3D turbulence, have their analogues in the theory of shallow flow. In three-dimensional cases, the turbulence regime of these types of flows is determined by the ratio between advective and viscous forces, which is expressed by the Reynolds number (Re). In the corresponding quasi-two-dimensional cases, this friction is more important than the molecular viscosity, therefore, the behavior of these shallow flows is determined by the ratio between horizontal transverse shear and bottom friction. These two values, respectively, determine the production and dissipation of kinetic energy of 2DCS.

References

1. Jirka GH Large scale flow structures and mixing processes in shallow flows. *Journal of Hydraulic Research*. 2001;39(6):567–573.

2. GJF van Heijst. Zelf-organisatie van twee-dimensionale stromingen. *Nederlands Tijdschrift voor Natuurkunde*. 1993;59:321–325.

3. Avancha R and Pletcher RH. *Large eddy simulation of the turbulent flow past a backward facing step*. Proceedings of the 38th AIAA Areosciences Meeting and Exhibit. Reno, Nevada, USA; 2000;0542:1–7.

4. Bijlsma AC, Uittenbogaard RE and Blokland T. *Horizontal large eddy simulation applied to stratified tidal flows*. Proceedings of the International Symposium on Shallow Flows. Delft, Netherlands; 2003;559–566.

5. Breugem WP. *The influence of wall permeability on laminar and turbulent flows*. PhD thesis, Delft University of Technology. 2004.

6. Clercx HJH, Zoeteweij ML and GJF van Heijst. *Quasi two-dimensional turbulence in shallow fluid layers: the role of bottom friction and fluid layer depth.* Proceedings of the International Symposium on Shallow Flows, Delft, Netherlands; 2003;87–94.

7. Frohlich J and Rodi W. *Indroduction to Large Eddy Simulation of turbulent flows. Closure Strategies for Turbulent and Transitional Flows* (ed. BE Launder and ND Sandham), Cambridge University Press; 2000;8:267–298.

8. Kadota A, Suzuki K and Uijttewaal WSJ. *The shallow flow around a single groyne under submerged and emerged conditions*. Proceedings of the International Conference in Fluvial Hydraulics (River Flow), Lisboa, Portugal; 2006;673–682.

9. Labeur RJ. *Finite element modelling of transport and non-hydrostatic flow in en- vironmental fluid mechanics*. PhD thesis, Delft University of Technology. 2009.

10. Mittal R and Iaccarino G. Immersed Boundary Methods. *Annual Review of Fluid Mechanics*. 2005;37:239–61.

11. Schnauder I, Sukhodolov A, Uijttewaal WSJ and Labeur RJ. *Field experiments and numerical modelling on shallow mixing layers at a confluence of two parallel streams*. Proceedings of the International Conference in Fluvial Hydraulics (River Flow), Izmir, Turkey; 2008;883–892.

12. Talstra H, Uijttewaal WSJ and Stelling GS. *3D LES computations of a shallow lateral expansion using an immersed boundary method*. Proceedings of the International Conference on Hydroscience and Engineering (ICHE), Philadelphia, USA; 2006.

13. W van Balen. *Large-scale coherent structures in turbulent shallow flows*. Master's thesis, Delft University of Technology; 2005.

14. BC van Prooijen and Uijttewaal WSJ. The relevance of a back-scatter model for depth-averaged flow simulation. *Flow Turbulence Combust*. 2009;82:73–91.

About the Authors:

Sofia V Protsenko, Associate Professor of the Department of Mathematics, Researcher, Taganrog Institute named after A. P. Chekhov (branch) of RSUE (48, Initiative St., Taganrog, 347936, RF), PhD (Physical and Mathematical Sciences), ORCID, rab5555@rambler.ru

Elena A Protsenko, Associate Professor of the Mathematics Department, Leading Researcher, Taganrog Institute named after A. P. Chekhov (branch) of RSUE (48, Initiative St., Taganrog, 347936, RF), PhD (Physical and Mathematical Sciences), ORCID, eapros@rambler.ru

Claimed contributorship:

SV Protsenko: making calculations, drawing conclusions, text preparation, working with sources, making graphic materials. EA Protsenko: basic concept formulation, research objectives and tasks computational analysis, conclusions correction, text revision.

Received 03.04.2023.
Revised 18.05.2023.
Accepted 19.05.2023.

Conflict of interest statement

The authors do not have any conflict of interest.

All authors have read and approved the final manuscript.

Об авторах:

Проценко Софья Владимировна, доцент кафедры математики, научный сотрудник, Таганрогский институт им. А. П. Чехова (филиал) Ростовского государственного экономического университета (347936, РФ, г. Таганрог, ул. Инициативная, 48), кандидат физико-математических наук, ORCID, rab5555@rambler.ru

Проценко Елена Анатольевна, доцент кафедры математики, ведущий научный сотрудник, Таганрогский институт им. А. П. Чехова (филиал) Ростовского государственного экономического университета (347936, РФ, г. Таганрог, ул. Инициативная, 48), кандидат физико-математических наук, ORCID, eapros@rambler.ru

Заявленный вклад соавторов:

С.В. Проценко — проведение расчетов, формулирование выводов, подготовка текста, оформление научной статьи, работа с источниками, оформление графических материалов. Е.А. Проценко — формирование основной концепции, цели и задачи исследования, анализ результатов исследований, корректировка выводов, доработка текста.

Поступила в редакцию 03.04.2023.
Поступила после рецензирования 18.05.2023.
Принята к публикации 19.05.2023.

Конфликт интересов

Авторы заявляют об отсутствии конфликта интересов.

Все авторы прочитали и одобрили окончательный вариант рукописи.

MATHEMATICAL MODELING
МАТЕМАТИЧЕСКОЕ МОДЕЛИРОВАНИЕ

Review article

UDC 519.872.6

https://doi.org/10.23947/2587-8999-2023-7-2-60-72

Simulation of Vehicular Traffic using Macro- and Microscopic Models

Marina A Trapeznikova, Antonina A Chechina, Natalya G Churbanova

Keldysh Institute of Applied Mathematics RAS, 4, Miusskaya Sq., Moscow, Russian Federation

nataimamod@mail.ru

Abstract

To effectively regulate traffic on highways and networks of modern megacities, it is necessary to introduce Intelligent Transport Systems, which include many innovative solutions, in particular, mathematical models for describing the dynamics of traffic flows.

The article is devoted to a brief description of the current state in this area in its development — from the simplest macroscopic and microscopic models that have become classic to modern developments.

Special attention is paid to the original multilane models developed by the authors of the article within both approaches. The macroscopic model is based on the quasigasdynamic approach, while the microscopic one uses the ideology of cellular automata and constitutes a generalization of the Nagel-Schreckenberg model for the multilane case.

The difference in the representation method and the mathematical apparatus for the mac-roscopic and microscopic description of traffic flows is briefly described, followed by the review of the main models at different stages of their development, presented by foreign and Russian authors.

Special attention is paid to the three-phase theory of Boris Kerner and models built in the framework of this theory.

Examples of modern software for traffic modeling are given.

The original quasigasdynamic model of traffic flows, which uses the continuum approximation and is constructed by analogy with the well-known model of gas dynamics, is briefly described. Due to the introduction of the lateral speed, the model is generalized to the multilane case.

An original microscopic model based on the cellular automata theory and representing a generalization of Nagel-Schreckenberg model for the multilane case is described. The model has been further developed by taking into account various driving strategies and behavioral aspects.

The article presents a brief overview of the state of the art in the field of mathematical modeling of traffic flows, as well as original macroscopic and microscopic models developed by the authors for the case of multilane traffic.

Keywords: mathematical modeling, traffic flows, microscopic and macroscopic models, cellular automata, multilane traffic.

For citation. Trapeznikova MA, Chechina AA, Churbanova NG. Simulation of vehicular traffic using macro- and microscopic models. *Computational Mathematics and Information Technologies.* 2023;7(2):60–72. https://doi.org/10.23947/2587-8999-2023-7-2-60-72

Обзорная статья

Моделирование движения автомобильного транспорта с использованием макро- и микроскопических моделей

М.А. Трапезникова, А.А. Чечина, Н.Г. Чурбанова

Институт прикладной математики им. М. В. Келдыша РАН, Российская Федерация, г. Москва, Миусская пл., 4

nataimamod@mail.ru

Аннотация

Для эффективного регулирования дорожного движения на магистралях и сетях современных мегаполисов необходимо внедрение Интеллектуальных транспортных систем, включающих в себя множество инновационных решений, в частности, математические модели описания динамики транспортных потоков.

Статья кратко описывает современное состояние транспортных систем и их развитие: от простейших макроскопических и микроскопических моделей, ставших классическими, до современных разработок.

Особое внимание уделяется разработанным авторами статьи оригинальным многополосным моделям в рамках обоих подходов. Макроскопическая модель основана на квазигазодинамическом подходе, а микроскопическая использует идеологию клеточных автоматов и является обобщением модели Нагеля-Шрекенберга на многополосный случай.

Кратко описывается различие в способе представления и математическом аппарате для макроскопического и микроскопического описания транспортных потоков. Дальше следует обзор основных моделей на разных этапах их развития, принадлежащих зарубежным и российским авторам.

Рассматривается трехфазная теория Бориса Кернера и модели, построенные в рамках этой теории.

Приводятся примеры современного программного обеспечения для транспортного моделирования.

Кратко описывается оригинальная квазигазодинамическая модель транспортных потоков, использующая приближение сплошной среды и построенная по аналогии с известной моделью газовой динамики. Благодаря введению скорости перестроения модель обобщена на многополосный случай.

Описывается оригинальная микроскопическая модель, основанная на теории клеточных автоматов, которая является обобщением модели Нагеля-Шрекенберга на многополосный случай. Модель получила дальнейшее развитие путем учета различных водительских стратегий и поведенческих аспектов.

В статье представлен краткий обзор состояния в области математического моделирования транспортных потоков, а также представлены оригинальные макроскопическая и микроскопическая модели, разработанные авторами для случая многополосного движения.

Ключевые слова: математическое моделирование, транспортные потоки, микроскопические и макроскопические модели, клеточные автоматы, многополосное движение.

Для цитирования. Трапезникова М.А., Чечина А.А., Чурбанова Н.Г. Моделирование движения автомобильного транспорта с использованием макро- и микроскопических моделей. *Computational Mathematics and Information Technologies.* 2023;7(2):60–72. https://doi.org/10.23947/2587-8999-2023-7-2-60-72

Introduction. World experience shows that in large cities it is necessary to introduce an Intelligent Transport System (ITS) for the effective construction of new transport networks with a complex multi-level structure, as well as for the operational regulation of traffic on them. ITS is a set of systems based on information, communication and management technologies embedded in vehicles and road infrastructure. It combines many innovative solutions: from mathematical models and methods of traffic description to decision support systems for traffic management, not to mention technical and engineering aspects.

The proposed article is devoted to a brief description of classical and modern trends in the field of mathematical modeling of motor traffic flows. Two main directions in this field are considered: macroscopic and microscopic models.

An overview of ready-made software tools for modeling the flows of road transport is also provided.

Special attention is paid to the original multiband models developed by the authors of the article within the framework of both approaches. The macroscopic model considers the transport flow as the movement of a weakly compressible gas and uses the ideology of kinetically consistent difference schemes and a quasi-gas dynamic (QGD) system of equations [1]. Recently, modern ultra-high-performance computing technology has appeared and the popularity of microscopic models has increased significantly. However, due to their cost-effectiveness, macroscopic models do not lose relevance in determining the main characteristics of road traffic necessary for transport planning.

The original microscopic model is based on the theory of cellular Automata (CA), adapted to modeling traffic flows on multi-lane highways and the main elements of the road network (RN) [2]. This approach allows you to take into account many technical parameters of cars and features of driver behavior. Such models can include a detailed description of the movement of cars at intersections and in places of narrowing of roads, overtaking and rebuilding, providing a high degree of compliance with the model of the real situation.

Both proposed approaches have internal parallelism and are suitable for fast and efficient calculations on supercomputers, even for modeling large-scale road networks with several million vehicles.

1. State of the research area. Currently, the theory of traffic flows is an independent scientific direction, which is based on the so-called physics of traffic flows — mathematical and simulation modeling. Mathematical traffic models are used both in research and in practice to justify planning and management decision-making in the transport industry.

Modeling of motor traffic flows began to develop in the USA since the 30s of the 20th century. But due to the increasing volume of transportation everywhere, as well as increasingly accessible computerization, in the 1990s this area began to attract more and more attention. Two main directions of this development have emerged: macroscopic modeling and microscopic modeling, which differ in the way they represent real reality, and in their mathematical description.

In the first case, traffic uses the approximation of a continuous medium and considers the flow of cars similarly to the flow of a weakly compressible gas. The main studied values are the density field (the number of cars per unit length of the road and per lane) and the average speed field, as well as the flow (the number of cars that have passed a given point on the road per unit time). The model consists of a system of partial differential equations and is solved by well-known finite difference methods.

In the case of microscopic modeling, the subject of the study is the movement of one individual car and its interaction with other participants in the movement, the reaction to the environment and its possible changes in this situation.

Such models are described, as a rule, by ordinary differential equations, for the solution of which there are also known numerical methods, for example, the Runge-Kutta method of the second or fourth orders.

Using macroscopic models, it is convenient to describe a fairly dense flow of vehicles when all drivers are forced to adhere to the same strategies and drive at approximately the same speed. With the help of such models, general patterns of traffic are usually investigated. Microscopic models allow us to consider in more detail the movement of the transport unit "driver-car". This takes into account not only the characteristics of the car itself, but also the behavioral characteristics of the driver, and perhaps even his psychological type. With the help of such models, it is possible to describe not only a sparse flow, but also a dense flow of vehicles thanks to today's computing capabilities.

One of the first simplest macroscopic models is the Lighthill-Witham-Richards (LWR) model [3]. It is characterized by a single dynamic equation, which is a consequence of the law of conservation of the number of cars:

$$\frac{\partial \rho}{\partial t} + \frac{dQ_e(\rho)}{d\rho}\frac{\partial \rho}{\partial x} = 0,$$

where ρ is the automobile flow density; Q_e is the equilibrium flow.

In this model, it is assumed that the flow or average velocity is always in local equilibrium relative to the actual density and instantly changes with it, that is, unreasonably high accelerations occur: $V = V_e(\rho)$, $Q = Q_e(\rho)$. Models of this type, due to the lack of finite acceleration, cannot describe the growth of traffic waves and the instability of the traffic flow.

At the next stage, models appeared that include, in addition to the continuity equation, a second dynamic equation — the acceleration equation, which describes local acceleration as a function of density, velocity, their gradients and other

possible external factors. Such a class of models is known as a class of *second-order models*, in contrast to the LWR models, which are called *first-order models*.

The book [4] presents the Payne model [5], for which the acceleration equation has the form:

$$\frac{\partial V}{\partial t} + V\frac{\partial V}{\partial x} = \frac{V_e(\rho) - V}{\tau} + \frac{V_e'(\rho)}{2\rho\tau}\frac{\partial \rho}{\partial x}$$

with constant relaxation time and the Kerner-Conheuser model [6]:

$$\frac{\partial V}{\partial t} + V\frac{\partial V}{\partial x} = \frac{V_e(\rho) - V}{\tau} - \frac{c_0^2}{\rho}\frac{\partial \rho}{\partial x} + \frac{\eta}{\rho}\frac{\partial^2 V}{\partial x^2}.$$

Here an analogue of sound velocity $\pm c_0$ and dynamic viscosity η are introduced. This model is purely phenomenological.

The Payne model and many subsequently proposed second-order models, including those with diffusion corrections, have some disadvantages. In particular, with strong spatial inhomogeneities of the initial conditions, negative values of speeds and densities exceeding the maximum permissible may occur, and also, according to these models, cars behind have a noticeable effect on the movement of the car, which is unrealistic in the case of one lane. In the future, a lot of effort was spent on making macro models anisotropic, that is, according to these models, cars should respond only to the situation in front of them. The most well-known models that solve these problems are the Aba-Raskla [7] and Zang [8] models.

Within the framework of the microscopic approach, the simplest model was the model of following the leader [9], which could reproduce only the basic details and features of traffic flows. The simplest representative of this class of models is a continuous-time model of optimal speed:

$$\dot{v} = \frac{v_{\text{opt}}(s) - v}{\tau},$$

which describes the adaptation of the actual speed of the car v to the optimal speed $v_{\text{opt}}(s)$ for the time scale set by the *adaptation time* τ. Its analogue is the discrete-time Newell model [10]:

$$v_\alpha(t + \Delta t) = v_{\text{opt}}(s(t)) = \min\left(v_0, \frac{s}{\Delta t}\right),$$

$$x_\alpha(t + \Delta t) = x_\alpha(t) + \frac{v_\alpha(t) + v_\alpha(t + \Delta t)}{2}\Delta t.$$

Another interesting example of the simplest model of following the leader is the Pipes model [11], based on the safe driving rule developed in California: “the rule for following the vehicle in front at a safe distance is to keep the distance between your car and the car in front of you no less than the shortest length of the car on the every ten miles an hour of the speed at which you are traveling”. Translated into mathematical language, this model can be formulated as follows:

$$s_i(t)_{\min} = \frac{l_i}{0.44}\dot{x}_i(t) + l_{i-1},$$

where $s_i(t)$ is the gap between the current and the cars in front, l_i is the length of the i-th car.

The Intelligent Driver Model (IDM) was a further development of the models of following the leader. Continuous-time IDM is the simplest complete and trouble-free model, giving realistic acceleration profiles and plausible behavior in all single-lane traffic situations. The most well-known model of this class is the Driver model [12], which demonstrates realistic behavior during acceleration and braking.

Separately, it should be noted the microscopic Prigogine models based on the kinetic Boltzmann theory [13, 14]. The model introduces a distribution function type function in kinetic theory $f(x,u,t)$, which denotes the number of cars located

at time t at a point in space between x and $x+dx$ and having a speed between u and $u+du$. The concept of the desired distribution is also introduced, which is an idealization of the goal to which this traffic flow aspires. The real and desired distributions may differ for many different reasons: road conditions, weather conditions, interaction with other cars, etc. By themselves, these reasons may also change over time and, consequently, the real distribution will approach the desired for some relaxation time. Based on these assumptions , an equation of the Boltzmann equation type is written for the real distribution:

$$\frac{\partial f}{\partial t} + u\frac{\partial f}{\partial x} = \left(\frac{\partial f}{\partial t}\right)_{rel} + \left(\frac{\partial f}{\partial t}\right)_{int},$$

where $\left(\frac{\partial f}{\partial t}\right)_{rel}$ is the transition of the real distribution to the desired one in the absence of interaction of cars, $\left(\frac{\partial f}{\partial t}\right)_{int}$ is the change in the real distribution arising from interactions between cars.

The members on the right side can be set in various ways, the distribution function can also have a more complex form. Due to this, there are a sufficient number of varieties of this model: for example, in the Paveri-Fontana model [15], in addition to the real one, the “desired” speed of this car is introduced. Prigozhin’s approach was subsequently developed in the works of Helbing et al. [16, 17].

In the future, models of both macro- and microscopic types developed in the direction of taking into account the human factor. There were models with a safe speed of movement [18], non-equilibrium models with realistic acceleration [19], models describing traffic at complex road junctions [20, 21], describing mixed flows consisting of heterogeneous vehicles [22, 23], etc.

Modern studies of the dynamics of traffic flows are mainly on the path of complicating existing models. One can cite, for example, publications [24–26] devoted to macroscopic models of hydrodynamic type.

In the field of microscopic modeling, a separate specific direction has been rapidly developing recently, using the theory of cellular automata. These models can be divided into two groups: deterministic and stochastic. An example of a deterministic model is the 184 Wolfram Rule. This model belongs to the class of elementary cellular automata. This is a group of 256 (2^{2^3}) one-dimensional models with the number of neighbors 3, they can be found in the Wolfram Atlas on the website [27].

One of the first realistic stochastic models of traffic flows is the well—known Nagel-Schreckenberg model [28]. This model requires detailed consideration, since many modern models developed by researchers around the world are based on it.

The route in the Nagel-Schreckenberg model is represented as a one-dimensional lattice, each cell of which can be either empty or contain a particle denoting a vehicle. The particles move from one cell to another (free) in one direction. In the case of single-lane traffic, they cannot overtake each other. The whole system is the space, time, speed are discrete. The speed shows how many cells the car moves in one time step. Acceleration occurs instantly between steps. At each time step, the system status is updated according to certain rules:

1. Acceleration. The speed of i-th car is increased by one if the maximum allowed speed is not reached: $V_i \to \min(V_i+1, V_{\max})$.

2. Deceleration. The speed of the car is reduced by one if there is a threat of collision with the car in front: $V_i \to \min(V_i, D_i - 1)$, where D_i is the distance to the car in front.

3. Random disturbances. If the speed of the car is positive, then it can be reduced by one with some probability: $V_i \to \max(V_i - 1, 0)$ with probability p.

4. Motion. Each car moves forward by the number of cells corresponding to its new speed after completing the previous steps: $X_i \to X_i + V_i$.

To simplify the recording, we assume that speed and distance are measured in cells, and time is dimensionless. For this reason, the values can be added, subtracted and compared with each other.

To date, there are more complex and detailed CA models. The article [29] presents an interesting generalization of the theory of cellular automata for the case of maritime transport in application to maritime transport. In this case, the space discretization rules are supplemented by mapping rules. The authors of the article [30] investigate the capacity of a motorway with two entrances and one intermediate exit between them also using a model of cellular automata. The aim of the research is to maximize the throughput of the system by establishing the optimal flow for two entrances. The paper [31] presents a numerically reliable model of cellular automata aimed at accurately reproducing deceleration and acceleration in accordance with realistic reactions of drivers when considering vehicles with different deceleration capabilities.

It is possible to model large road networks using cellular automata. As an example, we will give a model created by A. P. Buslaev [32] and colleagues at MADI. Their approach is based on ring structures of cellular automata with common cells, for which there is competition. Similar ring structures may have different topologies, the movement along them simulates the movement along the UDS with intersections.

In the early 2000s, an alternative theory of traffic flows appeared, namely, Boris Kerner's three-phase theory was proposed. The first works date back to 2002, however, the main provisions of the theory were formulated later in books [33] and [34]. Unlike previous theories, where two main phases of traffic flows (free movement and dense flow) were considered, here the author considers the existence of three phases: free flow, synchronized movement and a wide moving cluster, that is, two phases are distinguished in a dense flow. This makes it possible to predict and explain the empirical properties of the transition from free to dense traffic, as well as the features of the resulting spatial-temporal traffic structures. The author himself calls his theory empirical, qualitative, based on observational data, which allows the creation of various mathematical models within the framework of this theory. The author and other researchers have created models based on cellular automata [35, 36]. In particular, the Kerner-Klenov model [37, 38] introduces the concepts of acceleration and synchronization distance to correspond to the theory of three phases. Due to the mathematical description of stochastic acceleration with delay and the adaptation effect inside the synchronized flow, in the developed model, the transition from free to dense flow is an $F \rightarrow S$ transition (according to Kerner's theory of three phases) in a metastable free flow, which is observed in all empirical data. Kerner and Klenov also proposed a deterministic model [39]. In [40, 41], variants of macroscopic models implementing the three-phase theory are proposed.

In general, models corresponding to Kerner's three-phase theory are characterized by the ability to describe instabilities that inevitably arise in real traffic. Such models demonstrate one of the main theses of the theory of three phases: transitions between phases from free flow to synchronized and from synchronized to wide moving clusters can occur under the influence of random processes and at different values of the flow, and not be tied clearly to its specific value of the flow. Most of the models that exist today do not have this property.

Currently, the theory of three phases is gaining more and more followers, as evidenced by many publications, for example, [42, 43]. The article [44] presents a recently modified KKW (Kerner-Klenov-Wolf) model, which includes various types of vehicles. Variable sensitivity of the driver to speed fluctuations is introduced. Conclusions are drawn about the effect of changes in the speed of one or more vehicles on the overall flow rate at different intensity of the initial flow.

Domestic developments in the field of transport modeling correspond to the main global trends. The work on Buslaev networks carried out at MADI was mentioned above, stochastic models are also studied there, as well as the application of queuing theory to solve transport problems. MIPT, together with foreign colleagues, actively conducts research based on the theory of three Kerner phases, develops models of cellular automata [35, 37–39], hydrodynamic models [45, 46], simulation models, develops numerical methods for finding equilibria in large transport networks [47]. It should be noted the work of a team of authors from Lomonosov Moscow State University [48, 49], dedicated to the organization of traffic and the study of flow instability based on hydrodynamic models. Solving problems of optimal control of traffic flows at the RN [50], including using genetic algorithms, is actively engaged in the FRS "Informatics and Managemen" of the Russian Academy of Sciences. A two-dimensional quasi-gas dynamic model of transport flows and a multi-band CA model developed at the Keldysh IAM of the Russian Academy of Sciences will be presented below.

2. Software for modeling traffic flows. There are a huge number of software solutions for transport modeling. The packages reviewed in the collection [51] continue to evolve. The most well-known among commercial packages are:

– PTV Vision Traffic Suite [52];

– Aimsun (TSS-Transport Simulation Systems) [53].

There is also free and open source software, for example:

– MATSim [54, 55];

– Eclipse SUMO [56, 57].

PTV Vision Traffic Suite includes products:

– PTV Visum (strategic planning, calculation of transport demand, analysis of the transport network of cities, megacities, countries and regions based on macro modeling);

– PTV Vissim (traffic simulation, hypothesis testing on traffic management);

– PTV Viswalk (simulation of pedestrian flows, planning of mass events, development of evacuation plans);

– PTV Vistro (work at the network level, taking into account several types of intersections at once — regulated and unregulated, optimization of regulation modes).

Aimsun has now evolved from a myostimulator into a fully integrated traffic simulation application that combines ride demand forecasting, macroscopic functions and a mesoscopic-microscopic hybrid simulator.

PTV and Aimsun products are implemented for the Windows operating system.

MATSim is based on a multi-agent approach for large-scale transport modeling, consists of several modules that can be combined or used separately. Modules can be replaced with custom implementations.

SUMO is an academic development for modeling transport systems involving cars, public transport and pedestrians. The programs are based on a microscopic approach. SUMO includes many auxiliary tools that automate the main tasks and allow you to import a network, calculate a route, visualize, as well as calculate emissions of pollutants and calculate noise. SUMO can be supplemented with customizable models and provide interfaces for remote control of modeling. The distinctive features of SUMO are portability and extensibility. Versions of the package have been developed for a number of popular operating systems, in particular, for Linux.

It should be noted that there are also software packages for implementing the concept of BIM, 3D modeling and creating digital counterparts in the field of integrated design of roads and transport infrastructure, in particular, products of Bentley Systems [58], including OpenRoads and OpenCities Planner.

Thus, the world has already accumulated quite a lot of experience in modeling traffic flows, effective software tools have been developed that become an integral part of both short-term and long-term transport planning, and lay the foundation for intelligent transport systems.

3. Quasi-gas dynamic model of transport flows. As mentioned above, many macroscopic models describe the movement of vehicles by analogy with the gas dynamic flow. Consequently, the basis of the models is a system of equations of gas dynamics. The authors of this article some time ago developed a two-dimensional multiband macroscopic model for describing traffic flows, constructed by analogy with the QGD system of equations [59]. The QGD system was created to describe gas-dynamic flows in a wide range of Mach numbers, including well-proven in modeling substantially subsonic flows. Therefore, it was natural to use it when constructing a model of traffic flows in the approximation of a continuous medium. The equations of the QGD system, unlike traditional gas-dynamic equations, contain additional diffusion terms in the right part. In the case of transport flows, they can be considered as a natural viscosity, which allows smoothing solutions at large gradients and implementing numerical algorithms by end-to-end counting, without distinguishing features.

A distinctive feature of the multiband model is the presence in the system of an equation for the "transverse" component of the velocity, which makes sense of the speed of lane-to-lane rearrangement. Therefore, the model can be used to simulate traffic on the highway, taking into account its real geometry. Multibandness and the change in the number of bands is taken into account by specifying a specific computational domain, and not using sources in the right-hand sides of the equations. A detailed description of the QGD model of transport flows is contained in [1, 60, 61]. The system of equations of the proposed model looks like this:

$$\frac{\partial \rho}{\partial t} + \frac{\partial}{\partial x}(\rho U) + \frac{\partial}{\partial y}(\rho V) = \\ = \frac{\partial}{\partial x}\frac{\tau_x}{2}\left(\frac{\partial}{\partial x}\left(\rho U^2 + P_x\right) - f_x + \frac{\partial}{\partial y}(\rho UV)\right) + \\ + \frac{\partial}{\partial y}\frac{\tau_y}{2}\left(\frac{\partial}{\partial y}\left(\rho V^2 + P_y\right) - f_y + \frac{\partial}{\partial x}(\rho UV)\right), \tag{1}$$

$$\frac{\partial \rho U}{\partial t} + \frac{\partial}{\partial x}\left(\rho U^2 + P_x\right) - f_x + \frac{\partial}{\partial y}(\rho UV) = \\ = \frac{\partial}{\partial x}\frac{\tau_x}{2}\left(\frac{\partial}{\partial x}\left(\rho U^3 + 3P_x U\right) - 3f_x U\right) + \frac{\partial}{\partial y}\frac{\tau_y}{2}\left(\frac{\partial}{\partial y}\left(\rho UV^2 + P_y U\right) - f_y U\right) + \\ + \frac{\partial}{\partial x}\frac{\tau_x}{2}\left(\frac{\partial}{\partial y}\left(\rho U^2 V + P_y V\right) - f_y V\right) + \frac{\partial}{\partial y}\frac{\tau_y}{2}\left(\frac{\partial}{\partial x}\left(\rho U^2 V + P_x V\right) - f_x V\right), \tag{2}$$

$$\frac{\partial \rho V}{\partial t} + \frac{\partial}{\partial y}\left(\rho V^2 + P_y\right) - f_y + \frac{\partial}{\partial x}(\rho UV) = \\ = \frac{\partial}{\partial x}\frac{\tau_x}{2}\left(\frac{\partial}{\partial x}\left(\rho U^2 V + P_x V\right) - f_x V\right) + \frac{\partial}{\partial y}\frac{\tau_y}{2}\left(\frac{\partial}{\partial y}\left(\rho V^3 + 3P_y V\right) - 3f_y V\right) + \\ + \frac{\partial}{\partial x}\frac{\tau_x}{2}\left(\frac{\partial}{\partial y}\left(\rho V^2 U + P_y U\right) - f_y U\right) + \frac{\partial}{\partial y}\frac{\tau_y}{2}\left(\frac{\partial}{\partial x}\left(\rho V^2 U + P_x U\right) - f_x U\right). \tag{3}$$

The following designations are used here: ρ is the traffic flow density; U is the longitudinal, along the road, speed component; V is the transverse speed component (speed of rebuilding); $P = \lambda\rho^{\beta}/\beta$ is the pressure analog; $f = a\cdot\rho$ is the force of acceleration or deceleration, where $a = (U_{eq} - U)/T$ is the acceleration.

The equilibrium longitudinal velocity is calculated according to the parabolic fundamental diagram:

$$U_{eq} = U_{free}(1 - \rho/\rho_{jam})/T. \tag{4}$$

$T = t_0(1 + r\rho/(\rho_{jam} - r\rho))$ can be considered as a relaxation time. The equations are also supplemented by a number of phenomenological constants.

The above system contains an equation for the transverse velocity, similar to the equation of the longitudinal velocity. However, the test calculations have shown that it is more convenient to use an algebraic equation instead of the differential equation (3):

$$V_1 = k_u\rho\frac{\partial U}{\partial y} - k_\rho U\frac{\partial \rho}{\partial y} + k_{des}\frac{U^2}{(x_{des} - x)^2}(y_{des} - y),$$

where the first term corresponds to the driver's desire to drive at a higher speed, the second — the desire to drive in a lane with a lower density and the third — to achieve a certain goal. Here k_u, k_ρ, k_{des} are the constants; (x_{des}, y_{des}) are the coordinates of the driver's target. The use of equation (4) simplifies the solution process and increases the stability of the difference scheme.

It should be noted that in some cases of an inhomogeneous, but not very complex route, qualitatively correct results can be obtained using a one-dimensional CGD model [60, 62]:

$$\frac{\partial \rho}{\partial t} + \frac{\partial Q}{\partial x} = \frac{\partial}{\partial x}\frac{\tau}{2}\frac{\partial\left(\frac{Q^2}{\rho} + P\right)}{\partial x} + F_\rho, \tag{5}$$

$$\frac{\partial Q}{\partial t} + \frac{\partial}{\partial x}\left[\frac{Q^2}{\rho} + P\right] = f + \frac{\partial}{\partial x}\frac{\tau}{2}\frac{\partial\left(\frac{Q^3}{\rho^2} + P\frac{Q}{\rho}\right)}{\partial x} + F_U. \tag{6}$$

In these equations, written in conservative form, the traffic flow is: $Q = \rho \cdot U$. The source terms are on the right side F_ρ and F_U are equal to zero on a homogeneous road and are not equal to zero if there are entrances or exits from the main road or there is a change in the number of lanes.

The proposed models are numerically implemented using finite-difference schemes. The system is approximated by explicit second-order difference schemes in space. Note that the structure of an explicit computational algorithm fits well on the architecture of multiprocessor computing systems with distributed memory and, if necessary, a large amount of calculations can be parallelized with sufficiently high efficiency [62, 63].

4. Multiband model based on the theory of cellular automata. The second model proposed by the authors earlier and which is promising for implementation in an interactive program is a multiband model using the ideology of cellular automata. A detailed description of this model is given in [2, 60, 64]. Here we will describe it briefly.

The calculated area is a two-dimensional lattice. The number of cells in the transverse direction corresponds to the number of lanes on the considered section of the highway, and the width of the cell is equal to the width of the real road lane (Fig. 1).

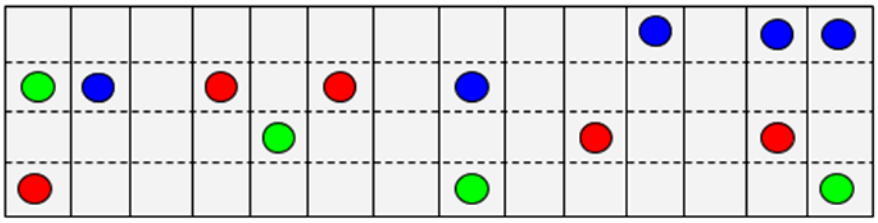

Fig. 1. Calculation area in the CA model

The number of cells along the road depends on the specific task, taking into account that the longitudinal size of the cell is equal to the average length of the car plus the width of the gap between the cars at maximum flow density, that is, in a “traffic jam”. In the literature, a length of 7.5 m is given as the standard cell size for passenger cars. The time in such models is discrete, the system is updated at each time step. With standard calculations, this step is equal to 1 s, although in more developed and realistic models this value may vary. At any given time, the grid cells can be in one of two states: the cell is either occupied (which corresponds to the presence of a car in it), or empty. Figure 1 shows the state of the computational domain at some point in time. The different color of the movement elements corresponds to different selected goals. At the next moment in time, the state of the cells is updated in two stages according to certain rules.

At the first stage, each driver checks whether he wants to change lanes and has the opportunity to do so. It is rebuilt if:

– it is necessary to achieve his goal (for example, to drive up to the exit from the road) or it is necessary to go around an obstacle;

– he gets an advantage after rebuilding — goes at a higher speed or with a lower density;

– there is a possibility for rebuilding — rebuilding is allowed and the neighboring cell is empty;

– the security conditions have been met.

After the chosen decision regarding the realignment and the action performed in accordance with it, forward movement takes place along the selected lane according to the Nagel-Schreckenberg single-lane traffic rules [28] given in section 1 of this article.

It should be noted that the initial, simplest version of the rebuilding strategy is described here. In more complex modifications of the model [65], the rules for rebuilding depend on the type of road element (X-shaped intersection, T-shaped intersection, U-turn, narrowing/widening section, etc.), road signs and markings. Various driving strategies and behavioral aspects are also taken into account. The concepts of “aggressive”, “cautious”, “polite” driver are introduced into the model. The percentages of a particular type of driver may change during the calculation process. A “slow start” algorithm has also been developed.

To implement the model, a CAM-2D software package has been developed [66], which has an integrated web interface and a visualization module in addition to computing modules. The parallel version is designed for calculations of road networks on the CPU of multiprocessor systems using MPI technology [62, 63].

Conclusion. The article presents an overview of works in the field of traffic flow modeling, covering a wide range of approaches — macro- and microscopic models, as well as models of cellular automata. Special attention is paid to the original developments of the authors of the article both in the field of macroscopic and microscopic (namely, cellular automata) modeling. Both developments have their advantages, such as, for example, the ability to simulate the movement of motor transport taking into account the actual geometry of the road, even in the case of macro modeling. The models have been repeatedly tested in calculations and, in addition, allow for effective implementation on supercomputers, since they have internal parallelism. The latter property is a special advantage in the conditions of traffic simulation on transport networks of multimillion megacities.

References

1. Sukhinova AB, Trapeznikova MA, Chetverushkin BN, et al. Two-dimensional macroscopic model of traffic flows. *Mathematical modeling*. 2009;21(2):118–126. (In Russ.).

2. Trapeznikova MA, Furmanov IR, Churbanova NG, etc. Modeling of multi-lane vehicle traffic based on the theory of cellular automata. *Mathematical modeling*. 2011;23(6):133–146. (In Russ.).

3. Lighthill MJ, Witham GB. On kinematic waves (Part II): A theory of traffic flow on long crowded roads. *In Proceedings of Royal Society*. Ser. A. 1955;229:317–345.

4. Treiber M, Kesting A. *Traffic flow dynamics. Data, models and simulation*. Berlin-Heidelberg: Springer; 2013. 503 p.

5. Payne H. Models of freeway traffic and control. In: Bekey, G.A. (ed.) *Mathematical Models of Public Systems. Simulation Council, La Jolla, CA*. 1971;1:51–61.

6. Kerner B, Konhäuser P. Structure and parameters of clusters in traffic flow. *Physical Review E*. 1994;50:54–83.

7. Aw A, Rascle M. Resurrection of "second order models" of traffic flow. *SIAM Journal on Applied Mathematics*. 2000;60:916–938.

8. Zhang HM. A non-equilibrium traffic model devoid of gas-like behavior. *Transportation Research*. B. 2002;36(3):275–290.

9. Gazis DC, Herman R, Rothery RW. Nonlinear follow-the-leader models of traffic flow. *Operations Research*. 1961;9(4):545–567.

10. Newell GF. A simplified car-following theory: a lower order model. *Transportation Research. Part B: Methodological.* 2002;36:195–205.

11. Pipes LA. An operational analysis of traffic dynamics. *Journal of Applied Physics.* 1954;24(3):274–281.

12. Treiber M, Hennecke A, Helbing D. Congested traffic states in empirical observations and microscopic simulations. *Physical Review E*. 2000;62(2):1805–1824.

13. Progogine I, Andrews FC. A Boltzmann like approach for traffic flow. *Operations Research.* 1960;8(6):789–797.

14. Prigogine I, Herman R. *Kinetic Theory of Vehicular Traffic*. Amsterdam, Elsevier; 1971.

15. Paveri-Fontana S.L. On Boltzmann like treatments for traffic flow. *Transportation Research*. 1975;9:225–235.

16. Helbing D., Treiber M. Enskog equations for traffic flow evaluated up to Navier-Stokes order. *Granular Matter*. 1998;1:21–31.

17. Treiber M, Hennecke A, Helbing D. Derivation, properties, and simulation of a gas-kinetic-based, non-local traffic model. *Physical Review E*. 1999;59(1):239–253.

18. Gipps PG. A behavioural car-following model for computer simulation. Transportation *Research Part B: Methodological.* 1981;15(2):105–111.

19. Kesting A, Treiber M, Helbing D. Enhanced Intelligent Driver Model to access the impact of driving strategies on traffic capacity simulations. *Philosophical Transactions of the Royal Society A*. 2010;368:4585–4605.

20. Su Z, Liu S, Deng W, et al. Transportation dynamics on networks of heterogeneous mobile agents. *Physics Letters A*. 2019;523:1379–1386.

21. Yao W, Jia N, Zhong S, et al. Best response game of traffic on road network of non-signalized intersections. *Physica A: Statistical mechanics and its applications*. 2018;490:P.386–401.

22. Dong P, Wang X, Yun L, et al. Research on the characteristics of mixed traffic flow based on an improved bicycle model simulation. *Simulation, SAGE Publications*. 2018;94(5):451–462.

23. Zeng JW, Qian YS, Wang H, et al. Modeling and simulation of traffic flow under different combination setting of taxi stop and bus stop. *Modern Physics Letters B*. 2018;32(25):1850301.

24. Zhou J, Zhang HL, Wang CP, et al. A new lattice model for single-lane traffic flow with the consideration of driver's memory during a period of time. *International Journal of Modern Physics C*. 2017;28(7):1750086.

25. Jin D, Zhou J, Zhang HL, et al. Lattice hydrodynamic model for traffic flow on curved road with passing. *Nonliear Dynamics*. 2017;89(1):107–124.

26. Kaur R, Sharma S. Analysis of driver's characteristics on a curved road in lattice model. *Physica A: Statstical Mechanics and its Applications.* 2017;471:59–67.

27. The Wolfram atlas of simple programs [Electronic resource]. URL: http://atlas.wolfram.com/ (date of application: 18.05.2023).

28. Nagel K, Schreckenberg M. A cellular automaton model for freeway traffic. *Journal de Physique I France*. 1992:2221–2229.

29. Qi L, Zheng Z, Gang L. A cellular automation model for ship traffic flow in waterways. *Physica A: Statistical Mechanics And Its Applications*. 2017;471:705–717.

30. Chen J, Jiang R, Lin L. Assigning on ramp flows to maximize capacity of highway with two on-ramps and one off-ramp in between. *Physica A: Statistical Mechanics And Its Applications*. 2017;465:347–357.

31. Guzman H.A., Larraga M.E., Alvarez-Icaza L., et al. A cellular automata model for traffic flow based on kinetics theory, vehicles capabilities and driver reactions. *Physica A: Statistical Mechanics And Its Applications*. 2018;491:528–548.

32. Bugaev A.S., Buslaev A.P., Kozlov V.V. et al. Generalized transport and logistics model as a class of dynamic systems. *Mathematical modeling*. 2015;27(12):65–87. (In Russ.).

33. Kerner BS. *The Physics of Traffic*. Berlin: Springer; 2004.

34. Kerner BS. *Introduction to Modern Traffic Flow Theory and Control*. Berlin: Springer; 2009.

35. Kerner BS, Klenov SL, Wolf DE. Cellular automata approach to three-phase traffic theory. *Journal Physics A: Mathematical and General*. 2002;35:9971–10013.

36. Jiang R, Wu QS. Spatial-temporal patterns at an isolated on-ramp in a new cellular automata model based on three-phase traffic theory. *Journal Physics A: Mathematical and General.* 2004;37:8197–8213.

37. Kerner B, Klenov S, Schreckenberg M. Simple cellular automaton model for traffic breakdown, highway capacity, and synchronized flow. *Physical Review E*. 2011;84:046110.

38. Kerner B, Klenov S, Hermanns G, et al. Effect of driver over-acceleration on traffic breakdown in three-phase cellular automaton traffic flow models. *Physica A: Statistical Mechanics and its Applications*. 2013;392(18):4083–4105.

39. Kerner B.S., Klenov S.L. Deterministic microscopic three-phase traffic flow models. *Journal Physics A: Mathematical and General.* 2006;39:1775.

40. Hoogendoorn S, Van Lint JWC, Knoop VL. Macroscopic modeling framework unifying kinematic wave modeling and three-phase traffic theory. *Transportation Research Record*. 2008;2088(1):102–108.

41. Laval JA. *Lane-changing in traffic streams.* In: Traffic and Granular Flow' 05. Proceedings of the International Workshop, ed. by A. Schadschneider, et al. Berlin: Springer; 2007. pp. 521–526.

42. Tian J, et al. Improved 2D intelligent driver model in the framework of three-phase traffic theory simulating synchronized flow and concave growth pattern of traffic oscillations. *Transportation Research*. 2016;41(F):55–65.

43. Xue Y, et al. Long-range correlations in vehicular traffic flow studied in the framework of Kerner's three-phase theory based on rescaled range analysis. *Communications in Nonlinear Sciences and Numerical Simulation*. 2015;22:285–296.

44. Qian YS, Feng X, Zeng JW. A cellular automata traffic flow model for three phase theory. *Physica A: Statistical Mechanics And Its Applications*. 2017;479:509–52.

45. Morozov II, Gasnikov AV, Tarasov VN, et al. Numerical study of transport flows based on hydrodynamic models. *Computer research and modeling.* 2011;3(4): 389–412. (In Russ.).

46. Kholodov Y., Alekseenko A., Kazorin V., et al. Generalization second order macroscopic traffic models via relative velocity of the congestion propagation. *Mathematics*. 2021;9(16):2001.

47. Kubentayeva M, Gasnikov A. Finding equilibria in the traffic assignment problem with primal-dual gradient methods for stable dynamics model and Beckmann model. *Mathematics*. 2021;9(11):1217.

48. Kiselev AB, Kokoreva AV, Nikitin VF, etc. Mathematical modeling of traffic flows by methods of continuum mechanics. Investigation of the influence of artificial road irregularities on the capacity of a road section. *Modern problems of mathematics and mechanics*. Applied Research, edited by VV Alexandrov and VB Kudryavtsev. Moscow: Publishing House of Moscow State University; 2009;1:311–322.(In Russ.).

49. Smirnov N, Kiselev A, Nikitin V, et al. Hydrodynamic traffic flow models and its application to studying traffic control effectiveness. *WSEAS Transactions on Fluid Mechanics*. 2014;9:178–186.

50. Diveev AI, Sofronova EA. The problem of optimal control of traffic flows in the urban road network. *Questions of the theory of security and stability.* 2018;20:89–99. (In Russ.).

51. *Fundamentals of Traffic Simulation*. In: International Series in Operations Research & Management Science. J. Barcelo (Ed.). Springer. 2010;145. 452 p.

52. PTV Vision Traffic Suite [Electronic resource]. URL: https://ptv-vision.ru/ (date of application: 18.05.2023).

53. Aimsun: Simulation and AI for future mobility [Electronic resource]. URL: https://www.aimsun.com/ (date of application: 18.05.2023).

54. *MATSim: Multi-Agent Transport Simulation* [Electronic resource]. URL: https://www.matsim.org/ (date of application: 18.05.2023).

55. Horni A, Nagel K, Axhausen KW (Eds.) *The Multi-Agent Transport Simulation MATSim*. London: Ubiquity Press; 2016.

56. *SUMO: Simulation of Urban MObility* [Electronic resource]. URL: https://www.eclipse.org/sumo/ (date of application: 18.05.2023).

57. Lopez PA, et al. Microscopic Traffic Simulation using SUMO. *21st international conference on Intelligent Transportation Systems (ITSC)*. 2018:2575–2582.

58. *Bentley Systems* [Electronic resource]. URL: https://www.bentley.com (date of application: 18.05.2023).

59. Chetverushkin BN. *Kinetic schemes and quasi-gas-dynamic system of equations*. Moscow: MAKS Press; 2004. 332 p. (In Russ.).

60. Churbanova NG, Chechina AA, Trapeznikova MA. Simulation of traffic flows on road segments using cellular automata theory and quasigasdynamic approach. *Mathematica Montisnigri*. 2019;XLVI:72–90.

61. Trapeznikova MA, Chechina AA, Churbanova NG, et al. Mathematical modeling of traffic flows based on macro- and microscopic approaches. *Bulletin of ASTU, Ser.: Management, Computer engineering and Computer Science.* 2014;1:130–139. (In Russ.).

62. Sokolov PA, Shkolina IV, Trapeznikova MA, et al. Simulation of vehicle traffic on supercomputers based on the SRG system of equations. *News of the SFU. Technical sciences*. 2019;7:159–169. (In Russ.).

63. Chetverushkin B, Chechina A, Churbanova N, et al. Development of parallel algorithms for intelligent transportation systems. *Mathematics*. 2022;10(4):643.

64. Trapeznikova MA, Chechina AA, Churbanova NG. Two-dimensional model of cellular automata for describing the dynamics of traffic flows on the elements of the road network. *Mathematical modeling*. 2017;29(9):110–120. (In Russ.).

65. Chechina A, Churbanova N, Trapeznikova M. Driver behaviour algorithms for the cellular automata-based mathematical model of traffic flows. *EPJ Web of Conferences*. 2021;248:02002.

66. Chechina AA, Herman MS, Ermakov AV, et al. Modeling and visualization of traffic flows on the elements of the road network using the SAM-2D software package. *Preprints of the IAM named after M. V. Keldysh*. 2016;124. 17 p. (In Russ.).

About the Authors:

Marina A Trapeznikova, Senior Researcher, Keldysh Institute of Applied Mathematics RAS (4, Miusskaya Sq., Moscow, 125047, RF), Cand.Sci. (Phys.-Math.), ORCID, mtrapez@yandex.ru

Antonina A Chechina, Junior Researcher, Keldysh Institute of Applied Mathematics RAS (4, Miusskaya Sq., Moscow, 125047, RF), Cand.Sci. (Phys.-Math.), ORCID, chechina.antonina@yandex.ru

Natalia G Churbanova, Senior Researcher, Keldysh Institute of Applied Mathematics RAS (4, Miusskaya Sq., Moscow, 125047, RF), Cand.Sci. (Phys.-Math.), ORCID, nataimamod@mail.ru

Received 11.04.2023.
Revised 16.05.2023.
Accepted 17.05.2023.

Conflict of interest statement

The authors does not have any conflict of interest.

All authors have read and approved the final manuscript.

Об авторах:

Трапезникова Марина Александровна, старший научный сотрудник, Институт прикладной математики им. М. В. Келдыша РАН (РФ, 125047, Москва, Миусская пл., 4), кандидат физико-математических наук, ORCID, mtrapez@yandex.ru

Чечина Антонина Александровна, младший научный сотрудник, Институт прикладной математики им. М. В. Келдыша РАН (РФ, 125047, Москва, Миусская пл., 4), кандидат физико-математических наук, ORCID, chechina.antonina@yandex.ru

Чурбанова Наталья Геннадьевна, старший научный сотрудник, Институт прикладной математики им. М. В. Келдыша РАН (РФ, 125047, Москва, Миусская пл., 4), кандидат физико-математических наук, ORCID, nataimamod@mail.ru

Поступила в редакцию 11.04.2023.
Поступила после рецензирования 16.05.2023.
Принята к публикации 17.05.2023.

Конфликт интересов

Авторы заявляют об отсутствии конфликта интересов.

Все авторы прочитали и одобрили окончательный вариант рукописи.

MATHEMATICAL MODELING
МАТЕМАТИЧЕСКОЕ МОДЕЛИРОВАНИЕ

UDC 519.6

Original article

https://doi.org/10.23947/2587-8999-2023-7-2-73-80

Existence and Uniqueness of the Initial-Boundary Value Problem Solution of Multicomponent Sediments Transport in Coastal Marine Systems

Valentina V Sidoryakina

Taganrog Institute named after A. P. Chekhov (branch) of RSUE, 48, Initiative St., Taganrog, Russian Federation

cvv9@mail.ru

Abstract

Introduction. This work is devoted to the study of a non-stationary two-dimensional model of sediment transport in coastal marine systems. The model takes into account the complex multi-fractional composition of sediments, the gravity effect and tangential stress caused by the impact of waves, turbulent exchange, dynamically changing bottom topography, and other factors. The aim of the work was to carry out an analytical study of the conditions for the initial-boundary value problem existence and uniqueness corresponding to the specified model.

Materials and Methods. Linearization of the initial-boundary value problem is performed on a temporary uniform grid. The nonlinear coefficients of a quasilinear parabolic equation are taken with a "delay" by one grid step. Thus, a chain of correlated by initial conditions is the final solutions of problems is built. The study of the existence and uniqueness of the problems included in this chain, and therefore the original problem as a whole, is carried out involving the methods of mathematical and functional analysis, as well as methods for solving differential equations.

Results. Earlier, the authors investigated the existence and uniqueness of the initial-boundary value problem of the transport of sediments of a single-component composition. In the present work, the result obtained is extended to the case of multi-fractional sediments.

Discussion and Conclusions. Based on the analysis of the existing results of mathematical modeling of hydrodynamic processes, a non-linear spatial two-dimensional model of sediment transport was previously investigated by the team of authors in the case of bottom sediments consisting of particles having the same characteristic dimensions and density (single-component composition). In this paper, the previous results of the study are extended to the case of sediments of a multicomponent composition, namely, the conditions for the existence and uniqueness of the solution of the initial-boundary value problem corresponding to the considered model are determined.

Keywords: multicomponent sediments' transport, coastal marine system, initial-boundary value problem, solution existence, solution uniqueness.

Funding information. The study was supported by the Russian Science Foundation grant no. 23-21-00509. https://rscf.ru/project/23-21-00509

For citation. Sidoryakina VV. Existence and uniqueness of the solution of the initial-boundary value problem of transport of multicomponent sediments of coastal marine systems. *Computational Mathematics and Information Technologies*. 2023;7(2):73–80. https://doi.org/10.23947/2587-8999-2023-7-2-73-80

Научная статья

Существование и единственность решения начально-краевой задачи транспорта многокомпонентных наносов прибрежных морских систем

В.В. Сидорякина

Таганрогский институт им. А. П. Чехова (филиал) РГЭУ (РИНХ), Российская Федерация, г. Таганрог, ул. Инициативная, 48

cvv9@mail.ru

Аннотация

Введение. Настоящая работа посвящена исследованию нестационарной двумерной модели транспорта наносов в прибрежных морских системах. Модель учитывает сложный многокомпонентный состав наносов; действие силы тяжести и тангенциального напряжения, вызванного воздействием волн; турбулентный обмен; динамически изменяемый рельеф дна и другие факторы. Целью работы являлось проведение аналитического исследования условий существования и единственности начально-краевой задачи, соответствующей указанной модели.

Материалы и методы. В работе на временной равномерной сетке выполнена линеаризация начально-краевой задачи, при которой нелинейные коэффициенты квазилинейного параболического уравнения берутся с «запаздыванием» на один шаг сетки. Тем самым строится цепочка задач, связанных по начальным условиям и финальным решениям. Привлекая методы математического и функционального анализа, а также методы решения дифференциальных уравнений, проводится исследование существования и единственности задач, входящих в данную цепочку, а потому и в целом исходной задачи.

Результаты исследования. На основе анализа существующих результатов математического моделирования гидродинамических процессов ранее была исследована нелинейная пространственно-двумерная модель транспорта наносов в случае донных отложений, состоящих из частиц, имеющих одинаковые характерные размеры и плотность (однокомпонентный состав). В настоящей работе предыдущие результаты исследования распространены на случай наносов многокомпонентного состава, а именно определены условия существования и единственности решения начально-краевой задачи, соответствующей рассматриваемой модели.

Обсуждение и заключения. Модель транспорта многокомпонентных наносов может быть полезна для прогноза распространения загрязняющих веществ, а также при исследовании динамики изменения рельефа дна как при антропогенном воздействии, так и в силу естественно протекающих природных процессов в морских системах.

Ключевые слова: транспорт многокомпонентных наносов, прибрежная морская система, начально-краевая задача, существование решения, единственность решения.

Финансирование. Исследование выполнено за счет гранта Российского научного фонда № 23-21-00509, https://rscf.ru/project/23-21-00509

Для цитирования. Сидорякина В.В. Существование и единственность решения начально-краевой задачи транспорта многокомпонентных наносов прибрежных морских систем. *Computational Mathematics and Information Technologies.* 2023;7(2):73–80. https://doi.org/10.23947/2587-8999-2023-7-2-73-80

Introduction. It is necessary to use a set of models of different spatial and temporal scales in solving practical tasks related to the environmental assessment of the water body's state [1–6]. The research of mathematical hydrophysical models, which are characterized by a variety of parameters, has been actively developed in recent decades [7–14]. The paper considers 2D mathematical model for calculating the transport of multicomponent sediments in relation to coastal marine systems. The set of convection-diffusion equations for each sediment component (or fraction) forms this mathematical model taking into account turbulent exchange, gravity, tangential stress, dynamically changing bottom relief and other factors [15–17].

The article presents the results of theoretical study of the initial boundary value problem existence and uniqueness based on the constructed model. In accordance with this goal, the initial boundary value problem for quasi-linear equation of parabolic type is considered, for which sufficient conditions for the existence and uniqueness of the solution are determined by methods of mathematical and functional analysis, as well as by methods of solving differential equations.

Materials and methods

1. Initial boundary value problem of multicomponent sediment transport. Let's write down the equation of multicomponent sediments transport [16, 17]:

$$(1-\varepsilon_r)\frac{\partial H}{\partial t}+\operatorname{div}\left(V_r k_r \vec{\tau}_b\right)=\operatorname{div}\left(V_r k_r \frac{\tau_{bc,r}}{\sin\varphi_0}\operatorname{grad}H\right)+\frac{w_{g,r}}{\rho_r}c_r,\quad r=\overline{1,R}. \tag{1}$$

Where $H=H(x,y,t)$ is the reservoir depth; ε_r is the porosity r-th component in the sediments composition; V_r is the r-th component's volume fraction; $\vec{\tau}_b$ is the tangential tangential stress vector at the reservoir bottom; $\tau_{bc,r}$ is the critical value of the tangential stress for r-th sediment component, $\tau_{bc,r}=a_r\sin\varphi_0$, a_r is the coefficient for r-th sediment component, φ_0 is the angle of the natural slope of the soil in the reservoir; $w_{g,r}$ is the hydraulic size or deposition rate of r-th component; ρ_r is the density of r-th bottom material component; $k_r=k_r(H,x,y,t)$ is nonlinear coefficient determined by the ratio:

$$k_r=\frac{A\tilde{\omega}d_r}{\left((\rho_r-\rho_0)gd_r\right)^{\beta}}\left|\vec{\tau}_b-\frac{\tau_{bc,r}}{\sin\varphi_0}\operatorname{grad}H\right|^{\beta-1},$$

where $\tilde{\omega}$ is the average wave frequency; d_r is the characteristic size of r-th component; g is the acceleration of gravity; ρ_0 is the aquatic environment density; A and β are the dimensionless constants.

Let the sediment transport process take place in an area D, $D(x,y)=\{0<x<L_x, 0<y<L_y\}$ with boundary S, representing a piecewise smooth line. We assume that a three-dimensional cylinder $Ц_T=D\times(0,T)$ of height T with a base D is the domain of equation (1). The boundary of this cylinder consists of a side surface $S\times[0,T]$ and two bases — $\overline{D}\times\{0\}$ and $\overline{D}\times\{T\}$.

Equation (1) is considered with the initial condition:

$$H(x,y,0)=H_0(x,y), \tag{2.1}$$

$$H_0(x,y)\in C^2(D)\cap C(\overline{D}), \tag{2.2}$$

$$\operatorname{grad}_{(x,y)}H_0\in C(\overline{D}), \tag{2.3}$$

$$(x,y)\in\overline{D} \tag{2.4}$$

and conditions on the region border $\overline{D}$:

$$\left|\overrightarrow{\tau_b}\right|\Big|_{y=0}=0, \tag{3}$$

$$H(L_x,y,t)=H_2(y,t),\ 0\le y\le L_y, \tag{4}$$

$$H(0,y,t)=H_1(y,t),\ 0\le y\le L_y, \tag{5}$$

$$H(x,0,t)=H_3(x),\ 0\le x\le L_x. \tag{6}$$

$$H(x,L_y,t)=0,\ 0\le x\le L_x. \tag{7}$$

Let assume:

$$\operatorname{grad}_{(x,y)}H\in C(\overline{Ц_T})\cap C^1(Ц_T),$$

$$\tau_{bx}=\tau_{bx}(x,y,t),$$

$$k_r\ge k_{0r}=\text{const}>0,\ \forall(x,y)\in\overline{D},\ 0<t\le T,$$

2. The initial boundary value problem linearization of multicomponent sediment transport. Let's build a time grid ω_τ, with step τ: $\omega_\tau=\{t_n=n\tau,\ n=0,1,...,N,\ N\tau=T\}$.

If n=1, then the reservoir depth $H^{(1)}(x,y,t_0)$ is known and is determined from the initial condition, i. e. $H^{(1)}(x,y,t_0)=H_0(x,y)$. If $n=2,...,N$, then the reservoir depth $H^{(n)}(x,y,t_{n-1})$ will also be known, since problem (1)–(7) is solved for the time interval, $t_{n-2}<t\le t_{n-1}$, i. e. $H^{(n)}(x,y,t_{n-1})=H^{(n-1)}(x,y,t_{n-1})$.

Denote:

$$k_r^{(n-1)}\equiv\frac{A\tilde{\omega}d_r}{\left((\rho_r-\rho_0)gd_r\right)^{\beta}}\left|\vec{\tau}_b-\frac{\tau_{bc,r}}{\sin\varphi_0}\operatorname{grad}H^{(n-1)}(x,y,t_{n-1})\right|^{\beta-1},\quad n=1,2,...,N. \tag{8}$$

After linearization, equation (1) and the initial condition will take the form:

$$(1-\varepsilon_r)\frac{\partial H^{(n)}}{\partial t}=\operatorname{div}\left(V_r k_r^{(n-1)}\frac{\tau_{bc,r}}{\sin\varphi_0}\operatorname{grad}H^{(n)}\right)-\operatorname{div}\left(V_r k_r^{(n-1)}\vec{\tau}_b\right)+\frac{w_{g,r}}{\rho_r}c_r,\quad r=\overline{1,R}, \tag{9}$$

$$t_{n-1} < t \le t_n,\ n = 1, 2,..., N,$$

$$H^{(1)}(x, y, t_0) = H_0(x, y),\ \ H^{(n)}(x, y, t_{n-1}) = H^{(n-1)}(x, y, t_{n-1}),\ \ (x, y) \in \overline{D},\ \ n = 2,..., N. \tag{10}$$

Boundary conditions (3)–(7) are assumed to be fulfilled for all time intervals $t_{n-1} < t \le t_n,\ n = 1, 2,..., N$.

Research results

1. Investigation of the linearized initial boundary value problem of multicomponent sediments transport solution existence. Let 's put $n = i,\ i = 1, 2,..., N$ in the equation (9).

We have:

$$(1 - \varepsilon_r)\frac{\partial H^{(i)}}{\partial t} = \operatorname{div}\left(V_r k_r^{(i-1)} \frac{\tau_{bc,r}}{\sin\varphi_0} \operatorname{grad} H^{(i)}\right) - \operatorname{div}\left(V_r k_r^{(i-1)} \vec{\tau}_b\right) + \frac{w_{g,r}}{\rho_r} c_r,\ \ r = \overline{1, R}. \tag{11}$$

Equation (11) is supplemented by conditions (10) and (3)–(7).

If $i = 1,$ then based on the assumptions made earlier, we can write:

$$V_r k_r^{(0)} \frac{\tau_{bc}}{\sin\varphi_0} \in C^1(\Pi_\infty),\ \ V_r k_r^{(0)} \vec{\tau}_b \in C^1(\Pi_\infty). \tag{12}$$

From [18] it can be concluded that if condition (12) is met, the solution of the initial boundary value problem (11), (10), (2) – (7), $t_0 < t \le t_1,\ \ i = 1,$ exists and belongs to the class:

$$H^{(1)}(x, y, t) \in C^2(\Pi_{t_1}) \cap C(\overline{\Pi}_{t_1}),\ \ \operatorname{grad}_{(x,y)} H^{(1)} \in C(\overline{\Pi}_{t_1}).$$

If $i = 2,$ then the initial-boundary value problem will have an initial condition $H^{(2)}(x, y, t_1) \equiv H^{(1)}(x, y, t_1)$. Its smoothness coincides with the smoothness of the initial condition for equation (11) of the number $i = 1$:

$$H^{(2)}(x, y, t) \in C^2(\Pi_{t_2}) \cap C(\overline{\Pi}_{t_2}),\ \operatorname{grad}_{(x,y)} H^{(2)} \in C(\overline{\Pi}_{t_2}).$$

It is obvious that the conditions from [18] and the solution of the problem are again applicable (11), (10), (2) – (7) for the number $i = 2$ exists.

Further, if $i,\ \ i = 3,..., N,$ then for each case we will have a mixed problem for a linear equation of parabolic type. The initial and boundary conditions have a smoothness sufficient for the functions existence $H^{(i)}(x, y, t),\ \ t_{i-1} < t \le t_i,\ \ i = 1, 2,..., N$ класса $C^2(\Pi_{t_i}) \cap C(\overline{\Pi}_{t_i}),\ \operatorname{grad}_{(x,y)} H^{(i)} \in C(\overline{\Pi}_{t_i})$, which are solutions to initial boundary value problems (11), (10), (2)–(7) [19].

2. The linearized initial boundary value problem solution uniqueness investigation of multicomponent sediments transport. Let's write equation (11) for $n = 1$:

$$(1 - \varepsilon_r)\frac{\partial H^{(1)}}{\partial t} = \operatorname{div}\left(V_r k_r^{(0)} \frac{\tau_{bc,r}}{\sin\varphi_0} \operatorname{grad} H^{(1)}\right) - \operatorname{div}\left(V_r k_r^{(0)} \vec{\tau}_b\right) + \frac{w_{g,r}}{\rho_r} c_r,\ \ r = \overline{1, R}. \tag{13}$$

Let us assume the existence of two different solutions to it:

$$H' = H'(x, y, t),\ \ H'' = H''(x, y, t),\ \ (x, y) \in \overline{D},\ \ t_0 < t \le t_1.$$

Denote:

$$w^{(1)}(x, y, t) \equiv H'(x, y, t) - H''(x, y, t),\ \ t_0 < t \le t_1,\ \ w^{(1)}(x, y, t) \not\equiv 0,\ \ w^{(1)}(x, y, t_0) \equiv 0.$$

The initial boundary value problem for the function $w(x, y, t) \equiv w^{(1)}(x, y, t)$ will have the form:

$$(1 - \varepsilon_r)\frac{\partial w}{\partial t} = \operatorname{div}\left(V_r k_r^{(0)} \frac{\tau_{bc,r}}{\sin\varphi_0} \operatorname{grad} w\right),\ \ r = \overline{1, R}, \tag{14}$$

$$w(x, y, 0) = 0,\ \ (x, y) \in \overline{D}, \tag{15}$$

$$\left|\vec{\tau}_b\right|\Big|_{y=0} = 0, \tag{16}$$

$$w(x, L_y, t) = 0,\ \ 0 \le x \le L_x, \tag{17}$$

$$w(0, y, t) = 0,\ \ 0 \le y \le L_y, \tag{18}$$

$$w(L_x, y, t) = 0,\ \ 0 \le y \le L_y, \tag{19}$$

$$w(x, 0, t) = 0,\ \ 0 \le x \le L_x. \tag{20}$$

We multiply both parts of equation (14) by the function $w(x,y,t) \not\equiv 0,\ t_0 < t \le t_1,\ (x,y) \in \overline{D},$ and then perform integration over variables $t,\ t_0 < t \le t_1$ and (x,y) in the domain D. We will get:

$$\int_{t_0}^{t_1}\left((1-\varepsilon_r)\iint_D w\frac{\partial w}{\partial t}\,dxdy\right)dt = \int_{t_0}^{t_1}\left(\iint_D w div\left(V_r k_r^{(0)}\frac{\tau_{bc,r}}{\sin\varphi_0}\operatorname{grad} w\right)dxdy\right)dt,\ r=\overline{1,R}. \tag{21}$$

After a series of transformations of equality (21), we obtain:

$$\frac{1}{2}(1-\varepsilon_r)\left[\iint_D w^2(x,y,t_1)dxdy - \iint_D w^2(x,y,t_0)dxdy\right] = \int_{t_0}^{t_1}\left(\iint_D w div\left(V_r k_r^{(0)}\frac{\tau_{bc,r}}{\sin\varphi_0}\operatorname{grad} w\right)dxdy\right)dt. \tag{22}$$

Equality (22) under condition (15) is written as:

$$\frac{1}{2}(1-\varepsilon_r)\iint_D w(x,y,t_1)^2 dxdy = \int_{t_0}^{t_1}\left(\iint_D w div\left(V_r k_r^{(0)}\frac{\tau_{bc,r}}{\sin\varphi_0}\operatorname{grad} w\right)dxdy\right)dt. \tag{23}$$

Let:

$$R(w) \equiv \int_{t_0}^{t_1}\left(\iint_D w div\left(V_r k_r^{(0)}\frac{\tau_{bc,r}}{\sin\varphi_0}\operatorname{grad} w\right)dxdy\right)dt. \tag{24}$$

There is equality:

$$\begin{aligned}&\iint_D\left[w\left(\frac{\partial}{\partial x}\left(V_r k_r^{(0)}\frac{\tau_{bc,r}}{\sin\varphi_0}\right)\frac{\partial w}{\partial x}\right)+\frac{\partial}{\partial y}\left(\left(V_r k_r^{(0)}\frac{\tau_{bc,r}}{\sin\varphi_0}\right)\frac{\partial w}{\partial y}\right)\right]dxdy = \\ &= \iint_D\left[\frac{\partial}{\partial x}\left(w\left(V_r k_r^{(0)}\frac{\tau_{bc,r}}{\sin\varphi_0}\right)\frac{\partial w}{\partial x}\right)+\frac{\partial}{\partial y}\left(w\left(V_r k_r^{(0)}\frac{\tau_{bc,r}}{\sin\varphi_0}\right)\frac{\partial w}{\partial y}\right)\right]dxdy - \\ &\quad - \iint_D\left[\left(V_r k_r^{(0)}\frac{\tau_{bc,r}}{\sin\varphi_0}\right)\left(\frac{\partial w}{\partial x}\right)^2+\left(V_r k_r^{(0)}\frac{\tau_{bc,r}}{\sin\varphi_0}\right)\left(\frac{\partial w}{\partial y}\right)^2\right]dxdy.\end{aligned} \tag{25}$$

On the other hand, taking into account the boundary conditions (16)–(20) and the Ostrogradsky-Gauss theorem [19], we have:

$$\iint_D\left[\frac{\partial}{\partial x}\left(w\left(V_r k_r^{(0)}\frac{\tau_{bc,r}}{\sin\varphi_0}\right)\frac{\partial w}{\partial x}\right)+\frac{\partial}{\partial y}\left(w\left(V_r k_r^{(0)}\frac{\tau_{bc,r}}{\sin\varphi_0}\right)\frac{\partial w}{\partial y}\right)\right]dxdy = 0. \tag{26}$$

From the equalities (25) and (26) we find:

$$R(w) \equiv -\int_{t_0}^{t_1}\left(\iint_D V_r k_r^{(0)}\frac{\tau_{bc,r}}{\sin\varphi_0}\left[\left(\frac{\partial w}{\partial x}\right)^2+\left(\frac{\partial w}{\partial y}\right)^2\right]dxdy\right)dt. \tag{27}$$

Taking into account (27), equality (22) will be written as:

$$\frac{1}{2}(1-\varepsilon_r)\iint_D w^2(x,y,t_1)dxdy = -\int_{t_0}^{t_1}\left(\iint_D V_r k_r^{(0)}\frac{\tau_{bc,r}}{\sin\varphi_0}\left[\left(\frac{\partial w}{\partial x}\right)^2+\left(\frac{\partial w}{\partial y}\right)^2\right]dxdy\right)dt. \tag{28}$$

Next, we transform the right side of equality (28). By involving the Poincare inequality [20], we obtain:

$$-\int_{t_0}^{t_1}\left[\iint_D V_r k_r^{(0)}\frac{\tau_{bc,r}}{\sin\varphi_0}\left(\left(\frac{\partial w}{\partial x}\right)^2+\left(\frac{\partial w}{\partial y}\right)^2\right)dxdy\right]dt \le -V_r k_r^{(0)}\frac{\tau_{bc,r}}{\sin\varphi_0}\int_{t_0}^{t_1}\left[\iint_D\left(\left(\frac{\partial w}{\partial x}\right)^2+\left(\frac{\partial w}{\partial y}\right)^2\right)dxdy\right]dt. \tag{29}$$

From the inequality (29) follows the assessment:

$$-\int_{t_0}^{t_1}\left[\iint_D V_r k_r^{(0)}\frac{\tau_{bc,r}}{\sin\varphi_0}\left(\left(\frac{\partial w}{\partial x}\right)^2+\left(\frac{\partial w}{\partial y}\right)^2\right)dxdy\right]dt \le -\pi^2 V_r k_r^{(0)}\frac{\tau_{bc,r}}{\sin\varphi_0}\left(\frac{1}{L_x^2}+\frac{1}{L_y^2}\right)\int_{t_0}^{t_1}\left[\iint_D w^2 dxdy\right]dt. \tag{30}$$

From the equalities (33) and (35) the inequality is obtained:

$$\frac{1}{2}(1-\varepsilon_r)\iint_D w^2(x,y,t_1)dxdy \le -\pi^2 V_r k_r^{(0)}\frac{\tau_{bc,r}}{\sin\varphi_0}\left(\frac{1}{L_x^2}+\frac{1}{L_y^2}\right)\int_{t_0}^{t_1}\left[\iint_D w^2 dxdy\right]dt. \tag{31}$$

Since $w(x,y,t) \not\equiv 0$, then $w^2(x,y,t^*) > 0$ is done. Due to the function continuity $w^2(x,y,t)$ in some neighborhood of the point t^* at $t_0 < t^* \le t_1$, we have $\iint\limits_D w^2(x,y,t)dxdy > 0$, and therefore:

$$-\pi^2 V_r k_r^{(0)} \frac{\tau_{bc,r}}{\sin\varphi_0}\left(\frac{1}{L_x^2}+\frac{1}{L_y^2}\right)\int\limits_{t_0}^{t_1}\left[\iint\limits_D w^2 dxdy\right]dt < 0. \tag{32}$$

From the resulting inequalities (31) and (32), a contradictory inequality will follow:

$$\frac{1}{2}(1-\varepsilon_r)\iint\limits_D w^2(x,y,t_1)dxdy < 0. \tag{33}$$

Therefore, the identity $w(x,y,t_1) \equiv 0$ is valid. Due to the arbitrariness of the time step τ, $\tau > 0$, we have:

$$w(x,y,t) = 0, \quad t_0 < t \le t_1.$$

Obviously, when $w(x,y,t) \equiv 0$ in case of $(x,y) \in \overline{D}$, $t_{n-1} \le t \le t_n$, $n = 2,...,N$.

Thus, the first step of induction at $n = 1$. Similarly , arguments are constructed for $n = s$, $s = 2,..,N$, which leads to equality:

$$w(x,y,t_s) \equiv 0.$$

The result of the reasoning is the following theorem.

Theorem. Let the equations (11) be given:

$$(1-\varepsilon_r)\frac{\partial H^{(n)}}{\partial t} = \operatorname{div}\left(V_r k_r^{(n-1)}\frac{\tau_{bc,r}}{\sin\varphi_0}\operatorname{grad} H^{(n)}\right) - \operatorname{div}\left(V_r k_r^{(n-1)}\vec{\tau}_b\right) + \frac{w_{g,r}}{\rho_r}c_r, \quad r = \overline{1,R},$$

$$t_{n-1} < t \le t_n,\ n = 1,2,...,N,$$

in a rectangular area:

$$D(x,y) = \{0 < x < L_x, 0 < y < L_y\},$$

where $k_r^{(n-1)} \equiv \frac{A\tilde{\omega}d_r}{((\rho_r-\rho_0)gd_r)^\beta}\left|\vec{\tau}_b - \frac{\tau_{bc,r}}{\sin\varphi_0}\operatorname{grad} H^{(n-1)}(x,y,t_{n-1})\right|^{\beta-1}$ with initial and boundary conditions (11), (3)–(7).

Then, if the conditions are met $k_r^{(n-1)} \ge k_{0r} > 0$, $k_r^{(n-1)} \in C^1(\overline{D})$, then $\forall n$, $n = 1,2,...,N$ the function $H^{(n)}(x,y,t)$, $t_{n-1} < t \le t_n$, $n = 1,2,...,N$ of the class $\operatorname{grad}_{(x,y)} H^{(n)} \in C(\overline{\amalg}_T)$ will be the solution of the equation of the number n in the cylinder $\amalg_T = D \times (0,T)$ and this solution is the only one.

Discussion and conclusions. The novelty of this work is determined by the formulation of a non-stationary spatial-two-dimensional mathematical problem of sediment transport, taking into account their complex multicomponent composition. The linearization of the corresponding initial-boundary value problem is performed on a grid in time and for an arbitrary time step $t_{n-1} < t \le t_n$, $n = 1,2,...,N$, the conditions for the initial-boundary value problem solution existence and uniqueness are obtained.

References

1. Leontiev IO. *Coastal dynamics: waves, currents, sediment flows*. Moscow: GEOS; 2001. 272 p. (In Russ.).

2. Xiaoying Liu, Shi Qi, Yuan Huang, et al. Predictive modeling in sediment transportation across multiple spatial scales in the Jialing River Basin of China. *International Journal of Sediment Research*. 2015;30(3):250–255. https://doi.org/10.1016/j.ijsrc.2015.03.013

3. Marchuk GI, Dymnikov VP, Zalesny VB. *Mathematical models in geophysical hydrodynamics and numerical methods of their implementation*. Leningrad: Hydrometeoizdat; 1987. 296 p. (In Russ.).

4. Gic-Grusza G, Dudkowska A. Numerical modeling of hydrodynamics and sediment transport — an integrated approach. *Ocean Dynamics*. 2017;67:1283–1292. https://doi.org/10.1007/s10236-017-1085-9

5. Ouda M, Toorman EA. Development of a new multiphase sediment transport model for free surface flows. *International Journal of Multiphase Flow*. 2019;117:81–102. https://doi.org/10.1016/j.ijmultiphaseflow.2019.04.023

6. Aksoy H, Kavvas ML. A review of hillslope and watershed scale erosion and sediment transport models. *Catena.* 2005;64(2–3):247–271. https://doi.org/10.1016/j.catena.2005.08.008

7. Sukhinov A, Sidoryakina V. Two-Dimensional-One-Dimensional Alternating Direction Schemes for Coastal Systems Convection-Diffusion Problems. *Mathematics*. 2021;9:3267. https://doi.org/10.3390/math9243267

8. Sukhinov A, Belova Y, Nikitina A, et al. Sufficient Conditions for the Existence and Uniqueness of the Solution of the Dynamics of Biogeochemical Cycles in Coastal Systems Problem. *Mathematics*. 2022;10:2092. https://doi.org/10.3390/math101220928

9. Sukhinov A, Belova Y, Panasenko N, et al. Research of the Solutions Proximity of Linearized and Nonlinear Problems of the Biogeochemical Process Dynamics in Coastal Systems. *Mathematics*. 2023;11:575. https://doi.org/10.3390/math11030575

10. Sukhinov AI, Chistyakov AE, Bondarenko YuS. Error estimation of the solution of the error diffusion equation based on schemes with weights. News of the SFU. *Technical sciences*. 2011;8(121):6–13. (In Russ.).

11. Sukhinov AI, Chistyakov AE, Shishenya AV. Estimation of the error of solving the diffusion equation based on schemes with weights. *Mathematical modeling*. 2013;25(11):53–64; *Mathematical Models and Computer Simulation*. 2014;6(3):324–331. (In Russ.). https://doi.org/10.1134/S2070048214030120

12. Sukhinov AI, Chistyakov AE, Ugolnitsky GA., et al. Game-theoretic regulations of mechanisms for managing the sustainable development of shallow-water ecosystems. *Automation and telemechanics*. 2017; 6:122–137; *Automation and Remote Control*. 2017;78(6):1059–1071. (In Russ.). https://doi.org/10.1134/S0005117917060078

13. Sukhinov AI, Sidoryakina VV. On the convergence of the solution of a linearized sequence of problems to the solution of a nonlinear sediment transport problem. *Mathematical modeling*. 2017;29(11):19–39. (In Russ.).

14. Sidoryakina VV., Sukhinov AI. Correctness study and numerical implementation of a linearized two-dimensional sediment transport problem. *Journal of Computational Mathematics and Mathematical Physics*. 2017;57(6):985–1002; Computational Mathematics and Mathematical Physics. 2017;57(6):978-994. (In Russ.) https://doi.org/10.7868/S0044466917060138

15. Sukhinov AI, Chistyakov AE, Protsenko EA. Construction of a discrete two-dimensional mathematical model of sediment transport. News of the SFU. *Technical sciences*. 2011;8(121):32–44. (In Russ.).

16. Sukhinov AI, Chistyakov AE, Sidoryakina VV. Parallel Solution of Sediment and Suspension Transportation Problems on the Basis of Explicit Schemes. *Communications in Computer and Information Science*. 2018;910:306–321. https://doi.org/10.1007/978-3-319-99673-8_22

17. Sukhinov AI, Chistyakov AE, Atayan AM., et al. Mathematical model of the process of deposition to the bottom of a multicomponent suspension and changes in the composition of bottom materials. Izvestiya IMI UdGU. 2022;60:73–89. (In Russ.). https://doi.org/10.35634/2226-3594-2022-60-05

18. Vladimirov VS. *Equations of mathematical physics.* Textbook. 4th ed., ispr. and add. Moscow: Nauka; 1981. 512 p. (In Russ.).

19. Ladyzhenskaya OA. *Boundary value problems of mathematical physics*. Moscow: Nauka; 1973. 407 p. (In Russ.).

20. Ladyzhenskaya OA, Solonnikov VA, Uraltseva NN. *Linear and quasi-linear equations of parabolic type*. Moscow: Nauka; 1967. 736 p. (In Russ.).

About the Author:

Valentina V Sidoryakina, Associate Professor of the Mathematics Department, Taganrog Institute named after A. P. Chekhov (branch) of RSUE (48, Initiative St., Taganrog, 347936, RF), PhD (Physical and Mathematical Sciences), MathSciNet, eLibrary.ru, ORCID, ResearcherID, ScopusID, cvv9@mail.ru

Received 18.04.2023.
Revised 24.05.2023.
Accepted 25.05.2023.

Conflict of interest statement

The authors do not have any conflict of interest.

All authors have read and approved the final manuscript.

Об авторе:

Сидорякина Валентина Владимировна, доцент кафедры математики, Таганрогский институт имени А. П. Чехова (филиал) РГЭУ (РИНХ), (РФ, 347936, г. Таганрог, ул. Инициативная, 48), кандидат физико-математических наук, MathSciNet, eLibrary.ru, ORCID, ResearcherID, ScopusID, cvv9@mail.ru

Поступила в редакцию 18.04.2023.
Поступила после рецензирования 24.05.2023.
Принята к публикации 25.05.2023.

Конфликт интересов
Автор заявляет об отсутствии конфликта интересов.

Автор прочитал и одобрил окончательный вариант рукописи.